

THESIS
2
2001

This is to certify that the
dissertation entitled

Studies of Microgravity Diffusion Flames

presented by

Robert W. Vance

has been accepted towards fulfillment
of the requirements for

Ph.D. degree in Mechanical Engineering



Major professor

Date 4/12/01

STUDIES OF MICROGRAVITY DIFFUSION FLAMES

BY

ROBERT W. VANCE

A DISSERTATION

Submitted to

Michigan State University

in partial fulfillment of the requirements

for the degree of

DOCTOR OF PHILOSOPHY

Department of Mechanical Engineering

2001

ABSTRACT

STUDIES OF MICROGRAVITY DIFFUSION FLAMES

By

Robert W. Vance

Various topics relating to flame stability are discussed. A linear stability analysis is performed on a set of simplified equations to discern regions of both cellular and oscillatory flame instabilities of diffusion flames. This is performed for a one-dimensional model and also for a two-dimensional model representing a simple version of an "edge flame". It is shown that the one-dimensional model agrees well with the two-dimensional model in a qualitative sense. A one-dimensional model of laminar premixed flame annihilation is examined to identify the effect of non-unity Lewis number on flame front extinction. Conclusions are drawn regarding the implications for turbulent flame stability. Additionally, a heat transfer analysis is performed for a slot-burner configuration of a diffusion flame. Here, characteristic profiles for the conductive heat loss from a lifted tri-brachial flame are examined. Correlations are presented and compared with experimental data.

ACKNOWLEDGEMENTS

I would like to acknowledge the members of my committee, Dr. I. Wichman, Dr. C. Somerton, Dr. M. Miklavcic, and Dr. M. Zhuang, who provided considerable support throughout. This dissertation is a product of their willingness to give their valuable time and a reflection of their commitment to excellent engineering education and research.

TABLE OF CONTENTS

LIST OF TABLES.....	v
LIST OF FIGURES.....	vi
CHAPTER 1	
INTRODUCTION.....	1
CHAPTER 2	
ONE-DIMENSIONAL DIFFUSION FLAME STABILITY.....	5
CHAPTER 3	
TWO-DIMENSIONAL DIFFUSION FLAME STABILITY.....	39
CHAPTER 4	
ONE-DIMENSIONAL LAMINAR PREMIXED FLAME ANNIHILATION.....	55
CHAPTER 5	
HEAT LOSS ANALYSIS OF A DIFFUSION FLAME LEADING EDGE	100
CHAPTER 6	
NUMERICAL TECHNIQUES	140

LIST OF TABLES

Table 5.1	Correction-factor coefficients.....	133
Table 5.2	Reaction information for Methane and Propane.....	124

List of Captions for Figures

Figure 2.1. Schematic Diagram of convective film diffusion flame.....	27
Figure 2.2. Qualitative plot of 1-D non-premixed flame Temperature vs Damkohler number. Three distinct branches are traditionally represented. The upper branch (above A) represents steady burning, the middle branch is unstable, and the lower branch corresponds to the ignition branch. In actual plots the lower turn appears at values of D many orders of magnitude higher than D at the upper turn.....	28
Figure 2.3. The response curve in the vicinity of the upper turning point. Here $Le=1.0$, $Pe=0.0$, $Ta=4$, $\phi=1.0$	29
Figure 2.4. Leading two eigenvalues for the case of $Pe=0$, $Le=1$, $Ta=4.0$, $To=0.05$. Here σ_2 has multiplicity 2 and is independent of D . Note that σ_1 is positive on the middle branch and negative on the upper branch (dotted curve).....	30
Figure 2.5. $1 < Le < Le_c$. Real eigenvalues σ_1 and σ_2 merge at B to form a complex conjugate pair until they split again at E. B moves up and E moves to the right as Le is increased. Here, $Pe=0.0$, $Le=1.01$, $Ta=4.0$, $To=0.05$	31
Figure 2.6. Leading two eigenvalues for $Le=2.0$ $Ta=4.0$, $Pe=0$, $To=0.05$. Upper branch instabilities are seen up to point C'. Oscillations are unstable between B and C' and stable beyond C'. Pure perturbation growth exists between A and B.....	32
Figure 2.7. When $Le < 1$, the third eigenvalue diverges from the constant value obtained when $Le = 1$ by moving lower. As $Le \rightarrow 1$ σ_3 merges with σ_2 . $Pe=0$, $Le=0.95$, $Ta=4$, $To=0.05$	33
Figure 2.8. The thermal-diffusive properties of the reactants plays a significant role in determining the flamelet size as well as the location of the onset of instability. Here $Pe=0.5$, $Ta=5.0$, $To=0.05$	34
Figure 2.9. The critical wave number for $Le=1$ for solutions along the unstable middle branch are relatively unaffected by the crossflow velocity. However, the increased cross flow results in a smaller flamelet after flame front breakup. $Le=1$, $Ta=5.0$, $To=0.05$	35
Figure 2.10 Experimental observations show a sinusoidal waveform prior to flame front breakup. (Colors inverted).....	36

Figure 2.11 After the flame breaks up, the flame pockets that form are dynamic in nature. The flame pockets do not behave uniformly in that different sizes are observed. (colors inverted).....	37
Figure 2.12. Transient solution for $Le=2$ $Pe=0$ $Ta=4$ $To=0.05$ at values of D on either side of point C' . In one case the oscillations grow with time and lead to instability. In the other, the oscillations decay leading to a stable solution.....	38
Figure 3.1 Schematic of 2-D edge-flame model with boundary conditions.....	47
Figure 3.2 Eigenvalue distribution for $Le=1$ $Pe=0.5$ $Ta=4$ $\phi=1.0$. Similar distributions are seen for the 1-D model when $Le=1$	48
Figure 3.3 Eigenvalue distribution for $Le=0.9$ $Pe=0.3$ $Ta=4$ $\phi=1.0$. σ_1 turns positive at the upper turning point, indicating instability along the middle branch. The third eigenvalue approaches σ_2 asymptotically along the middle branch.....	49
Figure 3.4 $Le=0.5$ $Pe=0.5$ $Ta=4.0$ $\phi=1.0$. When Le is decreased below a certain value, σ_3 crosses σ_2 . This behavior is not seen in the one-dimensional model. The Leading eigenvalue is not shown.....	50
Figure 3.5 Critical wave numbers for several different configurations. It is seen that 1) K_{crit} is not greatly affected by changes in Le or Pe and 2) The order of magnitude of K_{crit} is the same between the 1-D and 2-D models.....	51
Figure 3.6 $Le=1.1$ $Ta=4.0$ $Pe=0.0$ $\phi=1.0$. Stable oscillations exist on the upper branch while the entire middle branch is unstable. The regions within the circle represent eigenvalues along the middle branch.....	52
Figure 3.7 $Le=2.0$ $Pe=0.0$ $Ta=4.0$ $\phi=1.0$. The <u>upper</u> branch eigenvalues indicate regions of pure perturbation growth as well as oscillation growth leading to instability. The oscillations cease to exist when σ_3 becomes the leading eigenvalue.....	53
Figure 3.8 $Le=1.2$ $Ta=4.0$ $\phi=1.0$. The three leading eigenvalues for different Pe . Changes in Pe have only a small effect on the flame behavior which is consistent with $Le < 1$	54
Figure 4.1 Upstream extremum for H and location versus Le	85
Figure 4.2 $Le=2$, free stream.....	86
Figure 4.3 $Le=0.8$, free stream.....	87

Figure 4.4 $Le=1.0$, free stream.....	88
Figure 4.5 $Le=2$, T and Y profiles through reaction zone.....	89
Figure 4.6 $Le=0.8$, T and Y profiles through reaction zone.....	90
Figure 4.7 Free stream laminar flame speed as a function of Lewis number.....	91
Figure 4.8 $Le=1.0$ Reaction profile through annihilation.....	92
Figure 4.9 Reaction profile for $Le=2.0$ through annihilation.....	93
Figure 4.10 Reaction profiles for $Le=1.25$ through annihilation.....	94
Figure 4.11 Reaction profiles for $Le=0.8$ through annihilation.....	95
Figure 4.12 $Le=0.5$ reaction profiles during Flame propagation towards Junction.....	96
Figure 4.13 Temperature profiles for $Le=2.0$ through annihilation.....	97
Figure 4.14 Temperature profiles for $Le=0.8$ through annihilation.....	98
Figure 4.15 Annihilation time versus Lewis number.....	99
Figure 5.1 Model configuration and boundary conditions. The side and lower walls are porous to reactants. The vertical walls admit only diffusive fluxes. In the far field the diffusion flame is one-dimensional. The near field triple flame structure is shown, with (I) as the diffusion flame, (II) and (III) as rich and lean premixed flame arcs, and (IV) as the triple point or leading flame edge.....	128
Figure 5.2 Heat transfer model for infinitesimally thin flame sheet and isothermal boundary conditions. This model is the heat transfer simplification of the flame in figure 5.1 because by far the greatest heat release is along the diffusion flame arc.....	129
Figure 5.3 Model configuration of mixture fraction Z after conformal mapping. Note that the straight diffusion flame along $Z=Z_f$ occurs only in the case of zero convection. In addition, lines of constant Z are radially- directed arcs, $Z=\theta/\pi$	130
Figure 5.4 (a) Heat flux profiles comparison for straight flames $r_q=0.27$. Note the inaccuracy, generally, of the Burke-Schumann calculation of Equation(12.a,b) and the comparative similarity of the Finite-rate and Heat Transfer model results. A scaling factor renders the latter two visually	

indistinguishable. Heat flux comparisons for straight flame $r_q=0.9$. (b) Heat flux profiles comparisons for straight flames $r_q=0.9$. The comments to (a) apply here as well.....	131
Figure 5.5 (a) Heat flux profile comparisons for fuel lean flames $\phi=0.5$, $r_q=0.38$. For this non-symmetric case the flux distribution is asymmetric. The Burke-Schumann model is once again a poor approximation to the heat flux. (b) Heat flux profile comparisons for fuel rich flames $\phi=1.5$, $r_q=0.28$. See comments in figure 5.4a.....	132
Figure 5.6 Heat flux profile comparison for straight flame with convection $Pe=1, r_q=0.395$	134
Figure 5.7 Centerline temperature distributions for a straight flame $r_q=0.375$. The broadness of the actual flame moderates the temperature variation, compared with the sharp heat transfer profile. The τ values along the diffusion flame ($\eta>0.5$) agree to within $O(\beta^{-1})$	135
Figure 5.8 (a) Centerline temperature profile for a straight flame $r_q=0.525$. (b) Centerline temperature distribution for a straight flame $r_q=1.225$. For large quench distances the pure heat transfer temperature profile differs significantly from the finite-rate chemistry profile.....	136
Figure 5.9 Heat flux distribution for Methane/Oxygen combustion at various stoichiometries.....	137
Figure 5.10 Heat flux distribution for Methane/Oxygen combustion at various stoichiometries. The second reaction mechanism given in table 5.2 is used.....	138
Figure 5.11 Heat flux profile for Propane/oxygen configuration. Larger heat losses than Methane are predicted.....	139

INTRODUCTION

Let the reader be forewarned that the material herein does not consist, as is typically the case, of a thorough and complete analysis of a single problem. Rather, the topics, though comprising four chapters, are actually three non-related problems that can be considered as pertaining, either directly or indirectly, to the broad field of flame stability. Due to the inhomogeneity of this work, each chapter, save for perhaps the third for in truth it is an extension of the second, will be treated as a separate entity wherein pertinent literature will be discussed, results presented and conclusions drawn. Hence, this introduction shall serve only to provide the reader with a brief description of each problem and indications of its importance.

As noted above, the topics of flame stability are very broad. This is only to be expected given the complicated nature of the combustion processes. Instabilities can be caused by imbalances in thermal and mass diffusion (Chapters 2 and 3), concentrations of oxidizer or fuel that are insufficient to maintain steady burning, since combustion is a kinetically controlled process excessive heat losses can cause flame extinction (Chapter 5). Additionally, hydrodynamic concerns can cause flame instabilities. In turbulent flames large strain rates can effect flame behavior, flame front curvature (wrinkled flames) is dependant on not only the flow field but thermal-diffusive effects as well. Furthermore, the complex nature of turbulent flames show that flame fronts are often dynamic and interact leading to local flame front breakup and healing (Chapter 4). The above list of different types of instabilities is not complete but gives the reader an idea of the complicated behavior of reacting flow problems. It is due to the aforementioned complexity that any analysis seeking to understand the role of one particular element

must seek to systematically eliminate the effects of the others without ignoring the key characteristics of the problem that cause such instabilities to occur in the first place. In this spirit, each chapter consists of what may be termed a “minimalist model” in which it is believed only the barest terms are retained in order to facilitate examination of the phenomena in question. Such work, though not rigorously accurate, is simple enough that the conclusions drawn are not obfuscated by unneeded complexity.

In Chapter 2 a linear stability analysis is performed on a one-dimensional model of a diffusion flame in which the fuel is convected into the reaction zone while the oxidizer is diffused. Of particular interest is the effect on non-unity Lewis number (a ratio of thermal diffusion to mass diffusion) as well as the role of convection. The model produced allowed the examination of the eigenvalues for several parameters: Lewis number, Damkohler number (a ratio of characteristic flow time to a characteristic chemical reaction time), and the Peclet number (non-dimensional mass flux). Several types of instabilities were observed. The first consisted of pure flame extinction, the second involved regions of flame oscillations ($Le > 1$) that would either lead to extinction or dampen out to steady burning, and the third resulted in a cellular flame pattern ($Le \leq 1$).

The one-dimensional model can be considered a “classic” model having been examined extensively in the past using Activation Energy Asymptotics (AEA). The question that begs to be answered is, how well do one-dimensional models predict flame behavior? It is not expected that these simplified models will predict quantitative behavior but rather give an overview of flame characteristics. To begin to answer the above question a two-dimensional version of the model in Chapter 2 is examined. In this model the flame is examined in the presence of a cold, chemically inert wall. This

produces an “edge-flame” that better models real flame behavior. The linear stability analysis is carried out along similar lines as in Chapter 2. Such an analysis is very computationally costly but in the end offers reasonable support for the one-dimensional model.

Chapter 4 investigates the thermal-diffusive effects on laminar, premixed flame annihilation. Such a model can be thought of as representing the local flame interaction in turbulent flow fields. How these flames interact under different Lewis number conditions may offer some insight into how well turbulent flames can survive. The work in this chapter is a combination of theoretical approximations and numerical analysis, with the prior used as support for the latter.

The usefulness of one-dimensional models cannot be ignored. However, these models lack important features that real flames incorporate. Of particular interest is the interaction with a nearby surface. Such a feature was incorporated in Chapter 3 but was absent in Chapters 2 and 4. A two-dimensional model is presented in Chapter 5 in which a tri-brachial flame (“triple flame”) quenched a small distance above a “cold” wall. The model represents a slotted burner configuration in which the reactants are separated by an infinitely thin divider plate. Of particular interest is the conductive heat flux distribution along the cold adjacent boundary. By evaluating this heat flux profile, deductions can be made about the characteristic flame thickness; provide correlations that may be used in theoretical work; and when compared to experimental results, provide insight into which heat transfer mechanisms are important.

It is important to note, that although all the analysis performed in the above chapters has a theoretical bent, in all chapters some ties to existing experimental results

are made. In Chapter 2 (and subsequently Chapter 3) comparisons are made between predicted cellular flamelet sizes with cellular flames observed in micro-gravity drop tower flame spread experiments. The ties to turbulent flame stability are more anecdotal and compare only the observations made by several experimentalists about observed Lewis number effects on stability. The correlations obtained for the heat flux distribution are compared with two experiments burning methane gas. The maximum heat flux from the burner-attached flames is compared with the predicted values in Chapter 5.

A brief exposition on the numerical methods used to solve the various partial differential equations (PDEs) is provided in Chapter 6. The numerical work in this document does not represent in any way a novel approach to solving non-linear sets of PDEs. The description is included for sake of completeness.

ONE-DIMENSIONAL DIFFUSION FLAME STABILITY

2.1 Chapter Nomenclature

A – Pre-exponential factor for Arrhenius reaction rate, $k=A\exp(E/RT)$

A,B,C,E – Generic points along the “S” curve

D – Damkohler number, $D=Al\epsilon/(Y_{F_0} Y_{O_0})/\alpha$

E – Activation Energy

K – Wave number

Le – Lewis number

l – Half of separation distance between porous plates

m – Mass flux

Pe – Peclet number, $Pe=m\bar{l}/2\rho\alpha$

Q – Heat release

R – Ideal gas constant

T – Non-dimensional temperature, $T=\bar{T} (C_p Le)/QY_{O_0}$

t – Non-dimensional time

w - Non-dimensional reactivity = $Dy_O y_F \exp(-T_a/T)$

x,y - Non-dimensional spatial coordinates

Y – Species mass fraction

y - Non-dimensional species mass fraction, $y=Y_i/Y_{i_0}$

Z – Mixture fraction

Greek

β - Zeldovich number

ϕ - Global stoichiometric coefficient

ϕ - Generic scalar variable

λ - Wavelength

τ, δ, Γ - Arbitrary spatial function

Subscripts

a – Activation reference

c,crit – Critical value

F – Fuel

f – Flame

O – Oxidizer

o – Reference

max – Maximum

new – New

Superscripts

/ - Perturbation term

- - Steady state term

2.2 Introduction

In the study of diffusion flames the question of stability naturally arises when the words “ignition” and “quenching” are used. These are “near-limit” phenomena in the sense that either the temperature or the reactant concentrations (or both) can barely support combustion, making the transition to either a burning state for the former and a non-burning state for the latter a distinct possibility. These concepts can be broadened when other physical, geometric, and parametric influences are examined, such as nearby cold surfaces in the case of spreading flames over solid and liquid fuel, or multi-step

chemistry, or disparate Lewis numbers of the reactants, or radiant losses from the gas and from soot particulates near the flame. Before flame extinction concepts are broadened, however, the skeletal phenomenon should be understood in the clearest possible terms. The present article attempts to create such an understanding for a physically idealized model of diffusion flame stability.

In addition, a second goal is sought, namely a clear exposition of diffusion flame stability for pedagogical purposes. The authors believe this is absent in the literature. Our interest in diffusion flame stability lies in applications to flame spread. We found, however, that there was no complete exposition of the stability calculation for even the simplest model problems. The original study of Kirkby and Schmitz [1] comes closest to a full description but is hampered by the use of difficult terminology.

The mathematical analysis of the stability of partial differential equations has a long history. It has evolved in the last few decades into a theory based on the functional analysis of PDEs in terms of their eigenvalue spectra. The analysis of stability from a mathematical standpoint amounts to the examination of the eigenvalue spectrum of the linearized system of equations in relation to the original spectrum of the nonlinear system of equations. For infinitesimal disturbances the confluence of the two systems can be rigorously demonstrated, thereby rendering the analysis of the linearized problem mathematically representative of the original (nonlinear) problem.

The eigenvalue spectra can be examined in numerous ways. The study by Kim et al. [2] has, for the case $Le < 1$, postulated simplified forms of the conservation equations on either side of the flame sheet and then used asymptotic methods to derive “jump” conditions across the flame sheet with the goal of obtaining formulas for the dependence

of the eigenvalues on the parameters D , Le , and Pe . Extending this work with asymptotics, Kim [3] included higher order terms in the expansion of the inner zone solution in a more thorough examination of effects of non-unity Lewis number. The subsequent work of Kim et al. [4] employs no asymptotic methods in $Le > 1$ studies of diffusion flame stability. With regard to the latter work, which demonstrates a more complicated response¹ than the $Le < 1$ case, stability is examined by integrating the conservation equations numerically. Transient evolution of a monotonically growing solution indicates instability.

The overall nature of the spectrum of the eigenvalues for the diffusion flame can be understood both in a “physical” way and from experimental observations. Consequent to Linan’s analysis of diffusion flame structure [5], Peters [6] determined by physical arguments that the middle branch instability must be a “fast time” instability. The “fast time” stability discussion is the result of a simple scaling analysis: if the reaction sheet is thin, of order $[\text{activation energy}]^{-1}$, then in order to retain the transient term in the diffusion equation the temporal scale factor must be of order $[\text{activation energy}]^{-1}$ times smaller than the spatial scale. Laboratory observations have also produced a physical understanding of the nature and types of instabilities (cellular, oscillatory, etc.). Among these experimental works are ref. [7,8], which deal with flame instability in many configurations. In addition, many spectacular photographs can be found of ceiling flame instabilities, see especially reference [9].

Our analysis will demonstrate that the eigenvalue spectrum is vitally important, especially for the case $Le > 1$ examined recently by Matalon and Cheatham [10] and Kim

¹ The case for $Le < 1$ is less complicated in that no upper branch instabilities are seen and the middle branch is unstable. Furthermore, no oscillations are present for this case as are seen when $Le > 1$.

et al [4]. We shall demonstrate that the tracking of the leading eigenvalue is insufficient for understanding the instability process. The behavior of the second and third eigenvalues often signals imminent transitional behavior.

2.3 Model

The proposed model is a one-dimensional version of the film-diffusion flame examined by Kim et al. [2]. There, the authors were interested in the formation of striped, instability patterns in a one-dimensional flame sheet. A minimum of two spatial dimensions was required to describe the pattern of instability: one coordinate lay along the flame sheet, while the other lay perpendicular to the flame sheet. The coordinate along the flame sheet described the striping pattern. The fragmented flame sheets have been called “flame tubes” [11]. In this study, we are interested in the fundamental mathematical description of the instability mechanism. This does not require the formation of different sorts of flame patterns. For this reason, following Kirkby and Schmitz [1], we retain as little detail as required in order to produce a mathematical description of diffusion flame stability. The in-flame coordinate is thus deemed inessential for the stability analysis.

The proposed one-dimensional model consists of flowing fuel and diffusing oxidizer species on opposite sides of the reaction sheet. Radiative heat losses have been ignored, as have both Soret and Dufour diffusion. The flow is assumed uniform. The chemistry is modeled with a single-step, irreversible, Arrhenius reaction. Figure 2.1 shows a schematic of the one-dimensional model that has been used in previous stability analyses by Kim and colleagues [2,4] and Matalon and co-workers [10,12]. The latter investigators also describe a realistic physical configuration from which this model could,

in principle, be realized in a laboratory experiment. The problem formulation proceeds along similar lines as that of [2], producing the following set of non-dimensional equations.

$$\frac{\partial T}{\partial t} + Pe \frac{\partial T}{\partial x} = \frac{\partial^2 T}{\partial x^2} + w \quad (2.1.a)$$

$$Le \frac{\partial y_i}{\partial t} + PeLe \frac{\partial y_i}{\partial x} = \frac{\partial^2 y_i}{\partial x^2} - w, \quad i=O,F. \quad (2.1.b)$$

The equations are coupled through the non-linear reaction term, $w = Dy_O y_F \exp(-T_a/T)$. A single Lewis number is employed for both reactants. All terms in Eqs. (2.1) are defined in the Nomenclature.

The boundary conditions for Eqs. (2.1) are

$$T=T_o, y_F=1, y_O=0, \text{ at } x = -1 \text{ and } T=T_o, y_F=0, y_O=1, \text{ at } x = +1. \quad (2.2)$$

In this article we assume, for simplicity, that the fuel and oxidizer inflow temperatures are both equal to a reference temperature, T_o . The symmetry of Eqs.(2.1) and the boundary conditions implies that y_O and y_F are interchangeable; hence, from a stability perspective, this formulation describes both blowing fuel and blowing oxidizer.

The configuration of figure 2.1 is a generic, simplified version of many combustion problems. These include droplet combustion (blowing fuel from the droplet, inward oxygen diffusion form the ambient), spray flames, jet flames, flame spread, and diffusion flames in channels, among others. More complicated configurations require additional geometry dependent terms; and more complicated model formulations may require the inclusion of buoyancy or variable properties or pressure variations, or even

magnetic fields; but the qualitative nature of the solutions generated herein shall be representative, as a model, for all of these configurations.

2.4 Steady State Solutions

2.4.1 Analytical Burke-Schumann Solutions

The character of the steady-state solution provides insight into the influences of disturbances on the flame's ultimate stability or instability. For clarification of subsequent discussions, we present the steady Burke-Schumann solutions and briefly describe their structure. The solution for the mixture fraction is

$$Z = [\exp(\text{LePe}(1+x)) - 1] / [\exp(2\text{LePe}) - 1] \cong \frac{(1+x)}{2} [1 - \text{LePe}(1-x)/2 + O(\text{LePe})^2]. \quad (2.3)$$

When $\text{Pe}=0$, we have $Z=(1+x)/2$. It is relatively straightforward to show that when Pe is non-zero, Z is smaller everywhere (except at $x=\pm 1$) than the $\text{Pe}=0$ Z -distribution, i.e., $Z_{\text{Pe}>0} < Z_{\text{Pe}=0}$. The flame is shifted to the right by the blowing fuel, and this shift increases as Pe increases. We will not examine the large Pe case in this article.

At the flame sheet $Z=1/2=Z_f=[\exp(\text{LePe}(1+x_f)-1)/[\exp(2\text{LePe})-1]$, which can be solved to give $x_f=\ln[\cosh(\text{LePe})]$ for the flame sheet location. Burke-Schumann solutions for oxidizer, fuel, and temperature distributions are obtained by solving Eqs.(2.1) with w replaced with a delta function:

Oxidizer side ($-1 < x < x_f$):

$$Y_O=0 \quad (2.4.a)$$

$$Y_F = 1 - \frac{\exp(\text{LePe}(x/2)) \sinh(\text{LePe}(1+x)/2)}{\exp(\text{LePe}(x_f/2)) \sinh(\text{LePe}(1+x_f)/2)} \quad (2.4.b)$$

$$T - T_o = (T_f - T_o) \frac{\exp(\text{Pe}(x/2)) \sinh(\text{Pe}(1+x)/2)}{\exp(\text{Pe}(x_f/2)) \sinh(\text{Pe}(1+x_f)/2)} \quad (2.4.c)$$

Fuel side ($x_f < x < 1$):

$$Y_o = 1 - \frac{\exp(\text{LePe}(x/2)) \sinh(\text{LePe}(1-x)/2)}{\exp(\text{LePe}(x_f/2)) \sinh(\text{LePe}(1-x_f)/2)} \quad (2.4.d)$$

$$Y_F = 0 \quad (2.4.e)$$

$$T - T_o = (T_f - T_o) \frac{\exp(\text{Pe}(x/2)) \sinh(\text{Pe}(1-x)/2)}{\exp(\text{Pe}(x_f/2)) \sinh(\text{Pe}(1-x_f)/2)} \quad (2.4.f)$$

These distributions are applicable in the regions on either side away from the flame location. From these distributions it is possible to deduce some important facts (see [2]). First, the outer-zone formula for T_f produces a Le -dependence in which T_f increases as Le decreases and T_f decreases as Le increases. The roughly Le^{-1} dependence of T_f is well known and has been exploited in more detailed formulations of the non-dimensional combustion equations [2]. Second, the general shape of the profiles in response to the flow is ascertained, as is the response of the flame position to the fuel inflow.

2.4.2 Numerical Solutions

The steady state Eqs.(2.1.a,b) can be solved numerically by standard methods. The numerical solution produces the characteristic “S” curve which plots T_{\max} vs D , where T_{\max} is the maximum temperature in the domain. This “S” curve, to the knowledge of the authors, was first produced and thoroughly examined by Fendell [13]. The top branch of the curve corresponds to steady burning (under most *but not all* conditions), the middle branch is unstable; and the lower branch is known as the ignition branch, see Figure 2.2. The real “S” curve does not look like an actual S since the lower turn occurs at a value of D that is usually many orders of magnitude larger than its value at the upper turn. A representation of the upper turning point for $\text{Le}=1$, $\text{Pe}=0$, $T_a=4$ and $\phi=1$ is shown in Figure 2.3. At the lower turning point the Arrhenius exponential is $O(\exp(-E/RT_o))$

whereas at the upper turning point the Arrhenius exponential is $O(\exp(-E/RT_f))$. The “separation” in D between these two turning points is thus $O(\exp(E/R)(1/T_o-1/T_f))$, at least in the lowest approximation (i.e., without accounting for differences in reactant mass fractions at the two turning points). An analysis of the “S” curve using large activation energy asymptotics was carried out by Linan [5]. Combustion regimes in the various parts of the “S” curve were elucidated and canonical lowest order equations describing the mathematical character of each region were produced with accuracy that improved as the “Zeldovich number”, β , increased. The expansions, which proceed for both inner (flame zone) and outer (chemical equilibrium zones) in inverse powers of β , can be continued, at least in principle, indefinitely. Inner and outer solutions are matched in the characteristic fashion outlined in [14]. The expansions in β^{-1} are valid everywhere along the “S” curve but the relative accuracy of the solutions diminishes near the turning point where additional (higher-order) series terms are needed to maintain accuracy. The leakage of reactants was shown to be a cause of the transition from vigorous to non-vigorous burning. Numerous features of this S curve have been clarified since the work of Linan [5], but the fundamental distinctions made therein (and in the original work of Fendell[13]) remain valid. Though some aspects of the preceding description, such as the use of one-step chemistry, or the predominant leakage of the “wrong” reactant, etc. [15] are unsuitable for a more comprehensive approach, the appeal of the “S” curve remains strong. Discussions of diffusion flame stability are referred almost exclusively to “S” curve solutions [2,4,10]. Extending or broadening them to more realistic flame processes, geometries, and parametric ranges is desirable.

2.5 Stability Analysis

Equations (2.1.a,b) form a set of coupled semi-linear parabolic equations [16,17]. Hence the evolution of small disturbances is governed by linearized forms of these equations. These linearized equations are derived by writing the solution of each dependent variable as a combination of a steady solution and a perturbation

$$\phi(x, t) = \bar{\phi}(x) + \phi'(x, t), \quad (2.5)$$

where ϕ can be T , y_O , or y_F . Substituting Eq. (2.5) into Eq. (2.1) and retaining only the terms that are linear in ϕ' in the Taylor series expansion of w yields the following linear system:

$$\frac{\partial T'}{\partial t} + Pe \frac{\partial T'}{\partial x} = \frac{\partial^2 T'}{\partial x^2} + w', \quad (2.6.a)$$

$$Le \frac{\partial y'_i}{\partial t} + PeLe \frac{\partial y'_i}{\partial x} = \frac{\partial^2 y'_i}{\partial x^2} - w', \quad i=O,F, \quad (2.6.b)$$

$$w' = D \left[\bar{y}_O \bar{y}_F \left(\frac{T_a}{T^2} T' \right) + \bar{y}_O y'_F + y'_O \bar{y}_F \right] \times \exp \left(-\frac{T_a}{T} \right), \quad (2.6.c)$$

which is solved subject to the following boundary conditions (no disturbances at the boundaries):

$$T'(\pm 1, t) = y'_F(\pm 1, t) = y'_O(\pm 1, t) = 0. \quad (2.6.d)$$

Since the spatial part is a linear operator with compact resolvent [17], the evolution of small disturbances is determined by the eigenvalues of Eqs.(2.6.a-d). The eigenvalues are the complex numbers, σ , for which Eqs.(2.6) possess a nontrivial solution in the form

$$T'(x, t) = \tau(x) \exp(\sigma t) \quad (2.7.a)$$

$$y'_O(x, t) = \delta(x) \exp(\sigma t) \quad (2.7.b)$$

$$y'_F(x, t) = \Gamma(x) \exp(\sigma t). \quad (2.7.c)$$

If all eigenvalues have negative real parts, then all solutions of the nonlinear Eqs. (1) that originate as small disturbances of the steady state solution will decay exponentially to the steady solution [16,17]. In this case the steady state solution is said to be stable. On the other hand, if any of the eigenvalues has a positive real part then the steady state solution is unstable, meaning that there exists a threshold disturbance size such that some arbitrarily small initial disturbances of the steady state solution will evolve according to the nonlinear Eqs.(2.1.a,b) to grow eventually past the threshold [16,17].

With fixed parameters the steady state solution was found first, using Mathematica's NDSolve in the shooting algorithm for the boundary value problem. Error controls in the software enable the successive elimination of subsequent higher order error terms; the steady solution is for all practical purposes exact. In other words, the errors can be made as small as desired because it is known that the computed errors depend quadratically on grid size. Three different meshes were used (80, 160, 320 grid points) to reduce the computational errors.

This steady solution was used in Eqs.(2.6.a-d) along with Eqs.(2.7.a-c) for the disturbance quantities. The resulting disturbance equations are given below as equations 2.8.a.d.

$$\tau\sigma + Pe \frac{\partial \tau}{\partial x} = \frac{\partial^2 \tau}{\partial x^2} + w', \quad (2.8.a)$$

$$Le\delta\sigma + PeLe \frac{\partial \delta}{\partial x} = \frac{\partial^2 \delta}{\partial x^2} - w', \quad (2.8.b)$$

$$Le\Gamma\sigma + PeLe \frac{\partial \Gamma}{\partial x} = \frac{\partial^2 \Gamma}{\partial x^2} - w', \quad (2.8.c)$$

$$w' = D \left[\bar{y}_O \bar{y}_F \left(\frac{T_a}{T} \tau \right) + \bar{y}_O \Gamma + \delta \bar{y}_F \right] \times \exp \left(- \frac{T_a}{T} \right). \quad (2.8.d)$$

The equations were then discretized using a second order central difference scheme. The resulting matrix eigenvalue problem was also solved by using Mathematica. The computational errors of the eigenvalue also depend quadratically on the mesh size, hence we were able to reduce eigenvalue errors below a specified tolerance. For example, when $Pe = 0.5$, $Le = 0.9$, $To = 0.05$, $Ta = 5$, and $D = 21190000$ we found that the leading eigenvalue on the middle branch was equal to 0.1612, and on the upper branch it was equal to -0.1522 . Many spot checks were made by using different numerical methods. In particular, a Fortran based finite difference scheme was used (with no error controls) with 300 nodes to produce the steady solution, and the eigenvalues were calculated using standard Lapack subroutines.

The stability in the neighborhood of the upper turn, point A on figure 2.2, on the “S” curve has been investigated for a large set of parameters:

$$0 \leq Pe \leq 1, 0.1 \leq Le \leq 4, 1.5 \leq Ta \leq 6.5, 0.02 \leq To \leq 0.05.$$

A brief description of the findings appears below. In later sections lengthier discussions of their physical significance are presented. For larger values of Pe the eigenvalue behavior is more complicated; however, and more detailed analysis is needed before concrete generalizations are made.

Identifying the Le effect on the eigenvalue behavior is essential in understanding the various regimes of flame behavior. When $Le \leq 1$, the leading eigenvalue is negative on the upper branch, implying stability, and positive along the middle branch, implying instability. The leading eigenvalue is equal to zero at the turn, point A (see figures 2.3 and 2.6). When $Le = 1$ a linear combination of Eqs.(2.1) commonly called the Schvab-

Zeldovich procedure produces two stable linear, homogeneous heat equations with a convection term, and a nonlinear equation. The two heat equations are responsible for an eigenvalue of multiplicity two that does not change with D (see figure 2.4 curve denoted “ σ_2 ”). This constant eigenvalue is given by

$$-(\pi/2)^2/Le - (Pe/2)^2/Le. \quad (2.9)$$

This result is obtained for $y_O - y_F$ derived from Eq.(2.6.b) which is a linear heat equation with a convective term, and can be solved explicitly. When $Le=1$, the solution has multiplicity two because $2T + y_O + y_F$ satisfies the same equation. The remaining nonlinear equation produces the eigenvalue denoted “ σ_1 ” in figure 2.4. This eigenvalue is always positive on the middle branch, indicating instability as stated above. (Note that in all the figures pertaining to eigenvalue distributions, the dotted line indicates a position along the upper branch.) It is the character of the remaining two eigenvalues on this middle branch, however, that changes as Le is varied; the nature of this change dictates the stability of points along the sector ABC of the “S” curve of Figure 2.2.

When Le is slightly larger than unity, the eigenvalue that has multiplicity 2 when $Le = 1$ splits into 2 eigenvalues. One, σ_3 , is still given by Eq. (2.9) and the other one, σ_2 , interacts with σ_1 as shown on Figure 2.5. σ_1 and σ_2 are negative real numbers between the turning point A and point B on the upper branch (see figure 2.2). At point B they merge to form a complex conjugate pair with negative real parts (indicating decaying oscillations) until point E where they again split. At point C, σ_3 becomes the leading eigenvalue. As Le approaches unity the region between B and E shrinks to point C where σ_1 meets σ_2 on figure 2.4. As Le increases the value of σ_1 at B increases, B approaches A, and B reaches A at some critical value $Le_c > 1$.

When Le increases past the critical value Le_c , point B moves into the region of positive eigenvalues, $\text{Re}(\sigma) > 0$, and the characteristic behavior in region ABC of Figure 2.2 is changed completely (see figure 2.6). Notice that figure 2.6 ($Le > Le_c$) is qualitatively the same as figure 2.5 ($Le < Le_c$) with the point E (not shown) moving rapidly towards higher D as Le is increased. When $Le > Le_c$, the region between points A and B on the upper branch has eigenvalues that are real and positive, indicating that perturbation growth will occur and lead to flame extinction. Between B and C the two leading eigenvalues form a complex conjugate pair, whose real part is positive at B and decreases as D increases. The real parts become zero at a point C' between B and C indicating damped oscillations until point C (not shown) where the leading eigenvalue (σ_3) is independent of D.

On the other hand when Le is decreased *below unity*, σ_3 moves *under* the constant eigenvalue as shown in figure 2.7. The constant eigenvalue is still given by Eq. (2.9). Notice that along the upper branch all the eigenvalues are negative, while along the middle branch σ_1 is positive and $\sigma_{2,3}$ are negative. Thus, for $Le < 1$ the upper branch is stable and the middle branch is unstable. The remaining constant eigenvalue disappears in the case $Le_O \neq Le_F \neq 1$.

It has been shown that the system behavior changes when Le is increased passed unity. Damped oscillations appear when $1 < Le < Le_c$, but the entire upper branch remains stable. The beginning of the upper branch is unstable when $Le > Le_c$.

2.5.1 Cellular Flames

“Cellular flames” have been observed in both freely propagating premixed flames [18], burner attached diffusion flames [19,20], and micro-gravity flame spread. All these

systems are fairly complex, involving multidimensional processes that generally include flame-surface interactions. The qualitative nature of the cellular flame instability can be described by examination of the proposed one-dimensional problem.

In order to allow for spatial variation along a plane of unit depth, the $\partial^2/\partial x^2$ operator in Eqs.(1.a,b) needs to be replaced with the Laplacian $\partial^2/\partial x^2 + \partial^2/\partial y^2$ and perturbations take the form $\phi'(x, y, t) = f(x)\exp(\sigma t + iKy)$ in place of Eqs.(2.7.a-c). Here, K is a non-dimensional wave number in the new coordinate direction, y , which lies in the plane ((y, z) plane, where z is the unit-depth coordinate) of the flame sheet. This coordinate dependence will show the development of undulations in the flame, whereas the one-dimensional formulation merely produced fluctuations about the mean flame position, x_f . When $Le = 1$, the new eigenvalues, σ_{new} , are simply equal to the old eigenvalues σ shifted by K^2 , i.e. $\sigma_{new} = \sigma - K^2$. When $Le \neq 1$, the relation between σ_{new} and σ is far more complex but qualitatively identical. In particular, the introduction of K has a stabilizing influence on the flame. Two conditions need to be met in order to see the flame stripes in the y -coordinate plane. First, the boundary control requires that K be a multiple of $2\pi/L$ where L is the dimensionless length (y -coordinate) of the burner. If, for example, the ratio between the length and the width of the burner is 10, then K can take values 0.31, 0.63, ... Second, the new leading eigenvalue has to be very close to zero to ensure the temporal changes of the flame structure do not rapidly vary and destroy the striped flame pattern. The first condition, pertaining more to experimental aspects, will be ignored in the rest of the discussion. For each unstable steady state solution near point A on the "S" curve a K value is computed, called K_{crit} , such that the new leading eigenvalue on the middle branch is identically zero. When $0 < Le < Le_c$ on the middle branch away

from the upper turn on the “S” curve, K_{crit} gradually increases from zero at point A as D is increased. When $Le > Le_c$, the leading eigenvalue is positive near the turn A; and, hence, a finite K , sufficiently greater than zero, is needed to stabilize the unstable steady solution, see figure 2.8. Therefore, it is clear from figure 2.8 that cellular flames will be more easily witnessed for conditions satisfying $Le < Le_c$.

Of particular interest is how thermal-diffusive effects contribute to the determination of cellular flame size. Additionally, the convection of fuel as described by Pe is examined to identify the hydrodynamic effects. Thermal-diffusive effects are examined by varying the Lewis number and holding Pe constant at 0.5. The results for this numerical experiment are illustrated in figure 2.8. It is apparent that the influences of varying Le are relatively small. The critical K values are only moderately changed between the cases $Le = 0.9$ and $Le = 0.3$. This suggests that thermal-diffusive effects play only a minor role in determining flame cell size. The distance, measured in D , away from the instability point A is the main determinant of the size of the flame cells

In order to determine the effects of fuel flow on the cellular flame size several different values of Pe were examined. The range of Pe was varied between zero and 0.75, and Le was set equal to unity so that the diffusion term and the convective term were approximately of the same order of magnitude. In this range of Pe , the “S” curves retain their characteristics and are simply shifted towards higher D ranges. Figure 2.9 shows the K_{crit} values for the three different flow rates, $Pe=0$, 0.5, and 0.75. There is little difference between the K_{crit} values for a zero convection diffusion flame ($Pe = 0$) and one for which convection is appreciable, i.e., $Pe=0.75$. This leads to the conclusion that for order-unity fuel crossflow the size of the cellular flames is little affected.

2.5.1a Experimental Results

Calculating the wavelength in the direction normal to flame is difficult because no physical length scale exists. There is, however, a diffusion length scale that appears in the Damkohler number. This length is used in making comparisons with experimental observations. Furthermore, as noted above, a smaller wave number does not necessarily mean a larger wavelength, as can be seen in equations (2.10-2.11). The following relationships were used to calculate a wavelength based on a diffusion length scale.

$$L = \left(\frac{4D\alpha}{Y_{OO}LeA} \right)^{\frac{1}{2}} \quad (2.10)$$

$$\lambda = \frac{L}{K} \quad (2.11)$$

Here D is the Damkohler number, α is the thermal diffusivity, Y_{OO} is the mass fraction of oxygen in the oxidizer stream, A is the Arrhenius pre-exponential factor, and λ is the disturbance wavelength. For comparisons with experimental results, where a thin cellulose sheet was burned, the parameters for A and α were approximated by using propane as the fuel. The values for K and Da were taken very near the turning point, i.e., $(D-D_{\text{tum}}) \sim 1000$, where D_{tum} was found to be $1.7984e7$ for the case where $Le=1$. It is noted that in this region, near the stable limit, all the curves from figure 2.9 seem to be in very good agreement. Based on these numbers, the estimated flamelet wavelength was found to be on the order of four centimeters. This result is compared with experiments that show the size of the flame pockets to be on the order of several centimeters. Figure 2.10 illustrates a sinusoidal waveform prior to breakup with the characteristic wavelength shown. The distance between the peaks is 3.5 cm. Similarly, Figure 2.11 shows several

flame pockets after breakup. It is clear from this photograph that not all the flame pockets behave identically. In this instance the flamelet size varies by a large percentage, but the relative order of magnitude is still several centimeters. These results show that the simplified one-dimensional model was capable of predicting the order of magnitude of the size of the flame pockets.

2.5.2 Oscillatory behavior ($Le > Le_c$)

Oscillatory behavior in flames has been observed in microgravity candle experiments aboard the Mir space station, as well as during droplet burning experiments [21]. Several numerical investigations have examined oscillatory flames [4,10]. The qualitative nature of this phenomenon can also be described with a linear stability analysis of a one-dimensional diffusion flame.

When $Le > Le_c$, the leading eigenvalues form a complex conjugate pair beyond the point B on the upper curve (see figure 2.2 and 2.5). The real part is positive at B and decreases as D increases. At point C' the real part reduces to zero although the imaginary part is non-zero. So, between point C' and C on the upper curve, small perturbations will result in damped oscillations. Between B and C', small perturbations will oscillate with growing amplitude leading to flame extinction. A stable periodic orbit was not found numerically near point C'. Near C', long lasting oscillations are expected with circular frequency equal to the imaginary part of the leading eigenvalue pair.

The oscillatory behavior predicted by the linear stability analysis was supported by solving Eqs.(2.1.a,b) directly using a second order correct finite-difference method. In doing so, a graphical representation of the transient nature of the flame was achieved as well as a search for possible steady oscillatory behavior. The results in Figure 2.12

represent transient solutions for two points along the upper branch. The unstable solution is representative of a D value below point C' ($D_C=1.961E+6$), while the stable solution is for a D larger than that at point C' . The numerical investigation of the oscillatory behavior is similar to that performed by Kim et al. [4]. Although the method is able to identify all the characteristics of this simplified problem that have been identified by the preceding stability analysis, it is time consuming and does not allow Le_c to be readily evaluated.

2.6 Discussion and Conclusions

The mathematical examination of Eqs.(2.1.a,b) and the linearized small perturbation Eqs.(2.6.a-d) in terms of the first three eigenvalues leads to a clear picture of the overall phenomenon. The principal virtue of the model considered here is its simplicity and the absence in it of complications that might difficulties of interpretation. It has been stated that convection is “essential” for instabilities to occur in the configuration of Figure 2.1 [2]. Our examination produces results for $Pe=0$ that are qualitatively identical with those for $Pe\neq 0$. It appears that a nonzero value of Pe does not alter the nature of the stability calculation, even though complications enter as Pe becomes large. The stability results for $Le < Le_c$ were qualitatively simple, as the results of section 2.5.1 demonstrate. The situation for $Le > Le_c$, however, was more complicated. Here, several possibilities existed, whose realization depended primarily on the movement of the locus of the first two eigenvalues as a function of D and Le . Since a complex conjugate pair is formed on the upper branch after point B , oscillatory behavior there is the norm. Between A and B there are no oscillations. The critical value Le_c is the value of $Le > 1$ for which point B is located at the turning point A of Figure 2.2.

It is possible that asymptotic analyses can provide approximate formulas for the information obtained here by numerical methods of eigenvalue computation. The asymptotic calculations, however, are tedious and lengthy (see e.g. [2] for the $Le < 1$ case), and provide results in terms of parameters that are, in practice, difficult to calculate. An example of a difficult parameter to calculate is the Damkohler number derivative [2]. The calculation of the first few eigenvalues as outlined here, however, in complete accord with the mathematical theory of systems of equations [16,17]. The eigenvalue computation provides an immediate and complete assessment of the diffusion flame response, not only in the vicinity of specially chosen points of analysis (such as A) but everywhere along the entire “S” curve.

The Nyquist-plot analysis of Kirkby and Schmitz [1] also provides mathematically rigorous results. Nevertheless, considerably greater effort is required to interpret and employ the results presented therein. The difference between this work and that of Kirkby and Schmitz [1] is not mathematical rigor but ease of interpretability and consistency with the function-theoretic analysis of partial differential equations.

For the reasons given in the previous two paragraphs, we believe that our examination provides a comprehensive and readily understood description of diffusion flame instability. Additional analysis of the eigenvalue spectrum is suggested by the present analysis for the case of large Pe (where the behavior of the eigenvalues gets more complicated) and when the values of Le differ for the two reactants. The permutations in the latter case are numerous, as there is a blowing reactant and a diffusing reactant; Le for both reactants may be small, large, one large the other small; and so on. In addition, the behavior of the solution on the upper branch for $Le > Le_c$ near point B may warrant

theoretical analysis because a bifurcation exists there (real parts of two complex conjugate eigenvalues cross from positive to negative values in the direction of increasing D).

2.7 References

1. L.L. Kirkby and R.A. Schmitz *Combustion and Flame* **10** 205-219 (1966)
2. J.S. Kim, F.A. Williams, and P.D. Ronney *Journal of Fluid Mechanics*. **327** 273-301(1996)
3. J.S. Kim *Combustion Theory and Modelling* **1** 13-40(1997)
4. C. H. Sohn, et Al. *Combustion and Flame* **117** 404-412(1999)
5. A. Linan *Acta Astronautica* **1** 1007-1039(1974)
6. N. Peters *Combustion and Flame* **33** 315-318 (1978)
7. Y. Zhang et al. *Combustion and Flame* **90** 71-83 (1992)
8. R.H. Chen, G.B. Mitchell, P.D. Ronney *Twenty-fourth Symposium (International) on Combustion* 213-221 (1992)
9. M. Kokkala *VTT Tutkimuksia* **586** (1989)
10. S. Cheatham and M. Matalon *Twenty-sixth Symposium (International) on Combustion* 1063-1070 (1996)
11. J. Liu, P.D. Ronney *Combustion Science and Technology* **144** 21-45 (1999)
12. M., Matalon *37th AIAA Aerospace Sciences Meeting, AIAA 99-0584 (Reno, NV)* (1999)
13. F.E. Fendell *Journal of Fluid Mechanics* **21** 281-303 (1965)
14. J. Cole *Perturbation Methods in Applied Mathematics*, Blaisdell Publishing(1968)

15. A. Linan, and F. A., Williams Fundamental Aspects of Combustion, Oxford University Press (1993)
16. D. Henry Geometric Theory of Semilinear Parabolic Equations, Lecture Notes in Mathematics, No. 840, Springer-Verlag (1981)
17. M Miklavcic Applied Functional Analysis and Partial Differential Equations, World Scientific (1998)
18. C. M. Dunskey *Twenty-fourth Symposium (International) on Combustion* 177-187 (1992)
19. Class et. Al *SIAM Journal of Applied Mathematics* **59** n.3 942-964 (1999)
20. R. Kuske and B.J. Matkowsky *Quarterly of Applied Mathematics* **52** n.4 665-88 (1994)
21. S.L. Olson Buoyant Low Stretch Stagnation Point Diffusion Flames over a Solid Fuel, Ph.D. Dissertation, CWRU (1997)

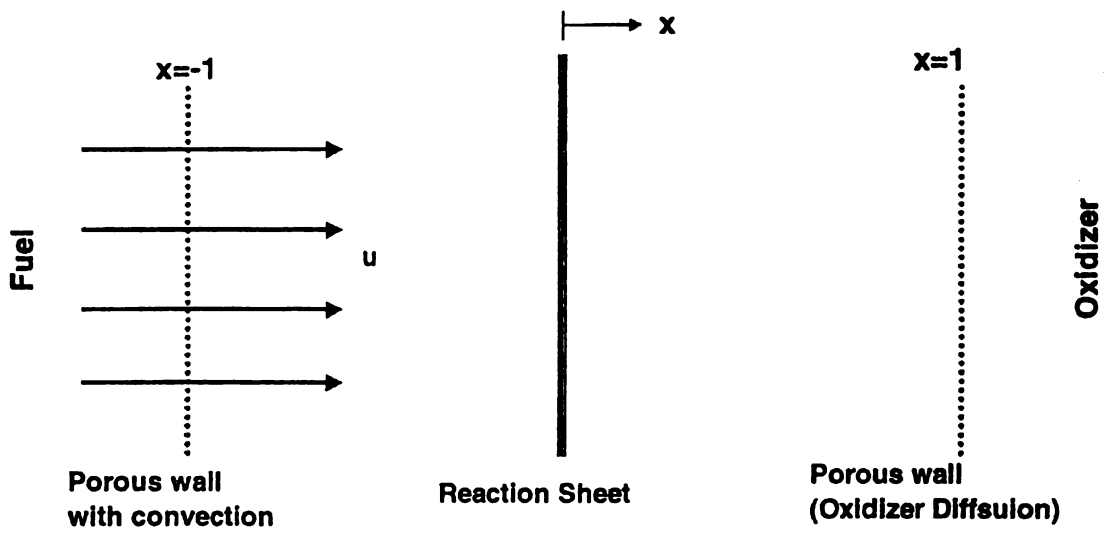


Figure 2.1 Schematic Diagram of convective film diffusion flame

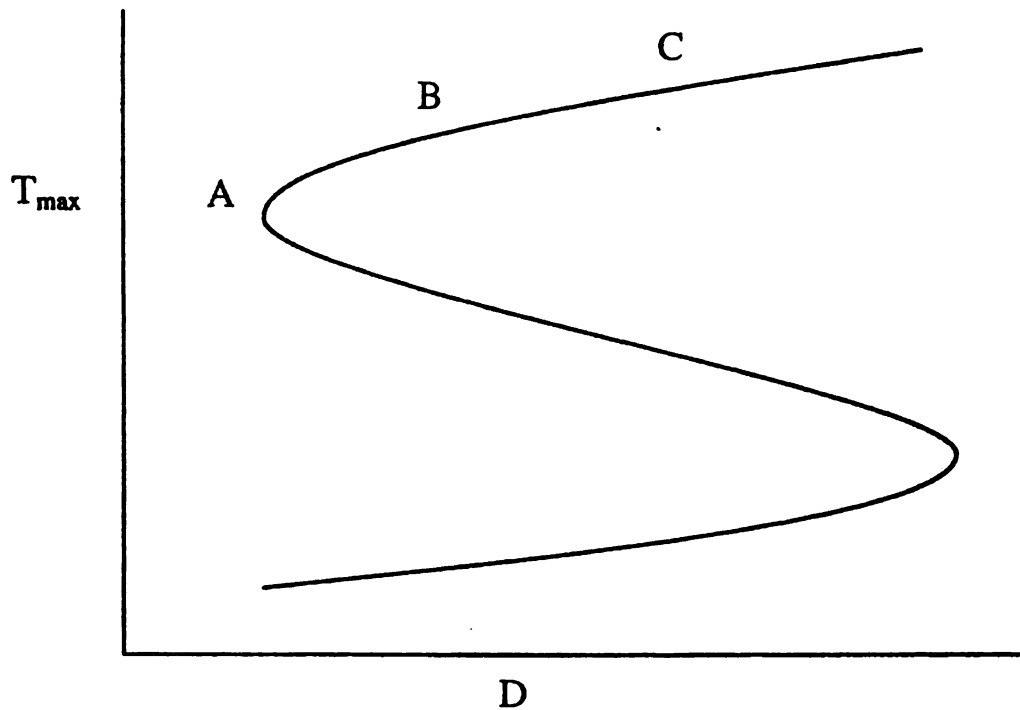


Figure 2.2 Qualitative plot of 1-D non-premixed flame Temperature vs Damkohler number. Three distinct branches are traditionally represented. The upper branch (above A) represents steady burning, the middle branch is unstable, and the lower branch corresponds to the ignition branch. In actual plots the lower turn appears at values of D many orders of magnitude higher than D at the upper turn.

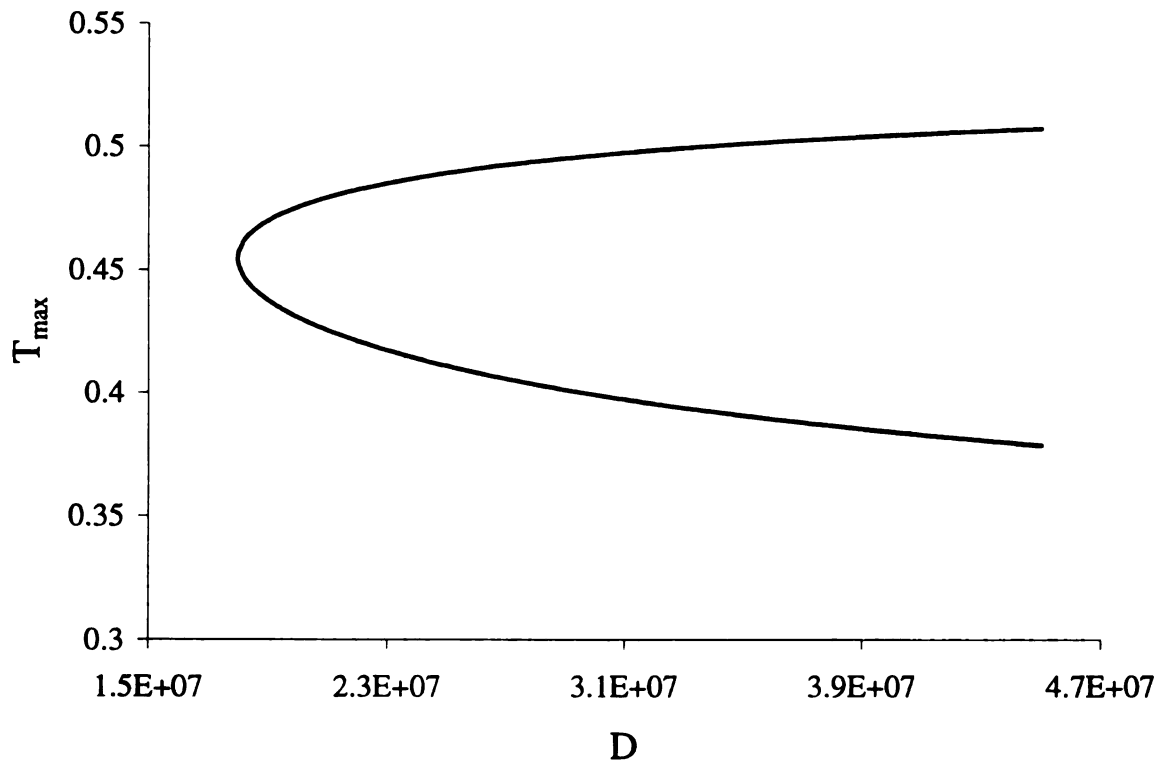


Figure 2.3. The response curve in the vicinity of the upper turning point. Here $Le=1.0$, $Pe=0.0$, $Ta=4$, $\phi=1.0$.

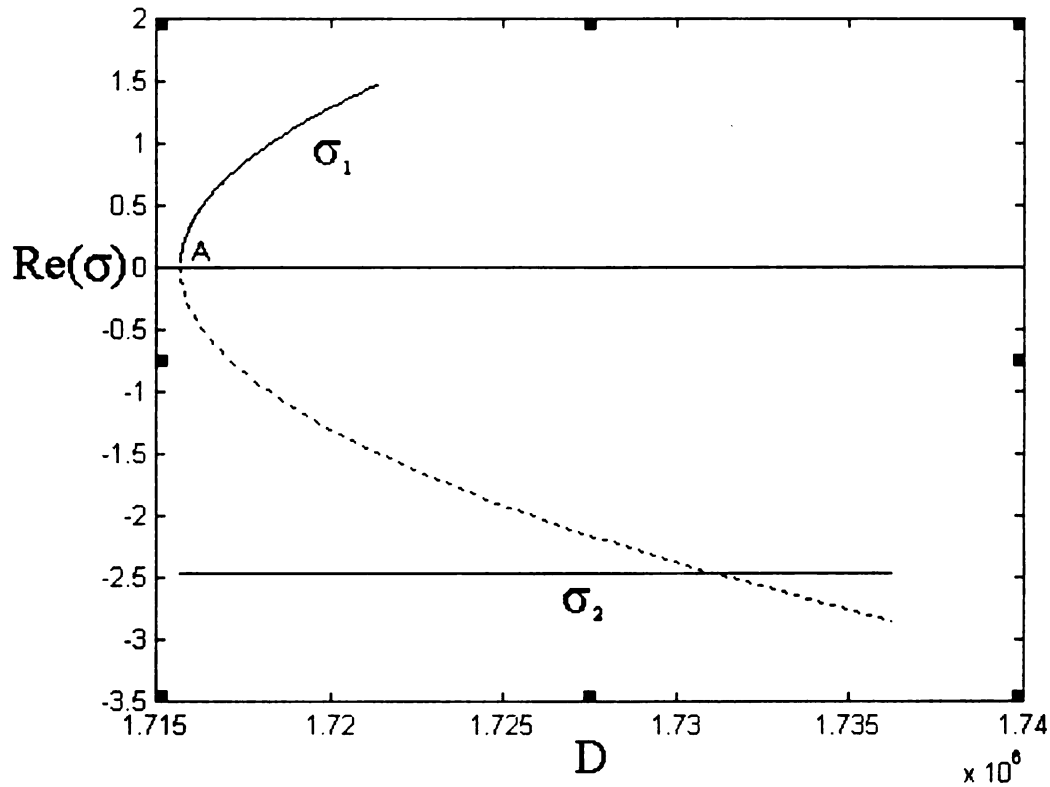


Figure 2.4 Leading two eigenvalues for the case of $Pe=0$, $Le=1$, $Ta=4.0$, $To=0.05$. Here σ_2 has multiplicity 2 and is independent of D . Note that σ_1 is positive on the middle branch and negative on the upper branch (dotted curve).

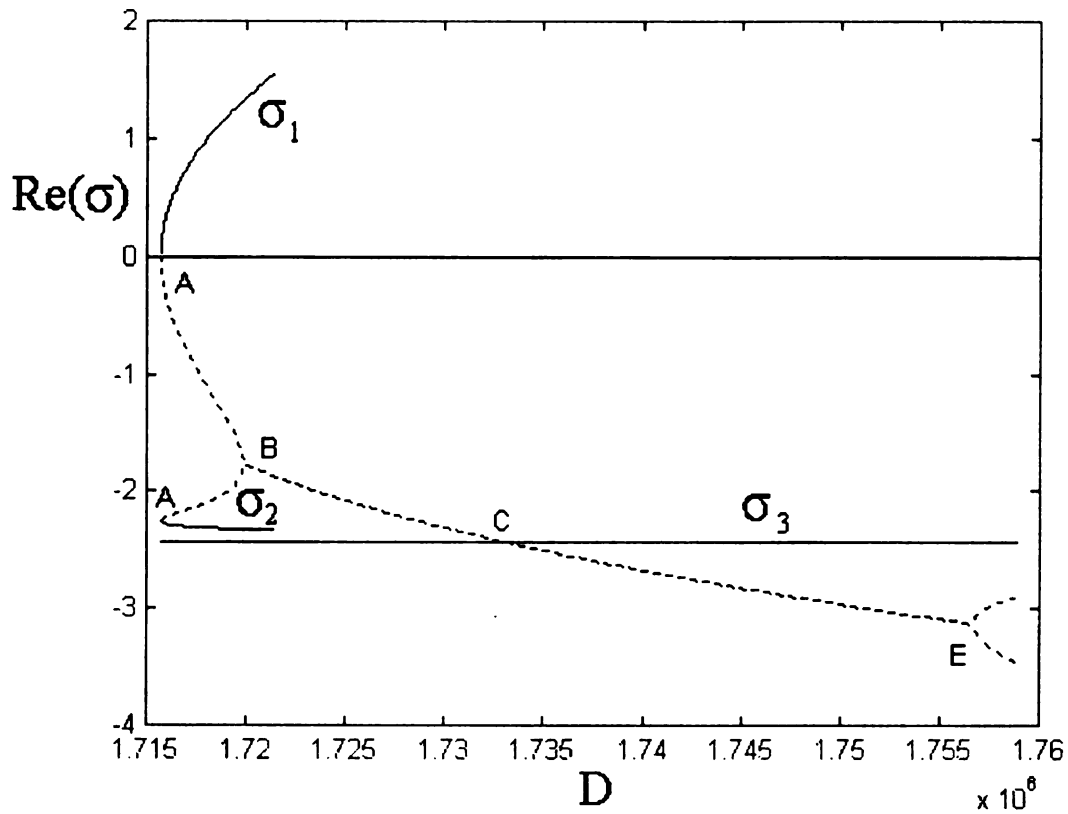


Figure 2.5. $1 < Le < Le_c$. Real eigenvalues σ_1 and σ_2 merge at B to form a complex conjugate pair until they split again at E. B moves up and E moves to the right as Le is increased. Here, $Pe=0.0$, $Le=1.01$, $Ta=4.0$, $To=0.05$.

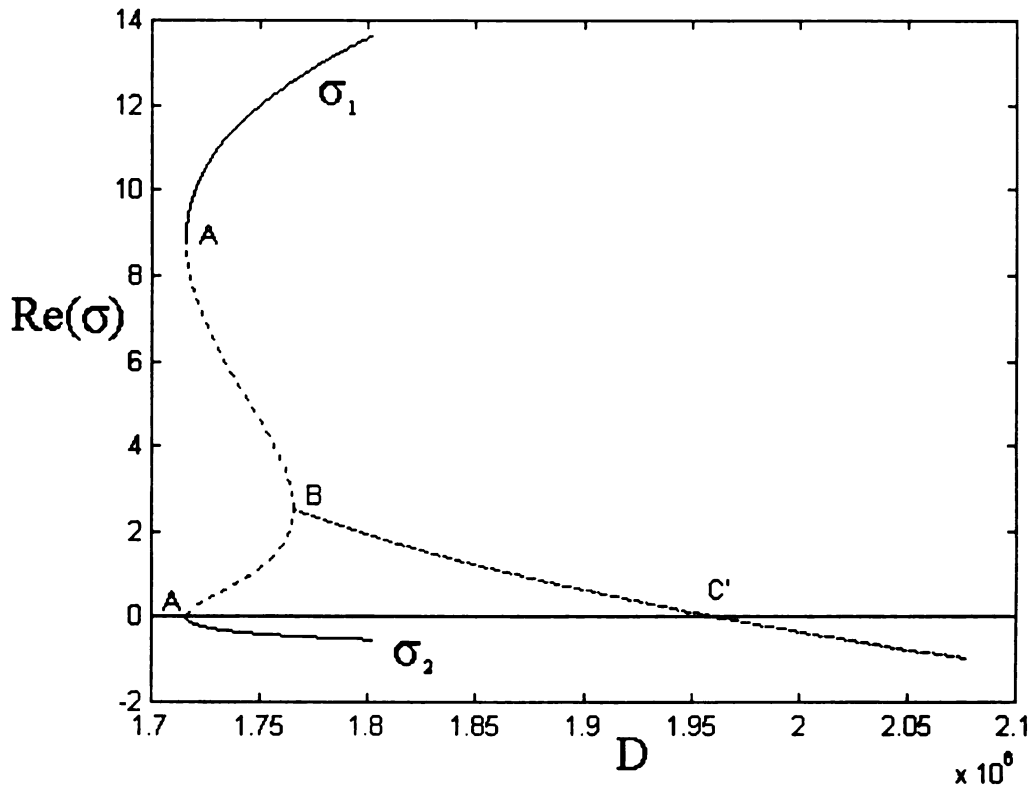


Figure 2.6. Leading two eigenvalues for $Le=2.0$ $Ta=4.0$, $Pe=0$, $To=0.05$. Upper branch instabilities are seen up to point C' . Oscillations are unstable between B and C' and stable beyond C' . Pure perturbation growth exists between A and B .

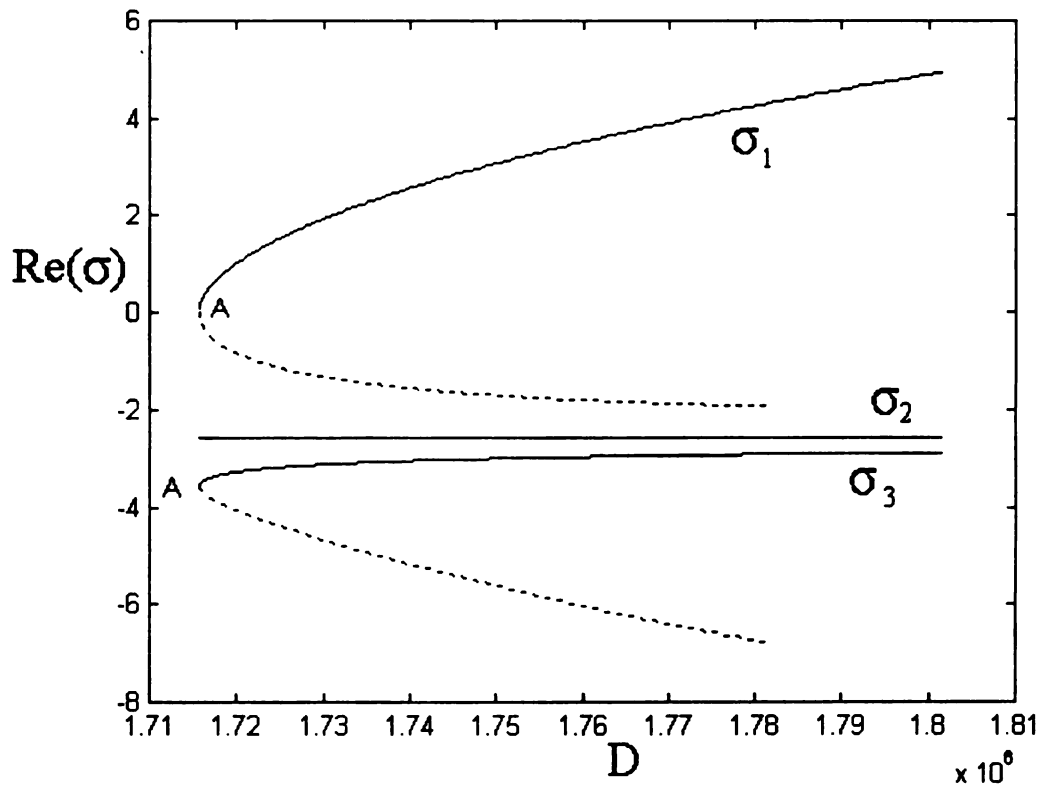


Figure 2.7. When $Le < 1$, the third eigenvalue diverges from the constant value obtained when $Le = 1$ by moving lower. As $Le \rightarrow 1$ σ_3 merges with σ_2 . $Pe=0$, $Le=0.95$, $Ta=4$, $To=0.05$.

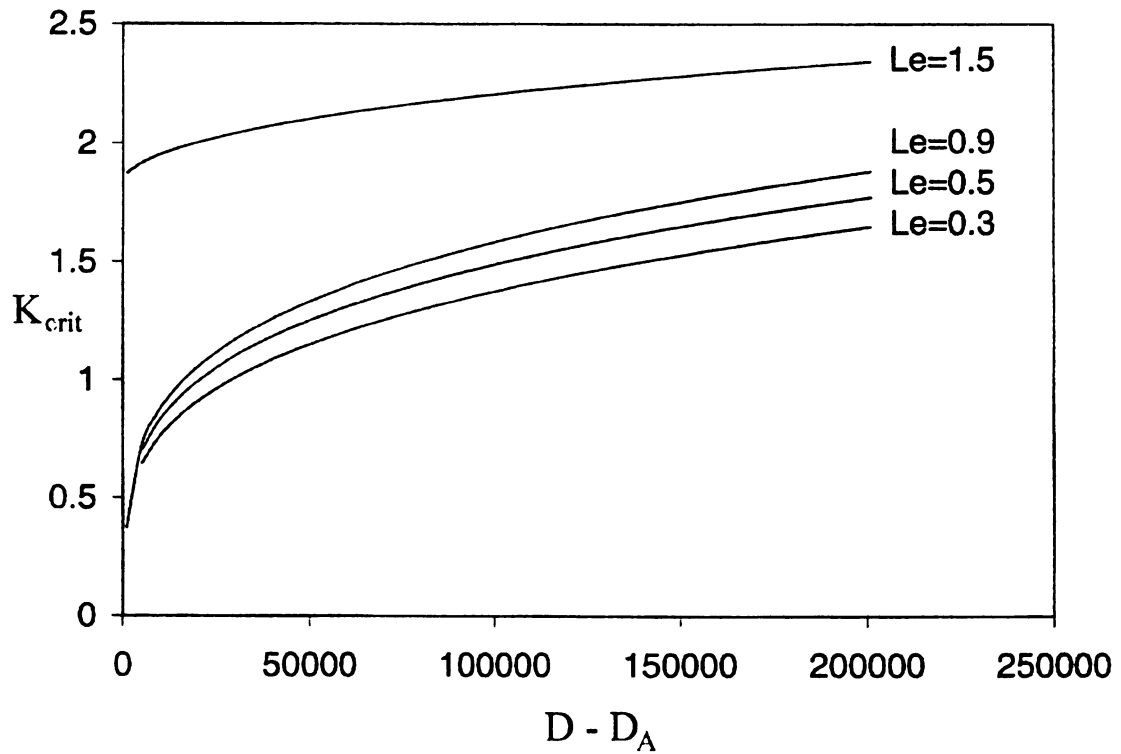


Figure 2.8. The thermal-diffusive properties of the reactants plays a significant role in determining the flamelet size as well as the location of the onset of instability. Here $Pe=0.5$, $Ta=5.0$, $To=0.05$.

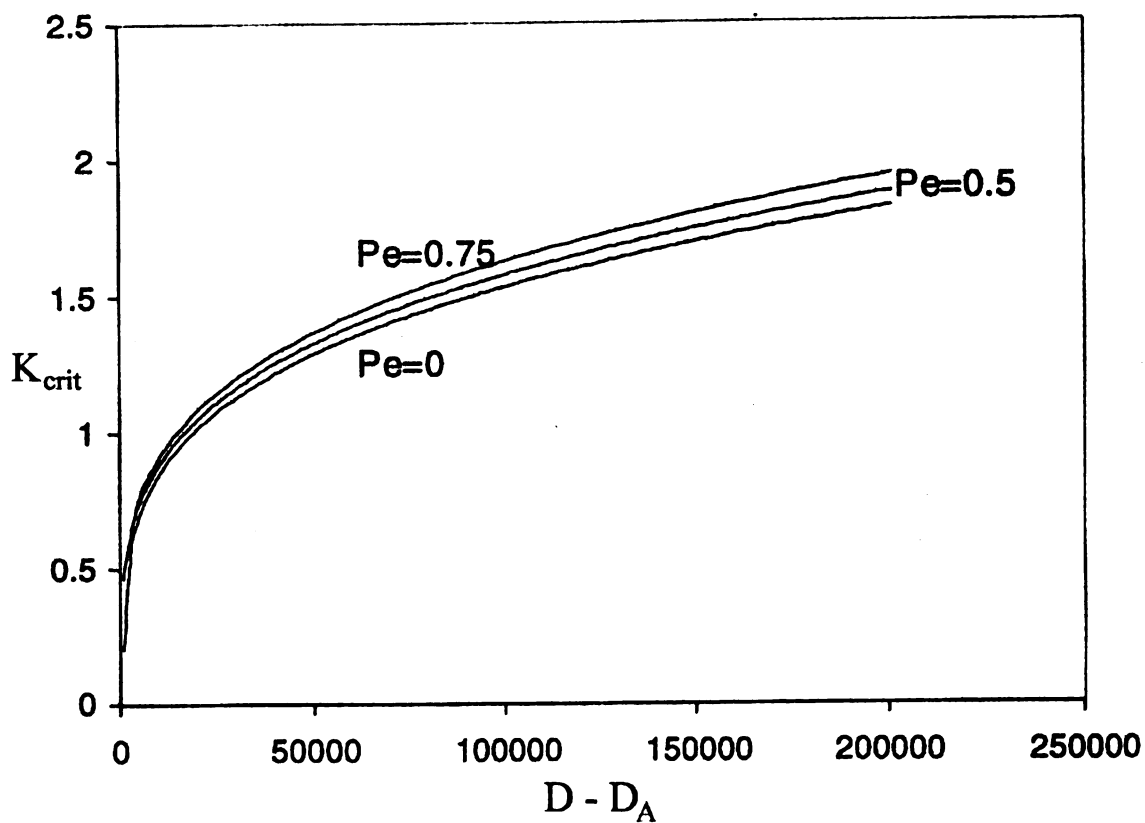


Figure 2.9. The critical wave number for $Le=1$ for solutions along the unstable middle branch are relatively unaffected by the crossflow velocity. However, the increased cross flow results in a smaller flamelet after flame front breakup. $Le=1$, $Ta=5.0$, $To=0.05$.

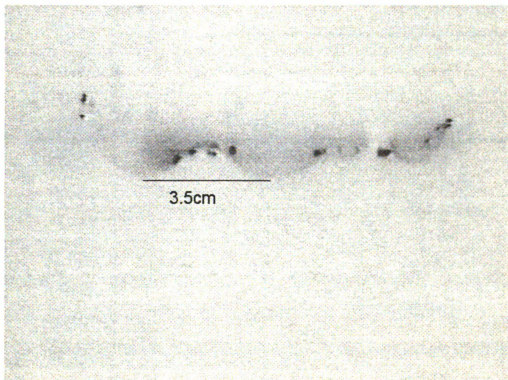


Figure 2.10 Experimental observations show a sinusoidal waveform prior to flame front breakup. (Colors inverted)

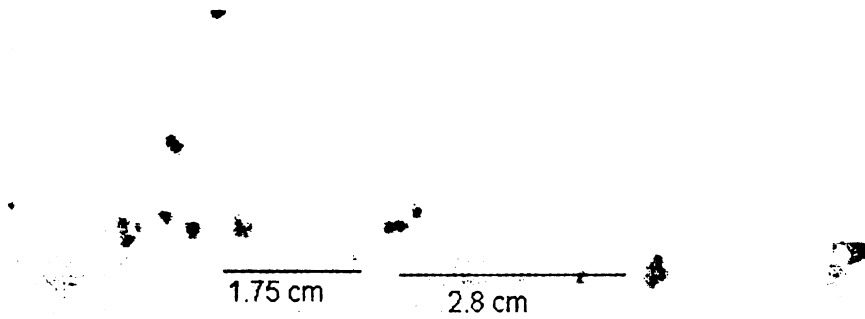


Figure 2.11 After the flame breaks up, the flame pockets that form are dynamic in nature. The flame pockets do not behave uniformly in that different sizes are observed. (colors inverted)

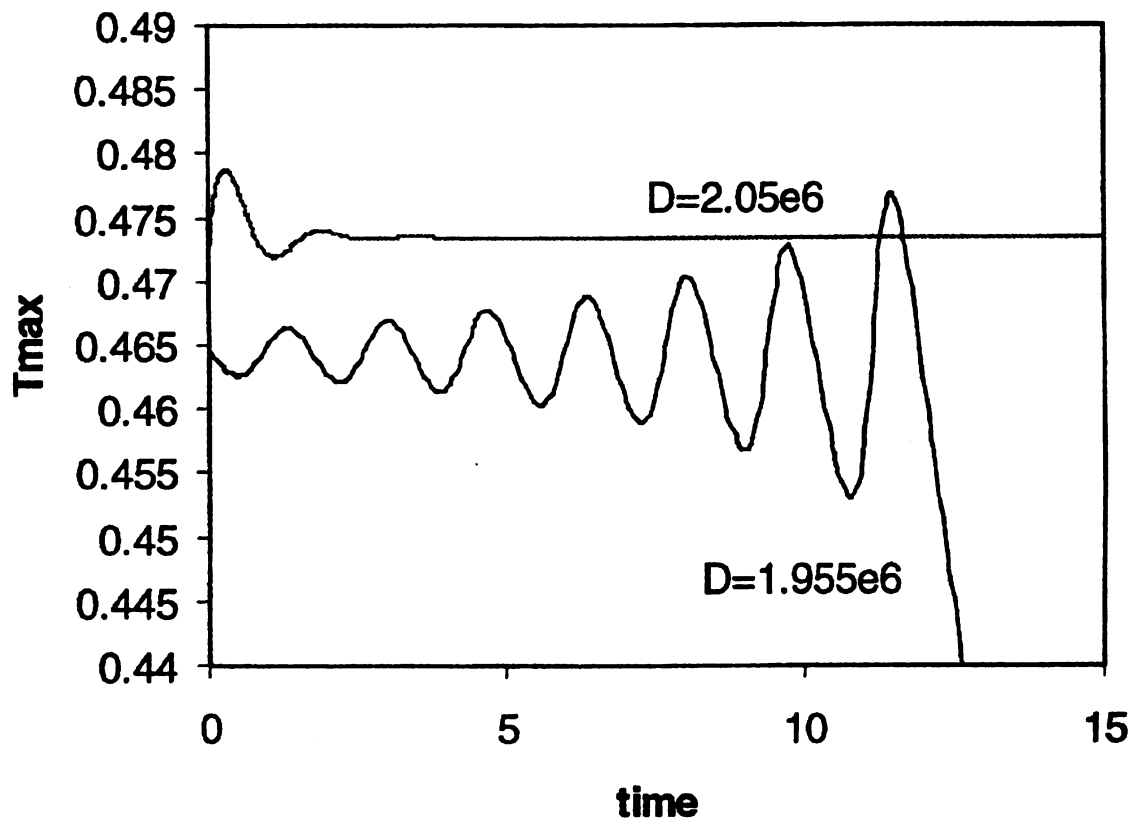


Figure 2.12. Transient solution for $Le=2$ $Pe=0$ $Ta=4$ $To=0.05$ at values of D on either side of point C' . In one case the oscillations grow with time and lead to instability. In the other, the oscillations decay leading to a stable solution.

TWO-DIMENSIONAL DIFFUSION FLAME STABILITY

3.1 Chapter Nomenclature

D – Damkohler number

K – Wave number

Le – Lewis number

Pe – Peclet number

T – Non-dimensional temperature

t – Non-dimensional time

w - Non-dimensional reactivity = $Dy_{O_2} \rho \exp(-T_a/T)$

x,y - Non-dimensional spatial coordinates

Y – Species mass fraction

y - Non-dimensional species mass fraction

Greek

ϕ - Global stoichiometric coefficient

λ - Wavelength

Subscripts

a – Activation reference

c,crit – Critical value

F – Fuel

f – Flame

O – Oxidizer

o – Reference

3.2 Introduction

The one-dimensional flame examined in Chapter 2 is a highly idealized model. However, with only one-dimension there is no possibility of the flame interacting with a nearby surface; and hence, some robustness may be lost. As noted in Chapter 2, there has been a large amount of work focused on various configurations of one-dimensional flames. There has not been, to the knowledge of the author, any work done involving multiple dimension, stability analysis to help support the validity of the one-dimensional model. Some work, in similar fashion to [1], states to be a multidimensional analysis solely because a dimension perpendicular to the base state is added, as in Chapter 2, to identify critical wave numbers even though the base state used is still one dimensional. Some interesting work has been done by Lingens et al. [2] in which experimental data is used to model the flow field of a burner-attached flame. The stability analysis that is carried out is done using a one-dimensional model in a radial coordinate but is applied at various locations above the burner, so in some sense the work took on a multidimensionality. Some numerical work has been done with two-dimensional models to identify cellular flames [3] for $Le < 1$, or flame oscillations [4] for $Le > 1$.

The question this chapter seeks to address is, “How does the flame behavior change with the addition of a second dimension?” Since real flames interact with surfaces it is important to know if the one-dimensional models are missing some important characteristics of this interaction.

3.3 Model

The governing equations are similar to those found in the previous chapter, with the exception of a second coordinate.

$$\frac{\partial T}{\partial t} + Pe \frac{\partial T}{\partial x} = \frac{\partial^2 T}{\partial x^2} + \frac{\partial^2 T}{\partial y^2} + w \quad (3.1.a)$$

$$Le \frac{\partial y_i}{\partial t} + PeLe \frac{\partial y_i}{\partial x} = \frac{\partial^2 y_i}{\partial x^2} + \frac{\partial^2 y_i}{\partial y^2} - w, \quad i=O,F. \quad (3.1.b)$$

The equations are coupled through the non-linear reaction term, $w=Dy_Oy_F\exp(-T_*/T)$. A single Lewis number is employed for both reactants. Figure 3.1 offers a graphical representation of the model.

The boundary conditions for equations (3.1) are

$$T=T_o, y_F=0, y_O=1, \text{ at } x = -1 \text{ and } T=T_o, y_F=1, y_O=0, \text{ at } x = +1. \quad (3.2.a)$$

$$T=T_o, y_F=0, y_O=0, \text{ at } y = 0 \text{ and } \frac{\partial(\bullet)}{\partial y} = 0 \text{ at } y = 3 \quad (3.2.b)$$

It is assumed that the far field flame, in the “in flame” coordinate, does not change with y and the flame is essentially one dimensional at this point. This assumption would be more valid if the “in-flame” boundary could be moved farther away from the “cold” lower wall, but computational limitations restrict the number of nodes available. Furthermore, we assume, for simplicity, that the fuel and oxidizer inflow temperatures are both equal to a reference temperature, $T_o \ll T_f$.

The present model offers a simplistic representation of a flame-spread configuration with blowing oxidizer and diffusing fuel. Additionally, the flame develops a “flame-edge” [3,5], which will offer generally qualitative characteristics of flame-edge behavior. It is possible to obtain a representative model for slot burners by changing the convective term to model flowing reactants in the in flame coordinate (y -direction), this configuration produces another edge flame namely a triple-flame structure (see Chapter 5). The present model, however, is closest to the one-dimensional model studied in

Chapter 2 with essentially the addition of a cold inert surface to add the multi-dimensionality.

3.4 Stability analysis

The stability analysis conducted is similar to that performed in chapter 2 and will not be expounded on here. There are, however, some limitations that arise when examining a two-dimensional base state. Namely, the eigenvalue calculations must be done over the whole domain, which makes the calculation very computationally inefficient. For this reason a relatively coarse grid was needed and, hence, some loss of accuracy near the static turning point (see figure 2.2 point A) is unavoidable. A finite difference algorithm was used employing a 92 x 92 uniformly spaced mesh. The eigenvalues were obtained by employing standard Lapack subroutines designed for large banded matrices. The coarse nature of the grid does not produce smooth, continuous eigenvalue curves, as does the one-dimensional model. However, it is believed that the results represent a qualitative picture of the flame behavior near the upper turning point of the “S” curve and will allow conclusions to be drawn about the usefulness of a one-dimensional model.

3.4.1 Eigenvalue results $Le \leq 1$

As discussed in the previous chapter, the governing equations can be reduced to a non-linear equation and two “heat equations”, which produce a constant eigenvalue of multiplicity two when $Le=1$. Because of this, the eigenvalue behavior for unity Le is not expected to vary greatly from the one-dimensional model. This is in fact the case as can be seen in figure 3.2. Here σ_1 represents the leading eigenvalue which is negative along the entire upper branch and turns positive (indicating instability) at the turning point. The

second two eigenvalues are independent of D and are always negative. This is qualitatively the same picture as the one-dimensional model (see figure 2.3). It is seen that the required coarse grid does not produce smooth curves in the vicinity of the upper turning point on the “S” curve. The solutions along the middle branch are difficult to obtain, and produce “ragged” curves.

The picture becomes slightly more complicated when Le is reduced below unity. As shown in the previous chapter (figure 2.6) there existed, among the three leading eigenvalues, only one constant eigenvalue. It is the behavior of what is labeled the third eigenvalue, σ_3 , that changes as Le is deviated from unity. In the one-dimensional model σ_3 departed from the constant value, σ_2 , by bending lower as the solution traveled along the upper branch and asymptotically approached the constant σ_2 as the middle branch was traversed. This behavior is also seen when Le is slightly less than unity in the two-dimensional model, see figure 3.3. The first qualitative difference appears for the two-dimensional model when Le is further reduced. If the Lewis number is too small σ_3 will not asymptotically approach σ_2 but will increase past this value as the middle branch is traversed, see figure 3.4. Although this difference does not change the physical behavior of the system, which still exhibits stable solutions along the entire upper branch, and unstable solutions along the middle branch with no oscillations present, one begins to see the effect of the flame edge and the cold boundary.

As noted in the previous chapter when $Le \leq 1$ the instability manifests itself in the form of cellular flames. The relative size of these “flamelets” is determined in part by the critical wave number for which the “new” leading eigenvalues become zero. This is discussed in detail in chapter 2. For the one-dimensional model it was found that K_{crit}

was not greatly affected by Le or Pe . This is seen also for the two-dimensional model as seen in figure 3.5. Here various Le and Pe configurations are presented along with the one-dimensional result for $Le=1$, $Pe=0$, and $T_a=4.0$. It is clear that the two-dimensional model produces critical wave numbers that are of the same order of magnitude as predicted with the one-dimensional model. Figure 3.5 also indicates that the critical wave number is only slightly affected by thermal-diffusive or hydrodynamic considerations.

It is therefore concluded, based on the above results, that for $Le \leq 1$, the one-dimensional model can accurately predict both the flame behavior, as described by the eigenvalue spectra, and the relative order of magnitude of the cellular flame instability.

3.4.2 Eigenvalue Results $Le > 1$

In the previous section it was shown that flame instabilities for $Le < 1$ result in cellular flames. When $Le > 1$ cellular flames are not observed, rather flame oscillations can occur that either decay to stable burning or oscillations that continue to grow resulting in flame quenching. This behavior was laid out in Chapter 2 for the one-dimensional model. Here it was seen that if Le is large enough the upper branch solutions exhibited pure perturbation growth or oscillation growth or decay. This behavior is described by the eigenvalue response examined below for the two-dimensional model. Note that in Chapter 2 the analysis was restricted to low Pe because the eigenvalue behavior became more complicated and wasn't the focus of the work. In this chapter, the restriction for low Pe is used because of the coarse nature of the grid needed to perform these calculations.

Small deviations from $Le = 1$ are first studied and are shown in figure 3.6. Small deviations from unity Le , as well as all the cases presented below, were discussed in detail in chapter 2 (see figure 2.4) and will not be expounded here again. If one compares the nature of eigenvalue behavior for figure 3.6 to that of figure 2.4, many similarities arise. Primarily, the entire upper branch is stable with decaying oscillations present over a small portion. Note figure 3.6 does not extend as far as figure 2.4 along the upper branch, but the behavior is similar. That is, the oscillations will persist until the complex conjugate pair $\sigma_{1,2}$ crosses σ_3 and σ_3 becomes the leading eigenvalue.

There exists a critical value of Le in the one-dimensional model for which larger values produce upper branch instabilities. This is the case also for the edge-flame model. Figure 3.7 shows the upper branch results for $Le = 2.0$ and as can be seen the complex conjugate pair extends into the positive region and then breaks up. This behavior indicates that not only do unstable oscillations exist but also pure perturbation growth. This is the same behavior seen in figure 2.5. Both figure 3.6 and 3.7 represent eigenvalue responses for the case of zero convection. It was seen that the characteristics of the flame behavior didn't change appreciably with changes in Pe when $Le < 1$. To identify any effect of Pe for $Le > 1$ the eigenvalue behavior was obtained for $Le = 1.2$ with $Pe=0.0$ and $Pe=0.5$. These results appear in figure 3.8. It is seen that the changes in Pe do not alter the behavior of the eigenvalues, with the exception that the curve is shifted towards higher D . This is consistent with the results seen for $Le < 1$.

3.5 Conclusions

A two-dimensional model of an edge-flame was examined to identify the validity of a simpler one-dimensional model. This work examined both the sub-unity Lewis

number regime whose instability is exhibited as cellular flame behavior and the $Le > 1$ regime which has the characteristic of producing oscillatory behavior. It was demonstrated that both of these regimes behave similarly to the one-dimensional model. Although a more exacting analysis, that is a more refined mesh, will be needed to more accurately predict the eigenvalue response. This will have to wait until more powerful computers are available. However, this analysis should provide strong support to all the previous, and future, work done with one-dimensional models. It is clear the basic characteristics and qualitative behavior of flames is predicted with only the barest of terms and dimensions.

3.6 References

1. Mukunda, H.S. and Drummond, J.P, *Applied Scientific Research*, **51**, 687-711, (1993)
2. Lingens, A. et al., *Twenty-sixth Symposium (International) on Combustion*, 1052-1061, (1996)
3. Thatcher, R.W. and Dold, J.W, , *Combustion Theory and Modelling*, **4**, 435-458, (2000)
4. Buckmaster, J. and Zhang, Y., Conference proceedings First Joint Meeting of the U.S. Sections of the Combustion Institute, 677-680, (1999)
5. Buckmaster, J., *Journal of Engineering Mathematics* , **31**, 269-284, (1997)

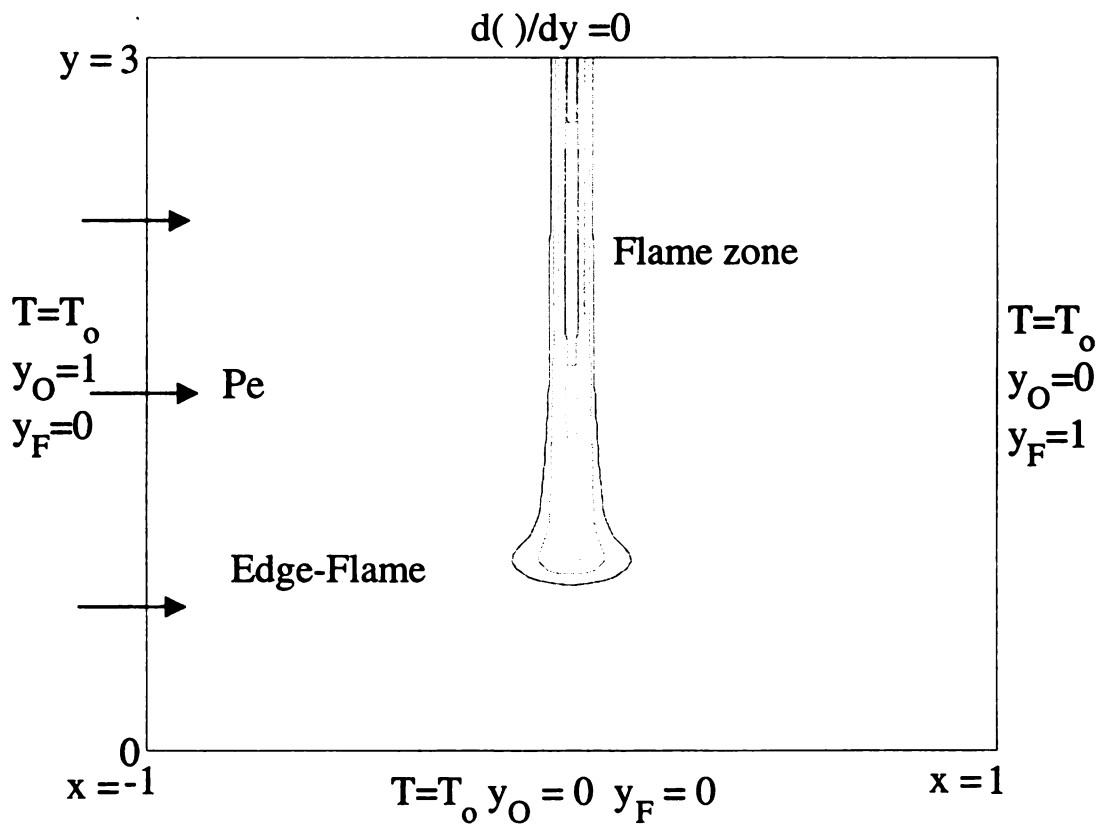


Figure 3.1 Schematic of 2-D edge-flame model with boundary conditions

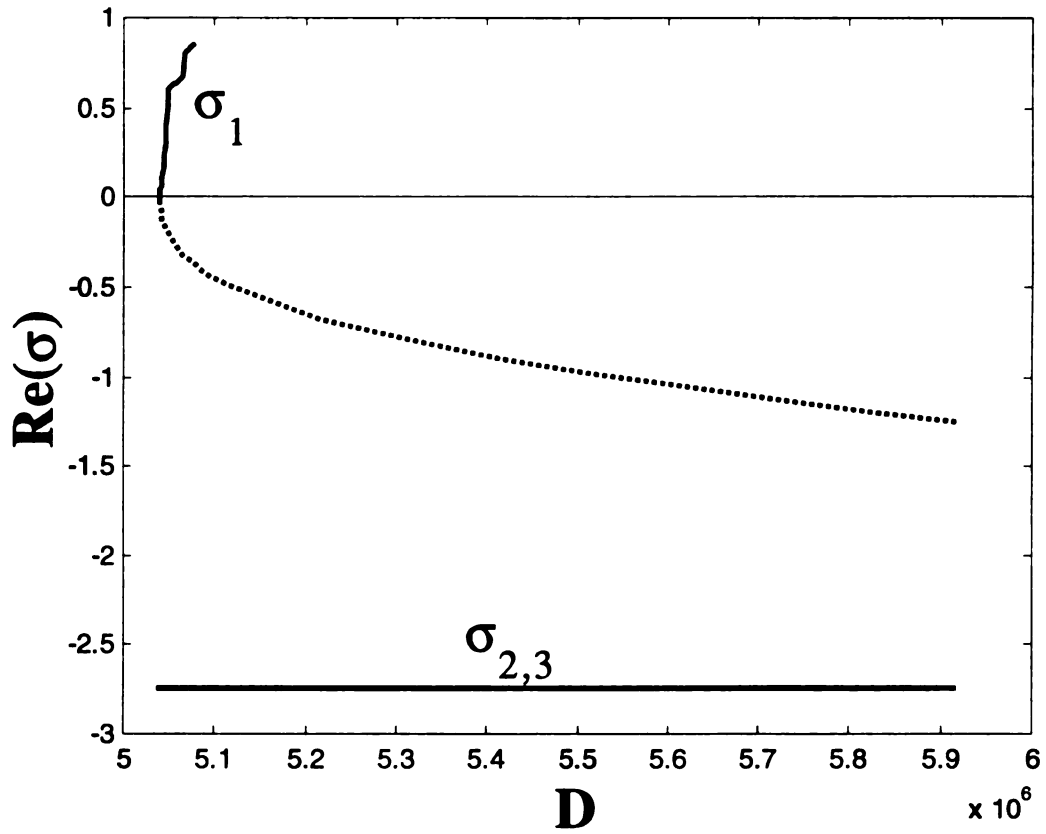


Figure 3.2 Eigenvalue distribution for $Le=1$ $Pe=0.5$ $Ta=4$ $\phi=1.0$. Similar distributions are seen for the 1-D model when $Le=1$.

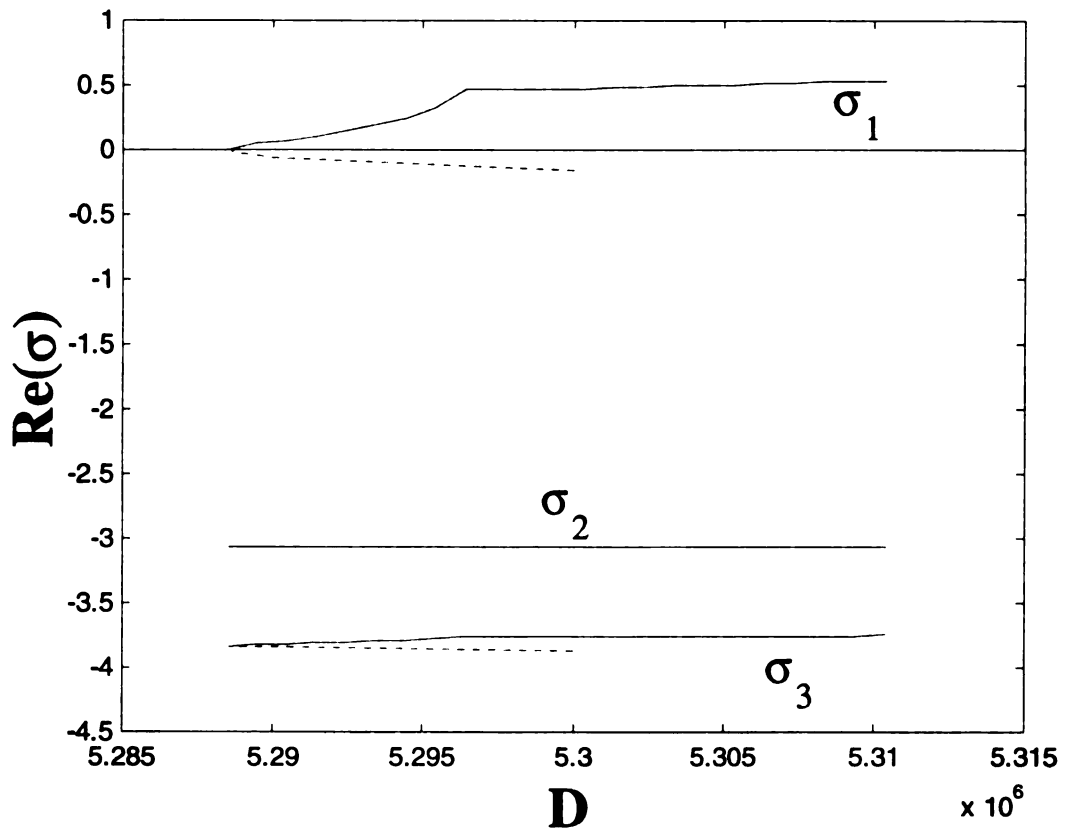


Figure 3.3 Eigenvalue distribution for $Le=0.9$ $Pe=0.3$ $Ta=4$ $\phi=1.0$. σ_1 turns positive at the upper turning point, indicating instability along the middle branch. The third eigenvalue approaches σ_2 asymptotically along the middle branch.

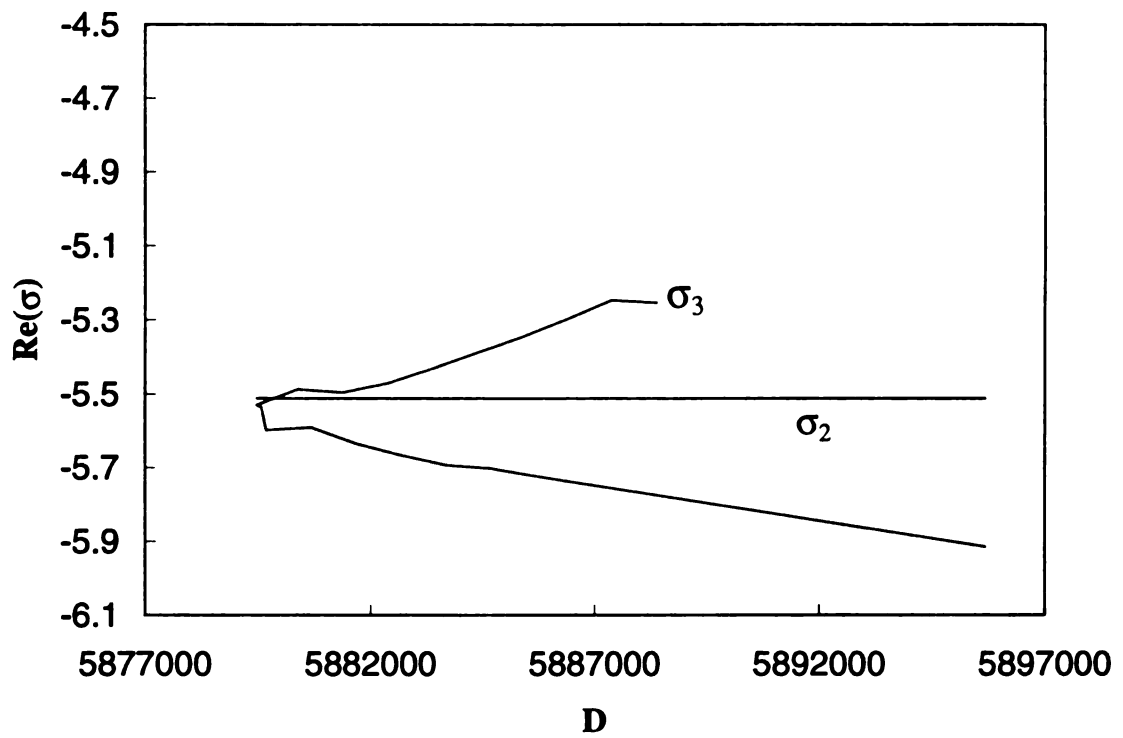


Figure 3.4 $Le=0.5$ $Pe=0.5$ $Ta=4.0$ $\phi=1.0$. When Le is decreased below a certain value, σ_3 crosses σ_2 . This behavior is not seen in the one-dimensional model. The Leading eigenvalue is not shown.

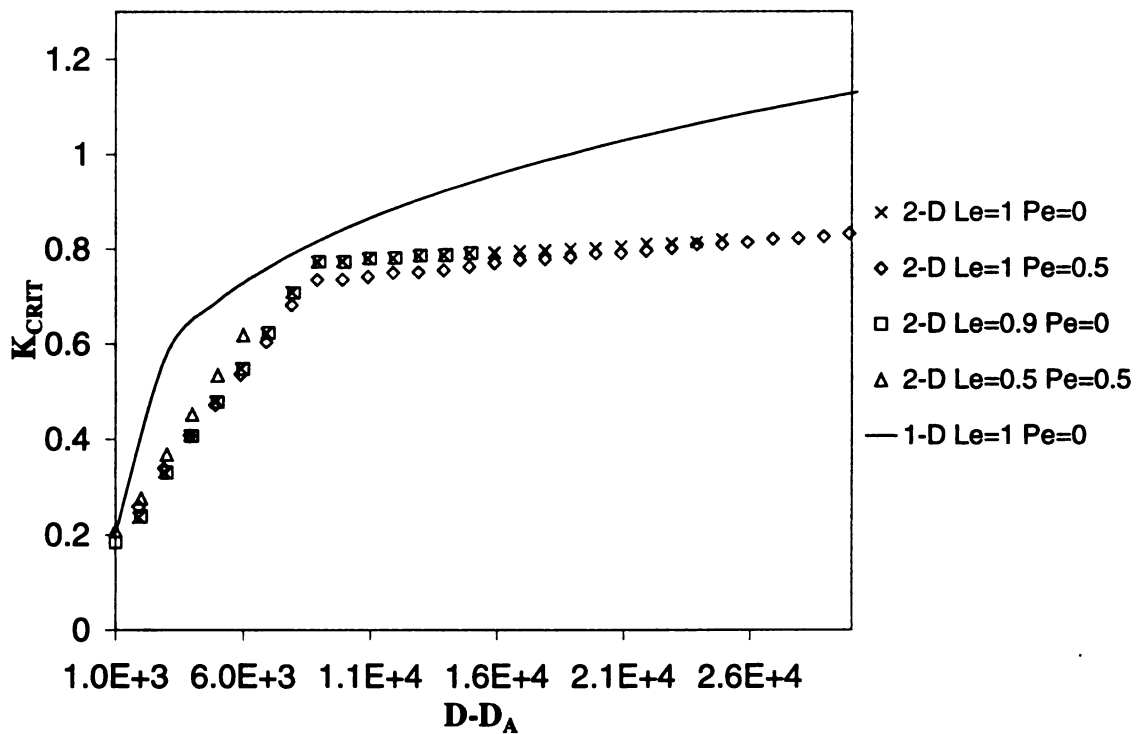


Figure 3.5 Critical wave numbers for several different configurations. It is seen that 1) K_{crit} is not greatly affected by changes in Le or Pe and 2) The order of magnitude of K_{crit} is the same between the 1-D and 2-D models.

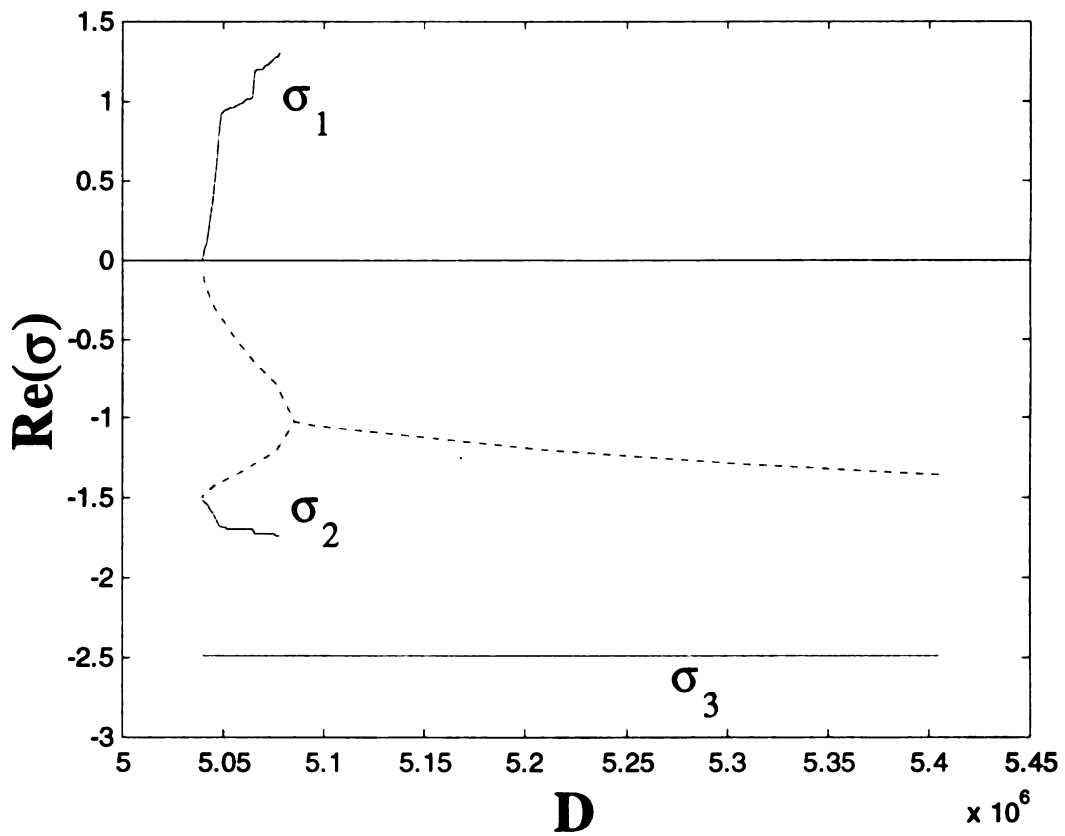


Figure 3.6 $Le=1.1$ $Ta=4.0$ $Pe=0.0$ $\phi=1.0$. Stable oscillations exist on the upper branch while the entire middle branch is unstable. The regions within the circle represent eigenvalues along the middle branch.

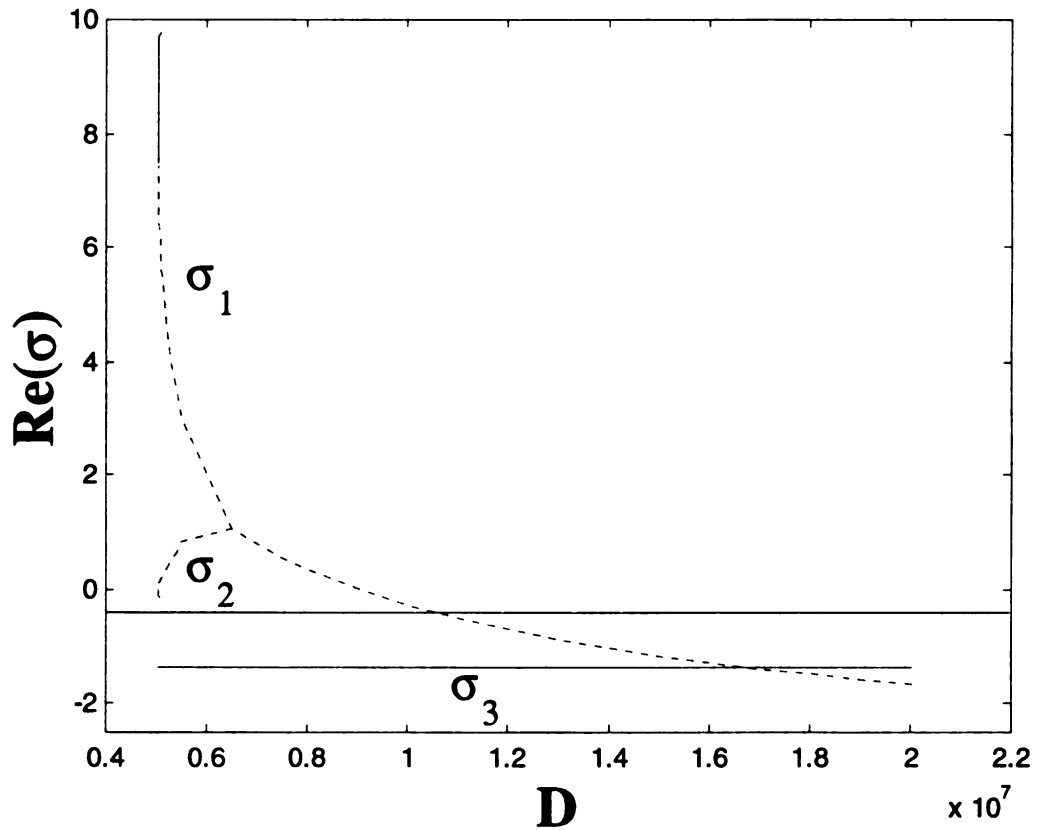


Figure 3.7 $Le=2.0$ $Pe=0.0$ $Ta=4.0$ $\phi=1.0$. The upper branch eigenvalues indicate regions of pure perturbation growth as well as oscillation growth leading to instability. The oscillations cease to exist when σ_3 becomes the leading eigenvalue.

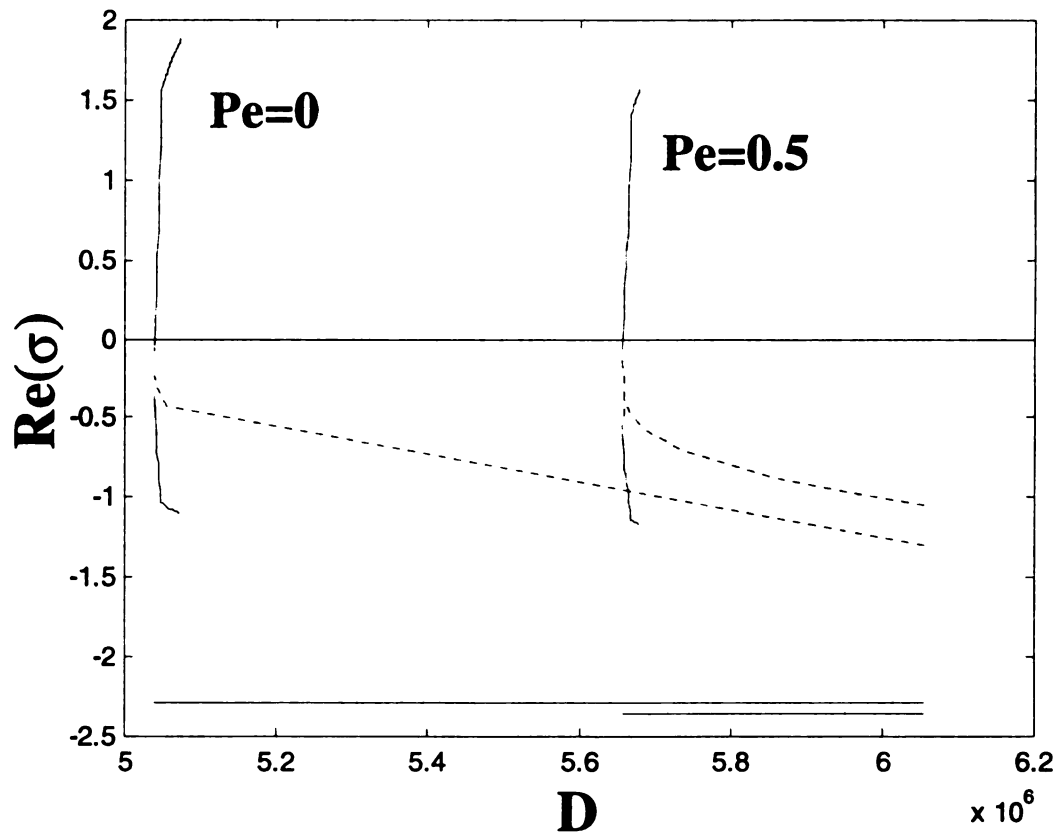


Figure 3.8 $Le=1.2$ $Ta=4.0$ $\phi=1.0$. The three leading eigenvalues for different Pe . Changes in Pe have only a small effect on the flame behavior which is consistent with $Le < 1$.

ONE-DIMENSIONAL LAMINAR PREMIXED FLAME ANNIHILATION

4.1 Chapter Nomenclature

A	Pre-exponential factor
C_p	Specific heat
D_i	Mass diffusivity of species i
E	Activation energy
H	Excess enthalpy, $H = \tau + y - 1$
I	Integral; see equation (4.19)
L	Characteristic length
Le	Lewis number, $Le = \lambda/\rho C_p D = \alpha_u/D_{fu}$
n	Reaction order
q	Chemical heat release
R	Non-dimensional reaction rate, $R = \Omega y^n \exp\{-\beta(1-\tau)/[1-\alpha(1-\tau)]\}$
t	Time
u	Flow velocity
x	Flow direction (physical spatial coordinate)
y	Reduced mass fraction of limiting reactant, $y = Y_F/Y_{Fu}$
Y	Mass fraction of limiting reactant
z	Mass coordinate, $z = \int_{-\infty}^x \rho dx$

Greek

α	Enthalpy ratio, $\alpha = 1 - T_u/T_b$ (also $\alpha_u = \lambda_u/\rho_u C_p$)
----------	--

β	Zeldovich number, $\beta = \alpha(E/R_u T_b)$
δ	Deviation of Le from unity, $\delta = Le - 1$
η	Stretched mass fraction, $\eta = \beta y$
λ	Thermal Conductivity
ν	Stoichiometric coefficient
ρ	Density
σ	Non-dimensional time, $\sigma = t/t_u$
τ	Non-dimensional temperature, $\tau = (T - T_u)/(T_f - T_u)$
ω	Reaction rate (units mass/vol-s)
Ω	Damkohler number
ξ	Transformed spatial mass coordinate
ζ	Normalized mass coordinate, $\zeta = z/z_u$

Subscripts

b	Burned
f	Flame or reaction zone
F	Fuel – limiting reactant
i	Species
m	Mass
t	Thermal
u	Unburned

Superscripts

*	At location of extremal H , i.e., where $dH/d\zeta = 0$
---	---

4.2 Introduction

Recent advances in the speed and accuracy of computational methods have made possible the numerical simulation of detailed flow and combustion problems involving interacting flames, complicated chemistry, turbulence, and real property variations. A particularly difficult feature of highly turbulent flames is the destruction and subsequent healing of flame fronts; a fraction of the flame surface per unit volume is, in all likelihood, continually changing through this complicated process. And though some aspects of flame destruction have been examined, like destruction through stretching, for instance [1,2], the difficult problem of mutual flame annihilation is virtually untouched.

Our goal in this study is to examine a simplified model for the mutual annihilation of two identical, oppositely propagating premixed laminar flames. Our intent is to develop a sound understanding so that the appearance of such flames in larger, complex calculations as a sub-problem does not cause unnecessary hardship in their interpretation and eventual use.

The direct inspiration for this study is the previous work of Echehki et al. [3] on mutual premixed flame annihilation. This work reviews the relevant, and quite scant, previous research and provides a rather extensive DNS examination with detailed chemistry. One of the main results was a rather clear demonstration that the dominant simple free flame balance between reaction and diffusion is completely upended during annihilation. Also, it was found that the light, fast hydrogen containing species had begun a mass diffusivity- based interaction before the thermal interaction took place: in other words, the Lewis number of the reactant was important. In particular, they determined that the flame acceleration during the final stage of the interaction is largely

produced by the diffusion of the hydrogen molecule (H_2) into the reaction zone. This alters the balance between reaction and diffusion in the reaction zone, and even for a stoichiometric CH_4 -air flame with a Lewis number of unity based on the deficient reactant, accelerations to as great as a factor of 20 over the unperturbed flame speeds were obtained. We shall see that for Lewis numbers very close to unity these sorts of accelerations do not occur in our simple model; in order to obtain such behaviors a model employing at least two-step chemistry is needed, with one species being light and highly diffusive. Another study with great relevance to our work is the recent study of Chen and Sohrab [4] on substantially the same problem. Their study, which is purely numerical, focuses on fundamental features of the interaction, using a chemical kinetic model that simulates real flame situations (asymptotically reduced four step methane chemistry). Influences of Lewis number were studied and flame accelerations and locally homogeneous explosions were observed. Accelerations to flame speeds seven times greater than free flame values were obtained. The general behaviors we shall describe here were explained on the basis of numerical, not analytical, calculations.

There has also been much research on the related problem of premixed flame destruction by cold walls [5-8]. This research is driven mostly by the study of combustion and pollutant formulation in engine cylinders, wherein the quenching layer and the various crevices are presumed to generate the bulk of the unburned hydrocarbon emissions. The early work was simplified, qualitative and inconclusive because the models were not examined thoroughly [5,6]. Subsequent work approached the opposite extreme: every possible ingredient was include in the numerical simulations, like real chemistry, thermal properties, etc.[7]. Still, these models, by their complexity, were

exceedingly unwieldy and the problem remained unresolved: the origins of the hydrocarbons from the quenching layer still could not be explained. Later work [8] emphasized the thorough examination of simple models. These have the virtue of producing desirability and understanding without interjecting cluttered detail. Nevertheless, some kind of realistic chemistry is needed to make further advances with this approach.

The specific aim of this study is to understand and describe the details of the interaction and ultimate annihilation of two oppositely directed planar, laminar premixed flames. We intend both to shed light on the extinction and to produce correlations that can describe the dominant features of the extinction. We limit ourselves to simple one step chemistry and simple property variations (constant $\rho\lambda$, ρ^2D_i , etc.). A good description of the equations and methodology of our work is given in the article of Peters [9], where he derives and explains at length the model we shall use here.

In this article we first derive the conservation equations and discuss their limitations (sec 2.). In sec. 3 we describe the various regimes of burning, with special emphasis on the final and most dramatic regime, the “strong interaction” stage or “homogenous explosion” stage [4]. In sec. 4 we present our numerical results. Finally, in sec. 5 we examine the results of sec. 4 in light of the theoretical work of sec. 3. Possible extensions and comparisons with the more detailed models of previous investigations are made in sec. 5.

4.3 The Model

We consider a perfect gas undergoing a one-step irreversible Arrhenius reaction at the flame front. The limiting component is denoted as Y_F , in which the reaction is of

arbitrary order, n . The transient one-dimensional equations for conservation of mass, limiting species, and energy are respectively

$$\rho_t + (\rho u)_x = 0, \quad (4.1a)$$

$$\rho C_p (T_t + u T_x) = (\lambda T_x)_x + q\omega, \quad (4.1b)$$

$$\rho (Y_{Ft} + u Y_{Fx}) = (\rho D_F Y_{Fx})_x - \nu_F \omega. \quad (4.1c)$$

We assume that ρD^2 , $\rho\lambda$ and C_p are constant and we transform to a mass-based coordinate, $z = \int_{-\infty}^x \rho dx$ where the symbol $-\infty$ denotes a distant, but not necessarily

infinitely far, boundary. We define the non-dimensional variables $\zeta = z/z_u$ ($z_u = \rho_u L_u$), $\tau = (T - T_u)/(T_b - T_u)$, $y = Y_F/Y_{Fu}$, $\sigma = t/t_u$ ($t = L_u^2/\alpha_u$), and we put $\nu_F = 1$ without loss of generality, and define the flame temperature as $T_b = T_u + qY_{Fu}/C_p$. We note that the characteristic length L_o is carried over from the steady flow propagation problem in which $\partial(\bullet)/\partial t = 0$ in the above equations, although an important clarification must be made. In the steady problem the characteristic length contains the eigenvalue mass burning rate $m = \rho_u S_L$ which must be derived as part of the solution. In our case we are concerned only with the unsteady evolution and an explicit eigenvalue calculation is not necessary. The non-dimensional equations reduce to

$$\frac{\partial \tau}{\partial \sigma} = \frac{\partial^2 \tau}{\partial \zeta^2} + R \quad (4.2a)$$

$$\frac{\partial y}{\partial \sigma} = \frac{1}{Le} \frac{\partial^2 y}{\partial \zeta^2} - R \quad (4.2b)$$

where

$$R = \Omega y^n \exp[-\beta(1-\tau)/(1-\alpha(1-\tau))] \quad (4.3a)$$

$$\Omega = AY_{Fu} e^{\frac{-E}{RT_b}} \quad (4.3b)$$

$$\beta = (E/R_u T_b)\alpha \quad (4.3c)$$

$$\alpha = 1 - T_u/T_b \quad (4.3d)$$

$$Le = \alpha_w/D_{fu} \quad (4.3e)$$

We note from equations (2) that the convective term has disappeared in the mass-coordinate formulation.

The initial and boundary conditions for equations (2) are now specified. At the symmetry line, $\zeta=0$, the gradients of species and temperature vanish,

$$\frac{\partial y}{\partial \zeta} = \frac{\partial \tau}{\partial \zeta} = 0 \quad \text{at } \zeta=0 \quad (4.4)$$

In the far field the chemical reaction has run to undisturbed completion with zero chemical potential. Hence,

$$y=0, \tau=1 \quad \text{at } \zeta = \infty. \quad (4.5)$$

Of course, in our numerical solution, we cannot impose conditions (4.5) at $\zeta = \infty$; we must choose a large downstream value instead. Our initial condition amounts to specifying the upstream distribution of species and temperature at the instant numerical integration begins. These distributions are derived in the following section. We note that the upstream distribution is somewhat idealized, since it obtained from the solution of the steady problem without the reaction term. This “preheat zone” solution gives $y=0, \tau=1$ at the flame, resulting in a discontinuous gradient across the flame, or better, flame sheet. A smoothing of this postulated distribution occurs in the first few instants of the numerical integration so the y and τ profiles soon resemble their undisturbed free stream values.

We observe that most of our discussion will center on the first order reaction, $n=1$.

For this case, the asymptotic estimate for the steady-state eigenvalue is [9],

$$\Omega = \frac{\beta^2}{2Le} \left[1 + \frac{2(3\alpha - 2.344 + Le)}{\beta} + O(\beta^{-2}) \right]. \quad (4.6a)$$

We shall assign to Ω a magnitude consistent with this estimate. The flame velocity is proportional to $\Omega^{-1/2}$, giving

$$S_L \propto \frac{Le^{1/2}}{\left(1 + \frac{2(3\alpha - 2.344 + Le)}{\beta} \right)^{1/2}}, \quad (4.6b)$$

suggesting that the flame speed increases with Le approximately as $Le^{1/2}$ for Le of the order of unity and large β . We shall use this correlation to test our numerical integrations in section 4.5.

4.4 Theoretical Discussion¹

In this section we shall discuss the theoretical basis for some of the behaviors we observe in the numerical solutions of section 4.5. In section 4.4.1, we discuss the influence of $Le \neq 1$ on the expected flame behavior. In section 4.4.2, we discuss the expected flame behavior during annihilation.

4.4.1 The $Le \neq 1$ Asymmetry

We begin our discussion of the influences of $Le \neq 1$, which we shall show are profound, by examining the combination $H=\tau+y-1$, called the excess enthalpy function, through the combination of equations (2). The physical significance of H is that it essentially defines the global thermal plus chemical enthalpy of the gas, normalized so

¹ The majority of the theoretical derivations in this section is the work of the author's major professor Dr. I.S. Wichman, and is included in this document for sake of completeness.

that an unchanged field produces $H=0$ everywhere. From the equations and boundary conditions given below, a number of conservation properties can be easily derived (e.g., integrate over the spatial coordinate ζ from $\zeta=0$ to $\zeta=\infty$, for instance). We write the equations and boundary conditions as

$$H_{\sigma} = H_{\zeta\zeta} + \left(\frac{1}{Le} - 1\right)y_{\zeta\zeta} , \quad (4.7a)$$

$$H_{\zeta} = 0 \quad \text{at} \quad \zeta = 0 \quad (4.7b)$$

$$H = 0 \quad \text{at} \quad \zeta = \infty \quad (4.7c)$$

$$H = 0 \quad \text{initially} . \quad (4.7d)$$

The initial condition (4.7d) was obtained by requiring $y=1$, $\tau=0$ everywhere in the gas prior to igniting the flame. We note that in equation (4.7a) the variables H and y are obviously interdependent; therefore, the third term cannot be considered as a source or sink term in the standard sense. However, if the third term can be shown to take a certain sign, then it can indeed be considered as a source or sink term and the solutions for H can be correspondingly interpreted.

When $Le=1$, the source term vanishes in the differential equation, so that $H=0$ is the solution everywhere for all time: there is no excess or defect of enthalpy. When $Le \neq 1$, however, the influences of reactant diffusion produce an upset of the H field. This upset is modified by the pre-factor $Le^{-1}-1$. When we let $Le=1+\delta$, where δ can be positive, zero, or negative we obtain for small δ ,

$$Le < 1: \frac{1}{Le} - 1 = |\delta|(1+|\delta|) + O(|\delta|^3) , \quad (4.8a)$$

$$Le > 1: \frac{1}{Le} - 1 = -|\delta|(1-|\delta|) + O(|\delta|^3) , \quad (4.8b)$$

indicating that the $Le < 1$ case is more sensitive to a fixed change of magnitude $|\delta|$ than the $Le > 1$ case. In the extreme case $Le \rightarrow 0$, the amplification $Le^{-1}-1$ becomes infinite, whereas on the other side the limit $Le \rightarrow \infty$ produces merely $Le^{-1}-1 \rightarrow -1$. We conclude that there is a great asymmetry between $Le < 1$ and $Le > 1$, the former being a greatly amplified influence, particularly as Le approaches zero.

To complicate matters further, we observe that $y_{\zeta\zeta}$ in equation (4.7a) changes sign at the inflection point. Upstream, $y_{\zeta\zeta}$ is negative, downstream it is positive. Hence, for $Le < 1$, the source term is negative upstream of the inflection point, and positive downstream of the inflection point: we expect $H < 0$ in front of the flame. When $Le > 1$, we correspondingly expect a region of enthalpy excess $H > 0$ to precede the flame front.

We shall understand the unsteady annihilation process much more thoroughly when we examine the enthalpy function for the steady flame. The governing equation is equation (4.7a) with the transient term replaced by H_{ζ} . Integration subject to upstream bounded constraints and vanishing downstream gradients gives, after a straightforward calculation,

$$H(\zeta) = \left(1 - \frac{1}{Le}\right)y(\zeta) \left[1 - \int_{\zeta}^{\infty} \frac{y(s)}{\zeta y(\zeta)} e^{-(s-\zeta)} ds\right] \quad (4.9)$$

which carries the sign of $1-Le^{-1}$ since the factor in square brackets is always greater than or equal to zero. For $Le < 1$, $H \leq 0$ everywhere; for $Le > 1$, $H \geq 0$ everywhere. As the simplest possible test case we specify $y(\zeta)$ as the flame sheet solution given by $y = 1 - \exp(Le\zeta)$ upstream of $\zeta=0$ and $y=0$ downstream of $\zeta=0$. Substitution into equation (4.9) yields

$$H(\zeta) = e^{\zeta} - e^{Le\zeta}, \quad \zeta < 0 \quad (4.10a)$$

$$H(\zeta) = 0, \quad \zeta > 0 \quad (4.10b)$$

The upstream vicinity of the flame sheet is a region of enthalpy defect when $Le < 1$, enthalpy excess when $Le > 1$, whereas the downstream side of the flame is a zero-excess enthalpy zone throughout. The gradient of H is discontinuous across the origin, with values $1 - Le$ at $\zeta = 0^-$ and zero at $\zeta = 0^+$. This is clearly unphysical and should be resolved easily by a standard asymptotic analysis of the flame zone. Nevertheless, we expect that the upstream solutions for H will be extremely accurate and, for this reason, we press ahead with our examination of the steady flame sheet.

Function H attains a local upstream extremum at the location ζ^* where $dH/d\zeta$ vanishes. From equation (4.10) we find

$$\zeta^* = -\frac{1}{Le-1} \ln(Le) \quad (4.11)$$

When Le is close to unity we let $Le = 1 + \delta$ to find

$$Le < 1: \quad \zeta^* = -1 - \frac{|\delta|}{2} \quad (4.12a)$$

$$Le > 1: \quad \zeta^* = -1 + \frac{|\delta|}{2} \quad (4.12b)$$

Consequently, when $Le < 1$ the upstream influence of non-zero H extends further, for a given increment $|\delta|$, than when $Le > 1$. A plot of $-\zeta^*$ versus Le is given in figure 4.1. We obtain the extremal of $H(\zeta)$ from equation (4.10) by substituting for ζ from equation (4.11), viz.,

$$H^* = Le^{-\left(\frac{Le}{Le-1}\right)} \times (Le - 1) \quad (4.13)$$

The curve of H^* versus Le is also shown in figure 4.1. We note that $H^*(Le)=-H^*(1/Le)$, so that H^* is anti-symmetric about $Le=1$ under the transformation $Le \rightarrow Le^{-1}$. In the vicinity of $Le=1$ we let $Le=1+\delta$ in equation(4.13) to obtain.

$$H^*(1+\delta) \approx \delta(1+\delta)^{-1}(1+\delta)^{-1/\delta} \quad (4.14)$$

As δ becomes small the factor $(1+\delta)^{-1/\delta}$ approaches e^{-1} . Hence,

$$Le < 1: \quad H^*(1-|\delta|) = \frac{-|\delta|}{e} \left(1 + \frac{|\delta|}{2}\right) \quad (4.15a)$$

$$Le > 1: \quad H^*(1+|\delta|) = \frac{|\delta|}{e} \left(1 - \frac{|\delta|}{2}\right) \quad (4.15b)$$

For a given $|\delta|$, the trough of H for values of Le smaller than 1 is deeper than the hill of H is high when Le is larger than 1.

The implications of this simplified steady flame analysis are that both the streamwise extent of the enthalpy change, and the magnitude of the change itself will be greater for an incremental decrease of Le to $1-\delta$ than for an incremental increase to $1+\delta$. For our flame annihilation problem, the vicinity of the symmetry plane should be much better informed of the arrival of a $Le < 1$ flame than a $Le > 1$ flame. For this reason, we expect gradual and undramatic extinctions when $Le < 1$, but sharp, well defined and dramatic extinctions when $Le > 1$.

4.4.2 Flame Annihilation Regimes

There are essentially three regimes of flame interaction, or non-interaction as the case may be. One of these is the strong interaction when two premixed flames (PF) are actively annihilating one another. A second is the weak interaction where thermo-diffusive contact has just recently begun. The third, and final, regime is the free flame

stage wherein the interaction is negligible and the two PFs behave as though their separation were infinite.

We shall analyze these separate regimes by transforming equations (4.2) into a more suitable coordinate system, namely one in which the peak of the reactivity R is always located at a fixed position, $\xi=1$. The transformation is $\xi=\zeta/\zeta_f$, which yields

$$\tau_\sigma - \left(\frac{\dot{\zeta}_f \xi}{\zeta_f}\right) \tau_\xi = \left(\frac{1}{\zeta_f^2}\right) \tau_{\xi\xi} + R \quad (4.16a)$$

$$y_\sigma - \left(\frac{\dot{\zeta}_f \xi}{\zeta_f}\right) y_\xi = \left(\frac{1}{Le\zeta_f^2}\right) y_{\xi\xi} - R \quad (4.16b)$$

where $\dot{\zeta}_f = d\zeta_f/d\sigma$ is the propagation velocity, which is negative because ζ_f decreases as time increases. The reactivity peak, R_{\max} , is located at $\xi=1$. As the annihilation process proceeds from start to finish, the gas between the symmetry plane at $\xi=0$ and the reactivity maximum at $\xi=1$ undergoes great changes. At first, in the free flame stage, the temperature and species mass fraction are essentially undisturbed because R occupies an infinitesimal volume fraction of the upstream gas. Here we use $\tau=0$, $y=1$ as the respective distributions. In the weak interaction stage, the flame is close enough to the symmetry plane that thermodiffusive communication begins to alter the undisturbed gas. In the final stage of strong interaction, a significant segment of the reactivity has entered the upstream gas; here the reaction term in equations (4.16) can no longer be ignored.

We begin by analyzing the strong interaction. We postulate that the spatial distribution of R has substantially eliminated the gradients τ_ξ, y_ξ and their derivatives $\tau_{\xi\xi}, y_{\xi\xi}$ leaving the lowest order balance between transient and reaction terms, as in homogeneous thermal explosions. This is reasonable because the upstream preheating,

confined to a finite pre-flame zone, eventually heats the gas to a nearly uniform condition, at least when the Lewis number is larger than one and the thermal layer is thicker than the mass diffusion layer. In the latter case of $Le < 1$ the two flames communicate via mass diffusivity which, in effect, chokes the approaching flames by rapidly depriving them of the needed reactant. In either case, the relevant equations are $\tau_\sigma \approx R$, $y_\sigma \approx -R$, which can be combined to give $(\tau + y)_\sigma \approx 0$. This integrates to $\tau + y = 1 + H = \text{constant}$, where the number H may be positive ($Le > 1$ or excess enthalpy case) or negative ($Le < 1$ or enthalpy defect case). We substitute $\tau = 1 + H - y$ into the equation $y_\sigma = -R$ to obtain, in the limit $\beta \rightarrow \infty$, the equation (recall we use $n=1$ presently)

$$y_\sigma = -\hat{\Omega} y e^{-\beta y} \Rightarrow \eta_\sigma = -\hat{\Omega} \eta e^{-\eta} = -\hat{\Omega} R(\eta), \quad (4.17)$$

where $\hat{\Omega} = \Omega \exp(H\beta)$ and $R(\eta) = \eta \exp(-\eta)$ is the lowest order asymptotic representation of the reaction rate, with $\eta = \beta y$ being the stretched species mass fraction. In the isenthalpic case we have $H=0$. Qualitatively, the difference between the isenthalpic case and the non-isenthalpic cases can be explained from the ratio

$$\frac{(\eta_\sigma)_{\text{isenthalpic}}}{(\eta_\sigma)_{\text{non-isenthalpic}}} = \frac{-\Omega \eta e^{-\eta}}{-\hat{\Omega} \eta e^{-\eta}} = e^{-H\beta} \quad (4.18)$$

When H is positive, the rate of change of η , in the non-isentropic case, is greater; when H is negative, the isentropic rate of change is greater. Equation (15) integrates to

$$\sigma = \hat{\Omega}^{-1} \cdot \int_{\eta}^{\eta_0} R(x)^{-1} dx \equiv \hat{\Omega}^{-1} I(\eta, \eta_0) \quad (4.19)$$

where η_0 is the initial value of η . Integral I is always positive. Consequently equation (4.19) predicts a monotonic decay of η that is hastened when $\hat{\Omega}$ increases. This, of

course, is the excess enthalpy case, $H > 0$. When $\hat{\Omega}$ decreases, the decay of y is slowed. We observe that these changes in the rate of decay of η are extremely sensitive to small changes in the non-isenthalpicity, H , since $\hat{\Omega}$ is proportional to $\exp(H\beta)$ and β is large. Once again, small changes in the excess enthalpy easily produce $O(1)$ changes in the reactant consumption rate.

In the weak interaction stage the reaction term R is essentially negligible in the vicinity of the symmetry plane $\xi \ll O(1)$, whereby

$$\tau_{\sigma} - \left(\frac{\xi \dot{\zeta}_f}{\zeta_f}\right) \tau_{\xi} = \left(\frac{1}{\zeta_f^2}\right) \tau_{\zeta\zeta} \quad (4.20a)$$

$$y_{\sigma} - \left(\frac{\xi \dot{\zeta}_f}{\zeta_f}\right) y_{\xi} = \left(\frac{1}{Le \zeta_f^2}\right) y_{\xi\xi} \quad (4.20b)$$

When properly normalized, i.e. with $\sigma \sim O(\zeta_f^2 \xi^2)$, the transient and diffusive terms are of the order unity and the convective term is of the order $\zeta_f \dot{\zeta}_f \xi^2$, which for small ξ is negligible. We are left with

$$g(\sigma) \tau_{\sigma} \approx \tau_{\xi\xi} \quad (4.21a)$$

$$g(\sigma) y_{\sigma} \approx \frac{1}{Le} y_{\xi\xi} \quad (4.21b)$$

where $g(\sigma) = \zeta_f^2$. The initial and boundary conditions for equations (4.21) are zero gradients at $\xi=0$, burned reactant at $\xi=\infty$, and given initial distributions when $\sigma=0$. The decrease of $g(\sigma)$ with increasing σ will raise the effective thermal diffusivity $g(\sigma)^{-1}$ and the effective mass diffusivity $(Leg(\sigma))^{-1}$, thereby accelerating the rate of increase of τ and the decrease of y near the centerline. Depending on whether Le is greater than or smaller

than unity the change in one will outweigh the other: when $Le < 1$ the y field should begin its' change before the τ field; vice-versa for $Le > 1$.

We note that a discussion based on length scales would determine only that the strong and weak interactions occur over the same spatial location. In the former case, spatial gradients of τ and y had become vanishingly small; in the latter case, the reaction R was negligibly small. The spatial scales, therefore, are the same as for the ordinary premixed flames: the standard conduction length based on flame speed; and the reaction-zone scale, which is the former divided by β . We observe that in this problem, as formulated, there is no characteristic physical length scale. Hence, the preceding length scales are of a secondary, or derivative, kind.

In the free stream stage we examine equations (4.16). We begin by integrating from $\xi=0$ to $\xi=\infty$ to find

$$\zeta_f = -\zeta_f \frac{\int_0^{\infty} R d\xi + \int_0^{\infty} y_{\sigma} d\xi}{\int_0^{\infty} y d\xi} \quad (4.22)$$

Since the flame is, in real terms, infinitely distant from the symmetry axis at $\xi=0$, we make negligible error by asserting that $R=0$ between $\xi=0$ and $\xi=1$. The integration of equations (4.16), with $R=0$, between $\xi=0$ and $\xi=1$ leads directly to

$$\zeta_f^2 \int_0^1 y_{\sigma} d\xi + \zeta_f \zeta_f \int_0^1 y d\xi = y_{\xi}(1) \quad (4.23)$$

which, by comparison to equation (4.22) yields $y_{\xi}(1) = -\zeta_f^2 \int_0^{\infty} R d\xi$.

Thus, equation (4.22) with the upper limits changed from ∞ to 1 becomes

$$\zeta_f = -\frac{[-y_{\xi\xi}(1) + \zeta_f^2 \int_0^1 y_{\sigma} d\xi]}{\zeta_f \int_0^1 y d\xi} \quad (4.24)$$

But $\int_0^1 y d\xi \approx 1$ and $y_{\xi}(1) = x_f dy/dx$; also since $y = 1 - \exp(x - x_f)$ in the upstream

region, we obtain finally $-y_{\xi}(1)=x_f$. These results, coupled with the observation

$\int_0^1 y_{\sigma} d\xi = 0$, yield from equation (4.24) the simple result

$$\zeta_f = -1 \quad (4.25)$$

Since $\zeta_f = (t_u/z_u)dz/dt = (t_u\rho(x_f)/z_u)dx_f/dt = -(\rho(x_f)/\rho_u)(t_u/L_u)S_L$, this constraint requires that the non-dimensionalization values t_u , L_u be chosen so that their ratio is given by $t_u/L_u = \rho(x_f)S_L/\rho_u$.

There are a sufficient number of degrees of freedom to allow this condition to be fulfilled. Hence with a suitable normalization of the characteristic length and time scales, the flame front propagates with unit negatively directed velocity. This undisturbed propagation is altered once the two PFs begin their thermo-diffusive interaction.

One important observation has not yet been mentioned, namely the absence in our problem of a single characteristic physical length. Our flame is laminar, which alleviates the need for Taylor, Kolmogorov, etc. length scales. Indeed, the only length scales are derived scales, like the characteristic thermal diffusion length (L_t), mass diffusion length (L_m) and the reaction zone thickness (L_r). The former two are combined in the Lewis number, $Le=L_t/L_m$; the latter appears only when the reaction zone is subjected to a careful

asymptotic analysis, where we find $L_f \sim O(L_f/\beta)$. Our analysis suggests the two PFs are aware of one another when their separation is $O(L_f)$ or $O(L_m)$, depending on whether Le is greater than or less than 1. Subsequently, the extinction is determined by the amount ϵ of excess enthalpy in the region between the flames. From Eq.(16) we obtain

$$\sigma = \hat{\Omega}^{-1} \left[\ln\left(\frac{\eta_0}{\eta}\right) + (\eta_0 - \eta) + \frac{1}{2 \cdot 2!} (\eta_0^2 - \eta^2) + \dots \right] \approx \hat{\Omega}^{-1} \ln\left(\frac{\eta_0}{\eta}\right) + \dots \quad (4.26)$$

since

$$\int_0^x \frac{e^s}{s} ds = \ln(x) + x + \frac{x^2}{2 \cdot 2!} + \dots \quad (4.27)$$

When $\eta/\eta_0 \sim O(10)$, we see that σ is still $O(\hat{\Omega}^{-1})$, indicating that the time to extinction is governed by parameter $\hat{\Omega}$, which is proportional to $\exp(H\beta)$. For large β , the time to ignition can decrease exponentially, for positive H . We suppose that the rate of change of H is much smaller than the extinction rate, hence H is expected to be nearly constant. When $Le > 1$ and H is positive, the elapsed time between the substantially undisturbed initial state and complete extinction is

$$\sigma \approx O(\hat{\Omega}^{-1}) = O\left(\frac{2Le}{\beta} e^{-H\beta}\right) \quad (4.28)$$

which can become very small as β increases. The constant of proportionality should be understood as a characteristic magnitude of the square brackets in equation (4.26); this requires choosing the initial state as represented by the rescaled mass fraction η_0 and the initial to final state ratio, η_0/η . Our subsequent numerical examination will discuss the choice of these “parameters”.

The influence of non-unity reaction order is easily assessed. When $n \neq 1$, the equivalents of Eq.(15) in the strong interaction stage became $y_\sigma = -\hat{\Omega}y^n e^{-\beta y}$ and $\eta_\sigma = -(\hat{\Omega}\beta^{1-n})\eta^n e^{-\eta}$. Thus, $\hat{\Omega}$ in our explosion equations (4.26) and (4.28) is replaced by $\hat{\Omega}\beta^{1-n}$. We obtain, for σ , equation (4.26) with β^2 replaced by β^{3-n} . Hence when $n < 1$, the extinction is made more abrupt by the algebraic factor $\beta^{-(1-n)}$, and when $n > 1$ the extinction is prolonged by the algebraic factor β^{n-1} .

Some additional speculations on the nature of the annihilation sequence are possible, especially when $Le > 1$. Here we observe that prior to the strong interaction the spatial distribution of R resembles a strongly peaked bell curve. As the centerline is approached, the upstream segment of the bell begins to rise. During the weak interaction, the qualitative nature of the bell remains unchanged: one maximum, two local minima, and two inflection points. During the strong interaction, a moment arrives when the reactivity upstream of the previous maximum (at the top of the bell) exceeds the bell-top maximum, meaning the upstream inflection point is lost. When this occurs, a distinct qualitative change has occurred and mutual annihilation is now assured.

4.5 Numerical Results

The primary emphasis of the numerical work is directed towards discerning the Lewis number effects on the flame propagation and annihilation. Cases of Lewis numbers greater and less than unity, as well as equal to unity, were studied to find the effects on the reaction term profiles and how it relates to the diffusive and convective terms, the temperature and species profiles, and the excess enthalpy. Furthermore, relationships

between the numerical flame speed, as well as the annihilation time, and the Lewis number were derived and compared to theoretical results.

4.5.1 Numerical Technique

Given the non-linear nature of equations (4.2 and 4.3) and the coupling between the energy and species equations through the reaction term, the solution of these equations is very critical. The numerical technique used was a finite difference model which incorporated a second order correct central differencing scheme. The non-linear reaction term was handled by performing a quasi-linearization around the previous iteration. This involved iterating at each time step until the new values of τ and y converged with respect to an arbitrary small positive value. This allowed larger time steps to be taken without sacrificing stability or numerical accuracy. Furthermore, the governing equations were solved simultaneously using Gaussian elimination and back substitution. To test the code the elemental lengths was reduced by one half with negligible change in the results. Hence, we are confident that the solution method used produces accurate results.

4.5.2 The Free Stream

To examine the free stream propagation, the three terms of equation (4.2a) were plotted along with the excess enthalpy for three cases of Lewis number equal to 1, 2, and 0.8. These plots appear as figures 4.2, 4.3, and 4.4. As can be seen the free stream term balances look very similar. For this reason it is concluded that, although the magnitudes of the terms are different, the primary mechanisms for flame propagation, i.e. a reactive-diffusive balance, are unaffected by the Lewis number. The excess enthalpy, however, has a different profile for all three cases. After the flame, the excess enthalpy is zero for

all three cases, but does not follow the same trend before the flame. For a Lewis number of unity H remains zero before the flame, but for a Lewis number greater than 1 the excess enthalpy becomes positive, whereas for Lewis less than 1, H is negative. These results support the theoretical conclusions drawn in section 4.4. We also note that the premixed flame enthalpy defect region is larger for $Le < 1$ than the enthalpy excess region is for $Le > 1$, in agreement with predictions.

To study the effect of diffusion and pre-heating, i.e. Lewis number effects, species and temperature profiles were plotted along with the reaction term for Lewis numbers of 2 and 0.8. These appear as figures 4.5 and 4.6. Comparing figures 4.5 and 4.6, it is evident that the species profiles are very different before the flame. For Lewis number of 2 there is very little diffusion towards the flame, whereas for Lewis number of 0.8, there is a significant reduction of species upstream of the flame, indicating that the upstream flame region is aware of the approaching flame front. This supports the results that the excess enthalpy for Lewis number greater than 1 is positive and for Lewis number less than one H is negative.

The final area of interest in the free stream is the laminar flame speed. As discussed in section 4.4, the flame propagation speed should have a nominally square root power dependence on the Lewis number (see the final equation of section 4.3). To examine how well the numerical flame speed corresponded to this, the various velocities were plotted against Le and then curve fitted. Figure 4.7 contains the plot and equation (4.29) shows the functional relationship,

$$S_L = 0.8926Le^{0.5025} \quad (4.29)$$

As can be seen, the free stream flame speed has the functional relationship expected for free stream flow. It should be noted that the theoretical relationship is based on propagation an infinite distance away from any boundary. This condition is impossible to obtain in a numerical code, however, it was assumed that a non-dimensional distance of 10 would provide an adequate approximation. Furthermore, the functional relationship becomes stronger as the flames become closer; more will be discussed on this in the next section dealing with the annihilation process.

4.5.3 Annihilation Zone

The examination of the “strong interaction” zone is the primary concern of this study. Examining the Lewis number effects on the reaction profiles, the temperature profiles; and correlating the annihilation time of the two flames is the aim of this section.

To begin the analysis of the reaction profiles through extinction, we will look at the $Le=1$ case. From this we will get a sense of some of the characteristics associated with flame annihilation. Figure 4.8 illustrates the reaction term profile as the two flames approach the symmetry line. As can be seen, the interaction of the two flames does not occur suddenly for this case, i.e. there is a small, low-grade reaction ahead of the flame, which is caused by the thermal upstream diffusion. For this reason, to get true free stream propagation it is necessary to start very far from the symmetry line. Further examination of figure 4.8 shows that there is an acceleration into the flame junction; this is indeed expected for the $Le \geq 1$ case. Furthermore, it is important to note that the most prominent parts of the flames have not yet come into contact. This occurs when the concavity of the reaction profile changes from positive to negative. After having come into contact we surmise that extinction is not very far away. It is this time, from first joining to when the

reaction term is essentially zero ($O(10^{-2})$), that we consider as the numerical annihilation time. Obviously, the theoretical time cannot be so nicely delineated hence our approach in comparing theory and numerics will be to scrutinize the functional dependencies. Reaction profiles for Lewis numbers of 2, 1.25, 0.8, and 0.5 will be compared to the $Le=1$ case to either support or refute the analytical work of the previous section. These additional plots appear as figures 4.9 through 4.12.

Primary examination of the various reaction profiles shows that as the Lewis number increases, the width of the reaction zone decreases; i.e. the reactions are much sharper and quicker with less upstream thermal and species diffusion. Furthermore, the acceleration of the flame for $Le>1$ becomes greater. For the case of $Le=1$ the acceleration is almost negligible, whereas for $Le=2$ it is clear that the reaction rate increases tremendously. As mentioned in the introduction, the previous work of Echehki et al.[3] can in fact produce accelerations when the value of Le of the deficient reactant is close to unity. However, we have not included multiple - and potentially very light - species into our one-step chemical model. We also observe that for $Le<1$ there is no acceleration, but rather a deceleration as the flame approaches the symmetry line. If one follows the time-labeled reaction profiles of figure 4.11, it is clear that when the two flames come into contact there is no jump in the reaction term, but conversely a slow, inevitable extinction. This effect is more pronounced as $Le \rightarrow 0$. It is for this reason that we expect the flame speed dependence on the Lewis number to become stronger as the flame becomes aware of its counterpart. The reaction profile in figure 4.11 shows that for $Le=0.5$ the reaction essentially dies out before the flames come into contact. These results support the theoretical assertions made in section 4.4 dealing with the Lewis number asymmetry.

Examination for the corresponding temperature profiles for $Le=2$ and 0.8 through annihilation will further shed some light on this problem. These can be found in figures 4.13 and 4.14.

The time-labeled temperature profiles for these two cases appear to have different characteristics. The case of $Le=2$ shows a change of concavity in the temperature profile, as discussed at the end of section 4.4.2. This is indeed the case for Lewis numbers greater than 1. Additional analysis shows that this change in inflection is consistent with the maximum reaction rate; that is, this profile change occurs immediately after the reaction rate reaches its maximum. This change in the temperature profile conducts heat away from the reaction and marks the beginning of the annihilation process. It should be noted that the flame does not extinguish itself because of the heat loss but rather by a defect of species through the burning process. However, this heat loss may add to the rate at which the flames annihilate one another. For the $Le=0.8$ case, the temperature profiles retain their positive concavity through annihilation. These profiles are consistent with all Lewis numbers less than 1, although as the Lewis number decreases the change in each profile becomes less dramatic. For the $Le<1$ case the thermal energy is being conducted into the flame junction, as blood is pumped into a dying patient, in hopes to maintain the flame. It is this additional energy input that may contribute to the slower annihilation times for Lewis number less than 1.

The final area of interest is finding a correlation between the annihilation time and the Lewis number. It is observed that the time to extinction from maximum reaction at the junction has a strong dependence on the Lewis number. We have noted that the criteria used in evaluating numerical annihilation times are not usable in theoretical

evaluations. Therefore, we expect some discrepancies between the theoretical and the numerical results. Theoretical flame quenching times can be shown, using equation (4.28), to be proportional to $Le\{\exp[-\beta(Le-1)/Le^{Le/(Le-1)}]\}$, where β is the Zeldovich number. The numerical results can be found graphically in figure 4.15, and give a Lewis number dependence, based on the theoretical result, described by equation (4.30),

$$\sigma_{ann} = 0.98Le \cdot \exp[-0.416\beta(Le-1)] \quad (4.30)$$

If the average value of $Le^{-Le/(Le-1)}$ is taken from $Le=0.1$ to $Le=2.0$, its value is found to be 0.404. This value is very close to the factor of 0.416 found in the correlation of equation (4.30). We can therefore surmise that the theoretical result corresponds with the numerical result within an average error of 16 percent. That is, the 16 percent is the average error between the correlation and the numerical results. The numerical results can be correlated to an average error of about three percent by using the following correlation:

$$\sigma_{ann} = 1.2e^{-0.71e} \quad (4.31)$$

The more accurate correlation does not remove any of the validity from the one found in equation (4.30). Given the good agreement with the theoretical result of equation (4.30) and the accuracy of the correlation given by the above equation, neither is to be preferred over the other, although equation (4.30) does provide further support that the numerical results are accurate.

4.6 Comparison with experimental observations

It has been suggested that this analysis could offer insight to turbulent flame stability. Examination of the numerical and theoretical results leads to the following

conclusions. For cases when $Le > 1$ the annihilation times are quite small, that is the event occurs rapidly with an associated increase in the excess enthalpy of the system. When $Le < 1$ the effect is quite the opposite, that is the annihilation occurs over a relatively long period of time and is associated with an enthalpy defect. Based on these observations re-ignition seems more possible when $Le > 1$. Hence, it is postulated that turbulent flames in which $Le > 1$ will be more stable than those when $Le < 1$.

Experimental observations for Methane/air turbulent premixed flames [10] concluded that local flame extinction for cases when $Le > 1$ is caused by excessive flame stretching. That is, the local flame does not propagate in a planar nature but rather becomes curved and essentially “stretched”. It was observed that when $Le < 1$ flame stretch and excessive heat losses play equally important roles. This is consistent with the excess enthalpy defect observed in the present study.

Along similar lines as the above study, and experimental examination of Propane/air mixtures [11] concludes that flame wrinkling is increased by as much as thirty percent when $Le < 1$ as compared to $Le > 1$. This result can be explained by the rapid annihilation and presumed quick re-ignition of $Le > 1$ flames. An additional observation made by the researchers is that for nearly freely propagating wave fronts, instabilities were observed when $Le < 1$.

A clear description of thermal-diffusive effects of propagating flame fronts is given in reference 12. This numerical model of turbulent premixed flames uses a two-step chemical kinetics scheme in which the Lewis number of the reactants is allowed to vary. The conclusions reached about flame curvature support those seen experimentally, though no comments of flame extinction were presented.

The above references do by no means represent a complete list of available data. However, all the results support in some way the results found by the one-dimensional laminar flame annihilation studied in this chapter.

4.7 Conclusions

We have demonstrated that a simple model of a premixed flame can describe many, if not most, of the principal features of mutual flame annihilation. These features can be anticipated theoretically, without requiring a numerical analysis. However, the numerical analysis provides a seamless connection between the disconnected theoretical submodels while also providing direct indication of the magnitudes involved. We see, consistent with reference 3, that the standard free flame reactive-diffusive balance is entirely upset during annihilation; we also see that Le has perhaps the strongest influence on the qualitative character of extinction, since $Le < 1$ extinctions are completely different from the $Le > 1$ extinctions. The former involve significant pre-extinction communication, hence the extinction is gradual, inexorable, and undramatic. By contrast, the $Le > 1$ extinctions occur with furious rapidity, partly because the two flames are largely ignorant of their mutual existence until they very close. Our correlation of the extinction times with the asymptotic formula predicts a dependence on $\exp[-\beta \cdot \text{constant} \cdot (Le - 1)]$, which we in fact observe numerically (see equation [4.30]). Thus, the sensitivity of extinction to Le is closely coupled to the magnitude of the Zeldovich number. When this is small, extinctions will be tame regardless of Le .

We can only speculate on what occurs in the post annihilation stage when this model is included in a larger problem of the kind discussed at the outset of this article. In this case we have many mutually interacting flames and “flamelets” that are in continual

relative motion due to turbulence and the other flow requirements. When the Lewis number of the principle limiting reactant is larger than unity, we expect dramatic annihilations accompanied by surges in the thermal enthalpy, as shown in figure 4.13. These local pockets of excess thermal enthalpy could seemingly serve as local hot spots for subsequent reignition of locally quenched mixtures. If the characteristic turbulent flow time is substantially larger than the characteristic annihilation time, the subsequent healing of the flame may occur quite rapidly; this would suggest that this flame might remain significantly intact with only minimal permanent destruction of flame surface. If, however, the Lewis number is small, the flames can annihilate one another while simultaneously depressing the thermal enthalpy (see figure 4.14). In this case, the prospects for reignition and flame healing are more remote. This is consistent with observed experimental results. We have not conducted a detailed comparison of our calculated annihilation times and turbulent flow time scales. Such a comparison would be interesting indeed. In real flames, however, there are many constituents, each with its' own characteristic Lewis number. It remains a challenge to determine the reactants whose influences through Le_i are greatest: some composite average of these Le_i 's may be used in a correlation such as equation (4.30) in order to attempt to describe these more complicated and more realistic flames. It would be interesting to repeat our analysis with a more realistic two- or even four-step mechanism, in order to determine, with greater precision, the relation between annihilation time and the relevant Lewis numbers. The previous work of Echehki et al.[3] suggests that with light, highly diffusive species like H_2 , the value of Le for the deficient reactant does not control the flame behavior as strongly as it does here. The qualitative nature of such a system should be evaluated with

a model 2-step reaction scheme, in which one of the intermediate species is much lighter than the others. Our findings therefore appear to be representative only for flames in which (1) The overall chemistry can be safely reduced to a global single step; (2) The Lewis numbers of all species are close to one another and to unity; and (3) The Lewis number of the limiting reactant (deficient species) is used in our formulae. We should caution the reader, however, because this study was not conducted with such a practical aim in mind. After more study, such practical questions might be completely addressed, but given the current paucity of hard evidence, we leave such questions to future work.

In a pedagogical sense, this simple model affords us yet another chance to examine non-trivial premixed flame propagation. That is, we are able to examine and appreciate a premixed flame process that does not conform to the restrictions obeyed by the steadily propagating one-dimensional laminar flame. The latter, though centrally important, is shown in this and other works [8] to be a singular special case. Future work may show that the entire concept of a “flame speed” in complicated transient flows, though useful for a preliminary understanding, is void of meaningful content.

4.8 References

1. Candel, S., and Poinso, T., *Combust. Sci. Tech.*, **70**: 1-15 (1990).
2. Poinso, T., Veynante, D., and Candel, S., *J. Fluid Mech.*, **228**: 561-606 (1991).
3. Echekki, T., Chen, J.H., and Gran, I., *26th Symposium (International) on Combustion, The Combustion Institute*, 323-329 (1997).
4. Chen, C.L., and Sohrab, S.H., *Combust. Flame*, **101**: 360-370 (1995)
5. Daniel, W.A., *Sixth Symposium (International) on Combustion*, Reinhold, New York, (1957).

6. Adamczyk, A.A., and Lavoie, G.A., SAE Transactiona 87, SAE paper # 780969 (1978).
7. Westbrook, C.K., Adamczyk, A.A., and Lavoie, G.A., *Combust. Flame*, **40**:81-99 (1981).
8. Wichman, I.S., and Bruneaux, G., *Combust. Flame*, **103**: 296-310 (1995).
9. Peters, N., *Numerical Methods in Laminar Flame Propagation, a GAMM Workshop*, Braunschweig : vieweg, (1982).
10. Yahagi, Y., Ueda, T, and Mizomoto, M., *24th Symposium (International) on Combustion, The Combustion Institute*, 537-542 (1992)
11. Lee, T., North, G, and Santavicca, D, *Combustion and Flame*, **93**, 445-456 (1993)
12. Rutland, C., and Trouve, A., *Combustion and Flame*, **94**, 41-57 (1993)

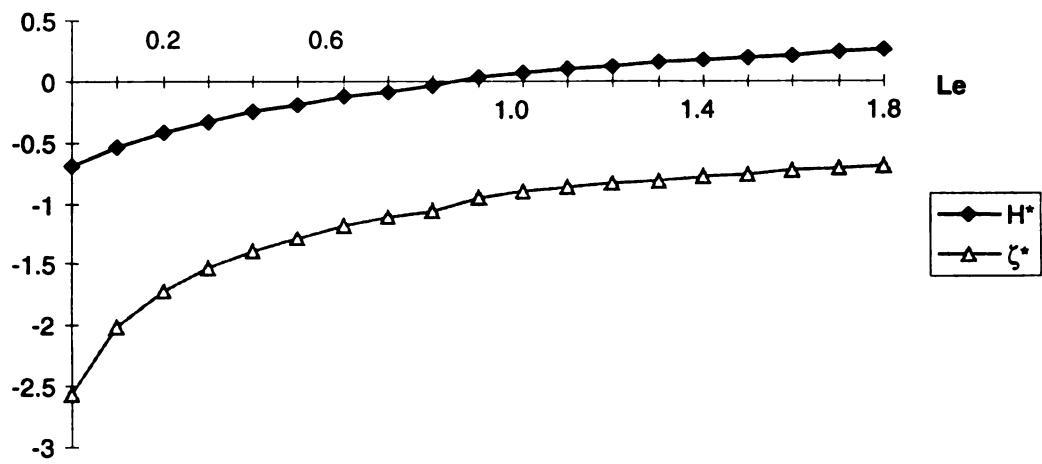


Figure 4.1 Upstream extremum for H and location versus Le .

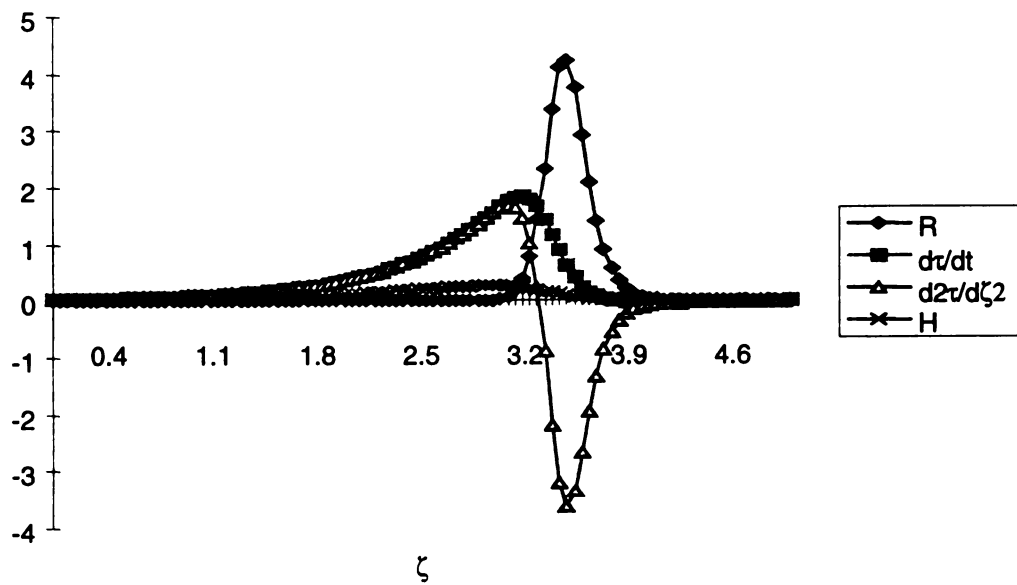


Figure 4.2 $Le=2$, free stream

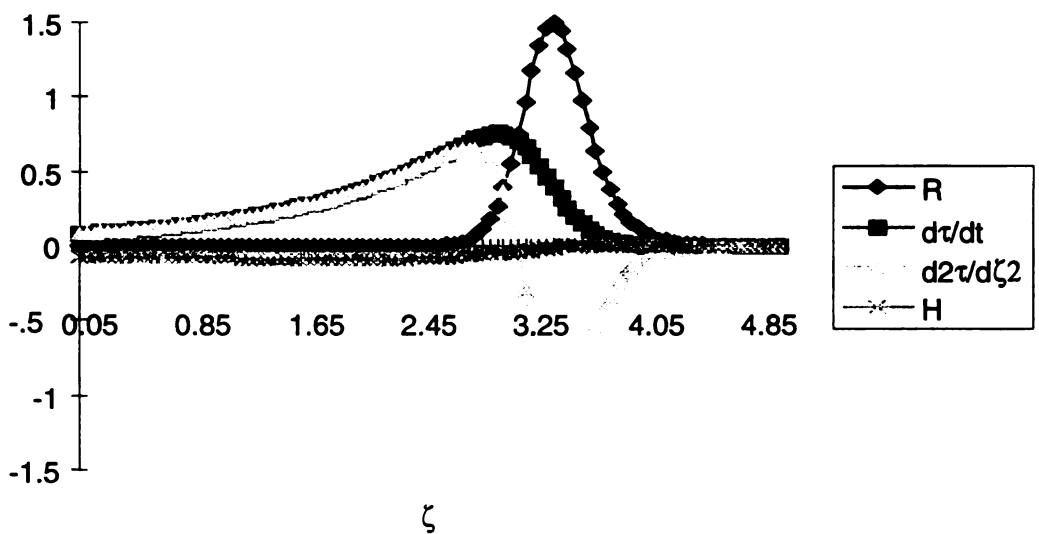


Figure 4.3 $Le=0.8$, free stream

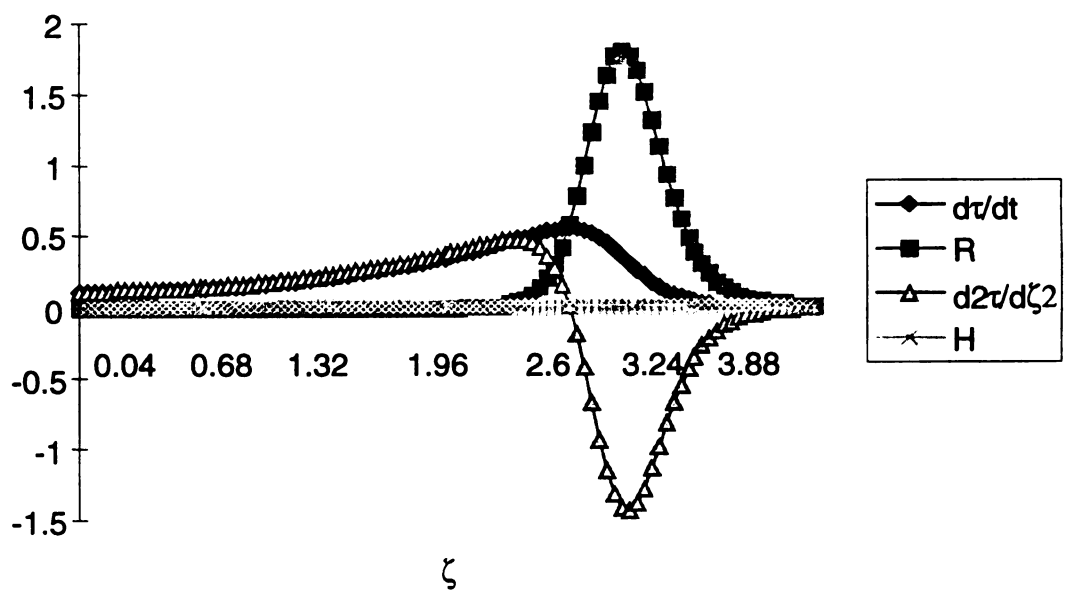


Figure 4.4 $Le=1.0$, free stream

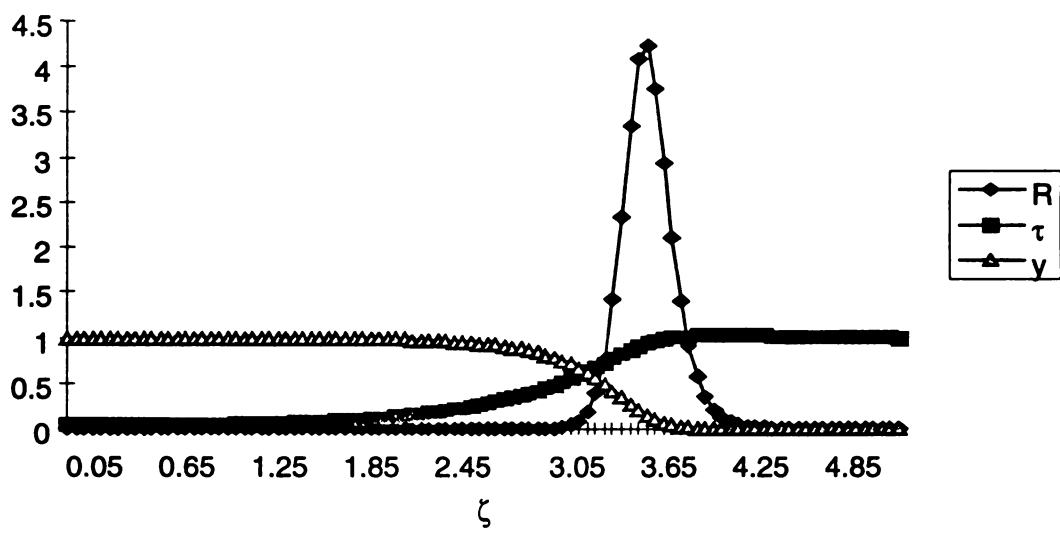


Figure 4.5 $Le=2$, T and Y profiles through reaction zone

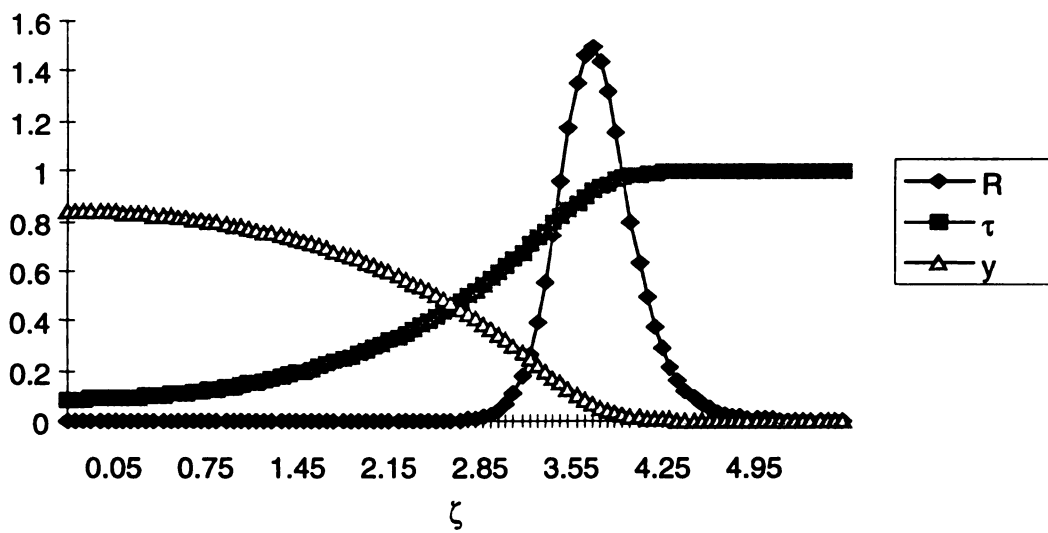


Figure 4.6 $Le=0.8$, T and Y profiles through reaction zone

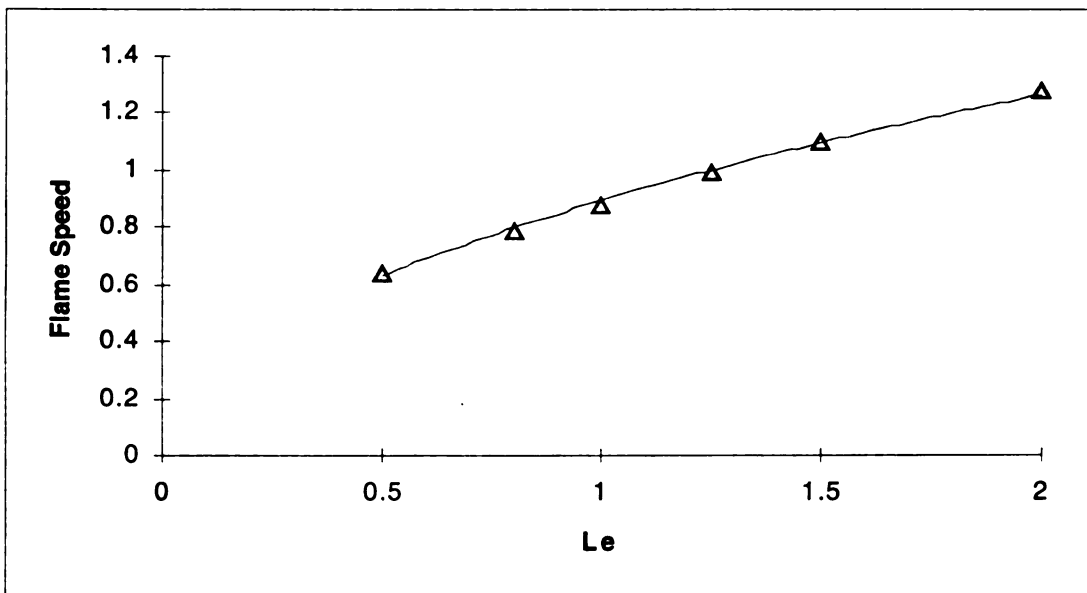


Figure 4.7 Free stream laminar flame speed as a function of Lewis number

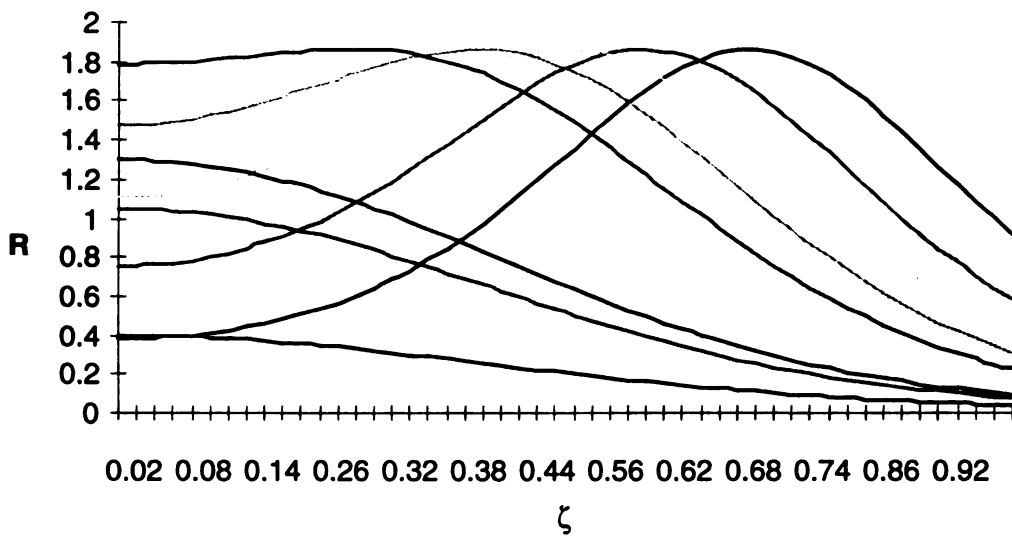


Figure 4.8 $Le=1.0$ Reaction profile through annihilation

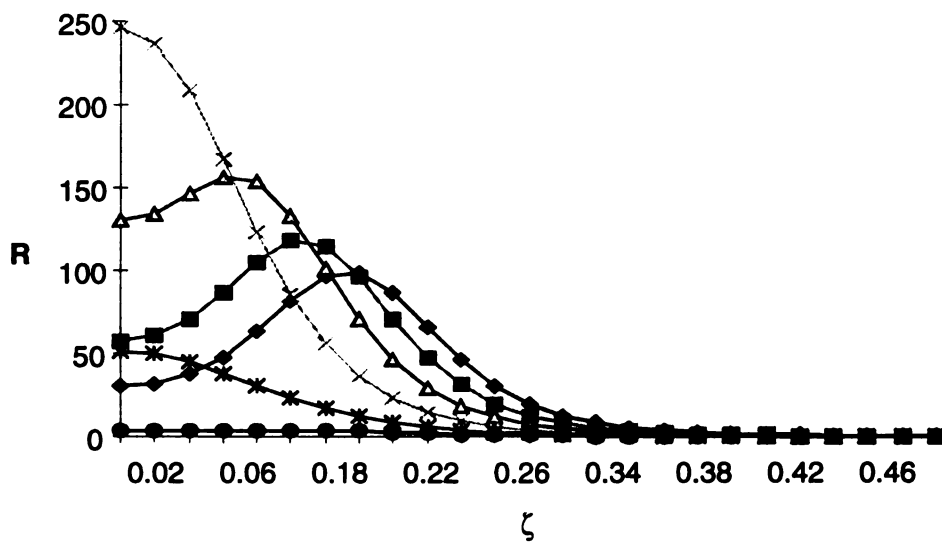


Figure 4.9 Reaction profile for $Le=2.0$ through annihilation

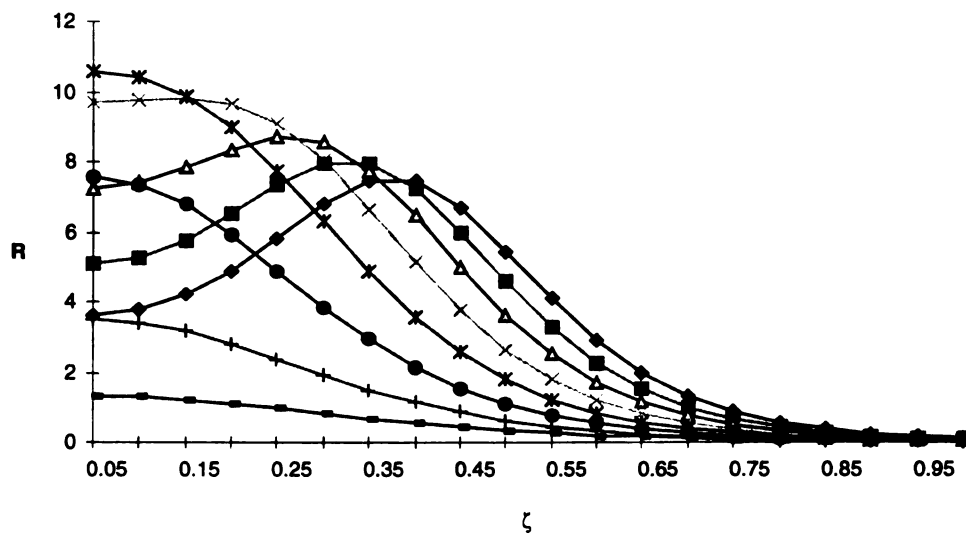


Figure 4.10 Reaction profiles for $Le=1.25$ through annihilation

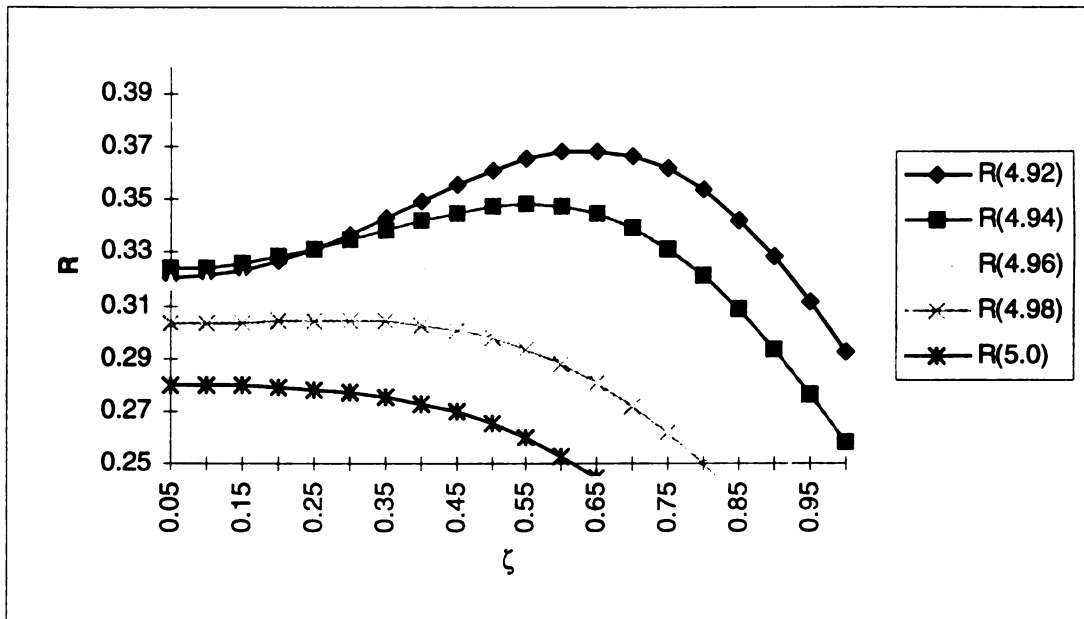


Figure 4.11 Reaction profiles for $Le=0.8$ through annihilation

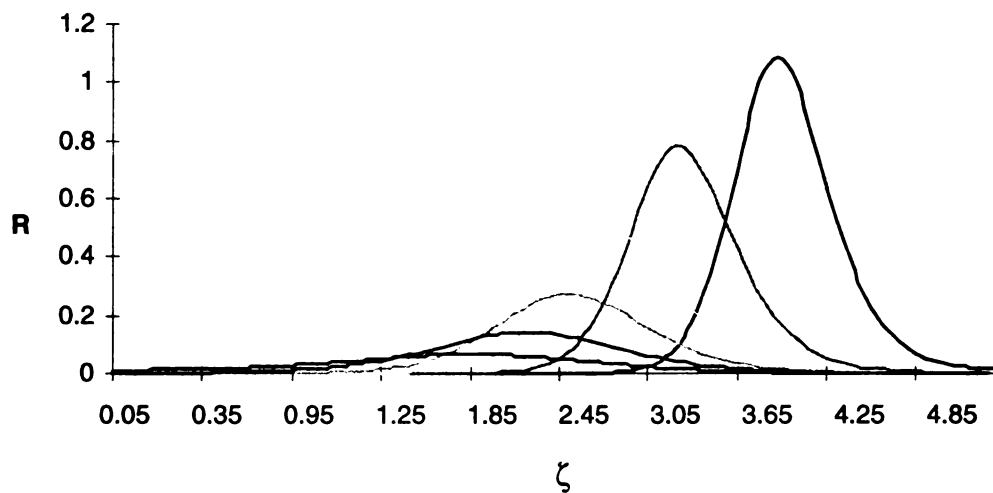


Figure 4.12 $Le=0.5$ reaction profiles during Flame propagation towards junction

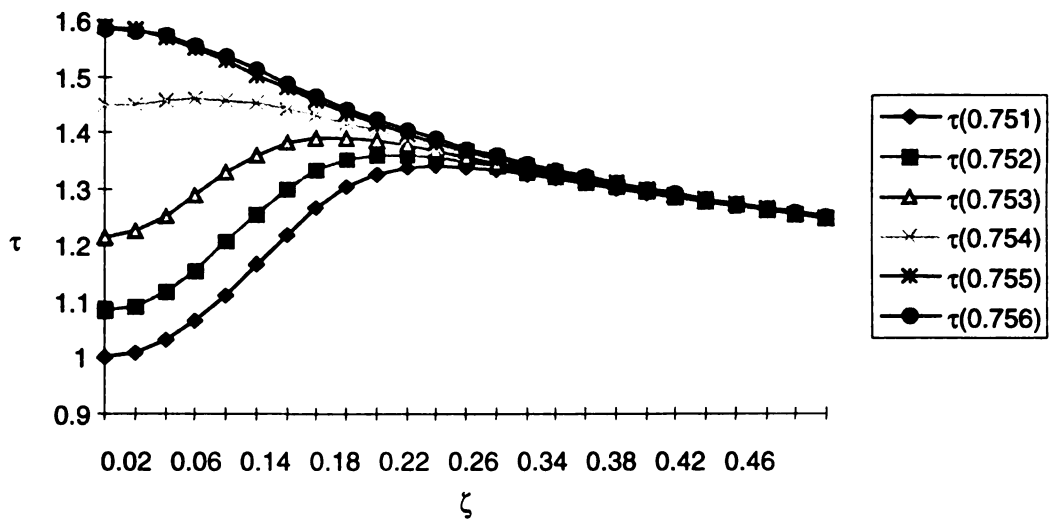


Figure 4.13 Temperature profiles for $Le=2.0$ through annihilation

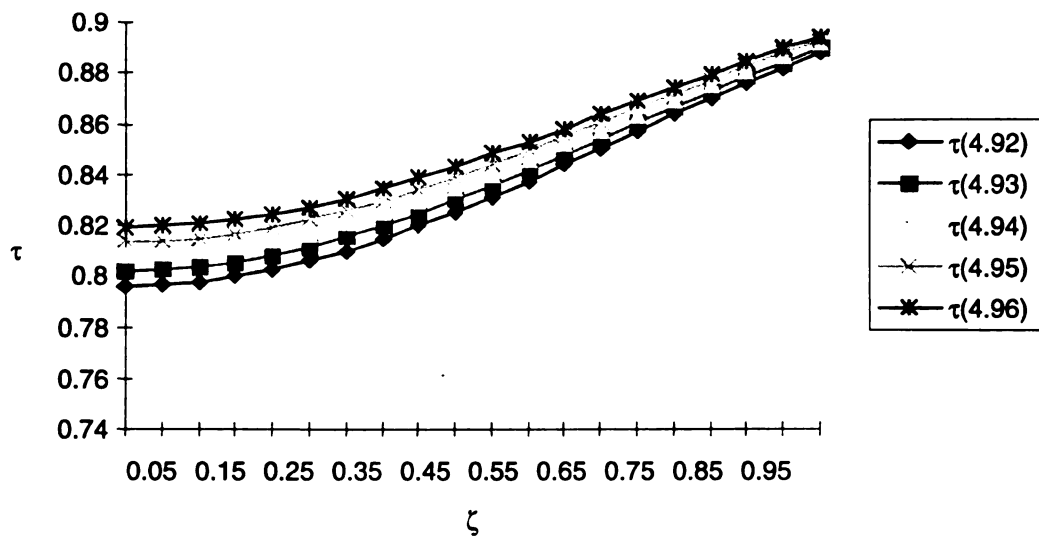


Figure 4.14 Temperature profiles for $Le=0.8$ through annihilation

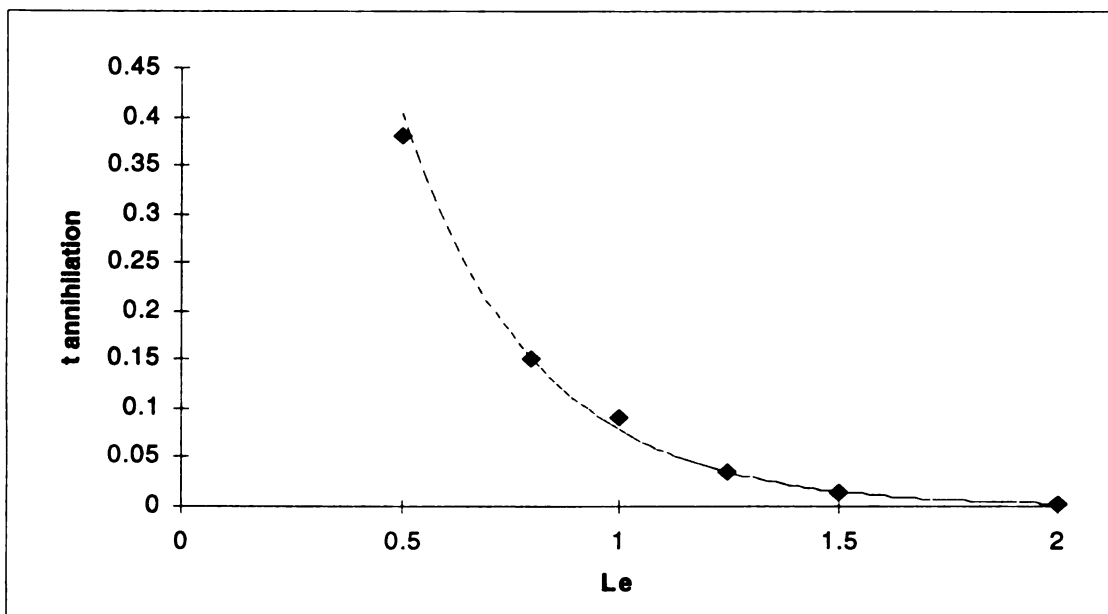


Figure 4.15 Annihilation time versus Lewis number

HEAT LOSS ANALYSIS OF A DIFFUSION

FLAME LEADING EDGE

5.1 Chapter Nomenclature

b	Reduced Damkohler number
C_p	Specific heat
D	Binary diffusion coefficient
Da	Damkohler number
H	Excess enthalpy
l	Half channel width
N	Non-dimensional spatial coordinate
Pe	Peclet number
q	Heat flux
R	Non-dimensional spatial coordinate
r_q	Quenching distance, $(\xi^2 + \eta^2)^{1/2}$ in ξ, η coordinates of figure 5.1
r_q	Quenching distance, $(u^2 + v^2)^{1/2}$ in u, v coordinates of figure 5.2
S	Scaling factor
T	Temperature
U, V	Non-dimensional coordinates $(u/r_q, v/r_q)$
u, v	Dimensional conformal mapping coordinates
v	Velocity
W	Reaction term
w	Non-dimensional reaction term

x,y Dimensional Coordinates
 Y_i Mass fraction of species i
 y_i Non-dimensional mass fraction of species i
 Z Mixture fraction

Greek

α Thermal diffusivity
 α $1-T_0/T_f$
 β Zel'dovich number, $\alpha(E/RT_f)$
 β_i Curve fit parameter
 ϕ Global stoichiometric index
 η Non-dimensional spatial coordinate
 ϑ Heat transfer parameter detailed in Equation(22.a)
 λ Thermal conductivity
 ν Ratio of oxidizer mass to fuel mass
 θ Non-dimensional spatial coordinate
 ρ Density
 τ Non-dimensional temperature, $(T-T_0)/(T_f-T_0)$
 Ξ,ξ Non-dimensional spatial coordinate

Subscripts

F Fuel
f Flame
O Oxidizer

- o Reference boundary value
- q Quench

5.2 Introduction

Real flames interact with surfaces. These interactions may be primary, in which case the interaction of the flame with the surface cannot be ignored in an analysis of flame behavior, or secondary, in which case the solid surface is largely incidental to the combustion process. The flame-surface interaction includes many physical processes: flame chemistry; fluid flow dynamics; and conductive, convective, and radiant heat transfer. For this reason a comprehensive theoretical model is exceedingly difficult, perhaps impossible, to construct. On the other hand, a pure numerical study without theoretical guidance is likely to make few novel observations. A similar statement applies of course to experimentation, thus suggesting that a “democratic” investigation, in which every conceivable influence is equally weighted and seriously considered will surely fail for not making distinctions between what is important and what is unimportant. Consequently, the development of theories for simplified limiting cases is a necessary part of a rational examination. Although theories almost by definition involve the suppression of some physics, this suppression ideally should have a positive, not a negative, aspect. This is adumbrated in the following quotation: “Idealization does not consist, as is commonly believed, in a subtracting or deducting of the petty and secondary. A tremendous expulsion of the principal features rather is the decisive thing, so that thereupon the others too disappear” [1]. Thus, it is the prominence of various model (theory) features that by necessity force the remaining features into the background. Finally, we note from practical experience that large-scale numerical

simulations often employ simplistic “sub-models” in order to describe processes that cannot be fully resolved by the global theory. It is imperative that such “sub-models” faithfully represent the “sub-problem” they purport to describe. They must also be sufficiently integrated with ease into the larger computation.

The purpose of this study is to first examine the leading edge of a flame in terms of the heat transfer during the quenching of a flame leading edge by an adjacent, cold, solid surface. The conductive heat transfer from a flame to a nearby surface is important for ensuring a continued supply of fuel, as in flame spread, or for ensuring flame survival, as in burner-attached flames. In the former case, the transfer of heat from the spreading flame gasifies the solid fuel beneath it, producing the fuel vapors that feed it with reactant. In the latter case, the heating of the burner rim by the flame minimizes transient heat losses, thereby maximizing reactant consumption while preventing possible flame extinction. Studies have recently been completed on various features of flame-wall interaction, in configurations reminiscent of both flame spread [2] and burner-attached flames [2,3].

A second feature of flame-surface interaction that we wish to investigate is the flame behavior as predicted by the relatively simple analysis of the conserved scalar mixture fraction combined with infinitely fast-rate chemical kinetics. As will be shown in comparisons to numerical solutions of the non-linear, finite-rate chemistry problem (model problem “A”), the examination of the mixture fraction field can provide valuable insight into the flame quenching mechanism. In addition, the study of model problem “A” provides the necessary impetus for examining the quenching problem discussed

previously. Nevertheless, certain analytical solutions obtained by these means shall exhibit almost no correspondence with our detailed examination.

From a practical viewpoint, and in terms of material response, the most important quantity to examine is the conductive heat flux, both to the surface and at various locations in the gas. Radiative heat losses are ignored for two primary reasons: in small scale combustion, conductive losses are dominant [4] and under micro-gravity conditions, soot and gas radiation are generally diminished. Currently, we know very little about such conductive fluxes, including their characteristic orders of magnitude or their functional shapes. Although some progress has recently been made in this area [2], we are far from a satisfactory understanding that might enable the use of such estimates in any engineering capacity. Our analysis herein has features in common with reference 5, where the nature of the opposed-flow flame spread over solid fuels was examined in detail. The simplifications provided by employing infinite rate chemistry and an idealized geometry for gas flow and flame spread enabled numerous deductions to be made, which might otherwise have remained hidden in excessive detail. One of these was the seemingly paradoxical result, long since confirmed by numerical examination [6] that the streamwise conductivity through the solid fuel bed plays a minor, almost negligible, role in the rate of flame spread. In addition to the heat flux into walls and surfaces, it is also worth examining heat fluxes across various planes in the gas [5].

Of particular interest in our model problem is the flux directed from the flame leading edge towards the nearby surface. As discussed in [2,7], this flux can change significantly from very large values near the leading edge, where the flame quenches, to much smaller values near the surface, where the gas loses thermal energy to the wall.

5.3 Background

In this chapter we shall examine a greatly simplified heat transfer model problem (model “B”) in the light of a fuller (but still simplified) model “A”. The latter includes finite-rate chemistry. It has been shown in past work that model “A” is an often quantitatively accurate representation of the actual, physical problem [8]. This conclusion was reached by comparing flame behavior in model “A” with a variable property Navier-Stokes simulation.

In this section we shall restate and examine various previous results from the analysis of model “A”. We shall also present various analytical results from this model for the infinite-rate chemistry limit. This examination will be conducted with the intent of providing motivation for a detailed examination of the pure heat transfer model “B” in sections 5.4-5.6 following.

Model “A” describes qualitatively a fuel injector problem and more rudimentarily a general lifted triple flame resembling but different in some features than a flame-spread problem. The model configuration is shown in figure 5.1. The fuel flows past one side of an impermeable, perfectly conducting divider and mixes with the oxidizer stream that flows past its other side. Permeable walls through which fuel and oxidizer separately diffuse are aligned with the bulk flow direction, which is vertical. Depending on the global stoichiometry, the diffusion flame inclines either to the left, to the right, or lies directly downstream of the divider. This model produces a triple flame configuration with a premixed flame arc anchoring the diffusion flame to the lower boundary. The diffusion flame extends downstream from the anchor point. Figure 5.1 shows a schematic of the triple flame configuration, including the fuel-rich and fuel-lean premixed

flames and the trailing downstream diffusion flame arc. The system is assumed to be steady. All boundaries except the divider plate are porous, non-reactive walls, whose temperature is T_o . The velocities, v , of the two streams are identical and specified at the inlet boundary [9,10]. The chemical reaction between the fuel and oxidizer occurs through a single irreversible step. It has been shown [11,12] that, although not capturing all the quantitative characteristics of the flame, single step chemistry captures many qualitative characteristics such as flame structure and temperature. Furthermore, even in multi-step kinetics models, only a few reactions are responsible for a majority of the heat released during combustion. The molecular weights of the reactants are assumed identical, the thermophysical properties ρ , λ , c_p , D are assumed constant, the Lewis numbers of the reactants are equal to unity, the influences are gravity and radiation (from the surface and the gas) are neglected, and Soret and Dufour terms are neglected. The diffusion velocities are given by Fick's law, and heat conduction is described by Fourier's law. Under these restrictions, the equations for conservation of species and energy become

$$\rho v \frac{\partial Y_o}{\partial y} = \rho D \nabla^2 Y_o - vW \quad (5.1.a)$$

$$\rho v \frac{\partial Y_F}{\partial y} = \rho D \nabla^2 Y_F - W \quad (5.1.b)$$

$$\rho v c_p \frac{\partial T}{\partial y} = \rho \lambda \nabla^2 T + qW \quad (5.1.c)$$

where $W = \rho A Y_o Y_F \exp(-E/RT)$ and the boundary conditions are

$$T = T_o, Y_o = Y_{oo}, Y_F = 0 \text{ at } (x = l/2, y \geq 0), (0 < x < l/2, y = 0) \quad (5.2.a)$$

$$T = T_o, Y_o = 0, Y_F = Y_{FF} \text{ at } (x = -l/2, y \geq 0), (-l/2 < x < 0, y = 0) \quad (5.2.b)$$

$$\partial T / \partial y = \partial Y_O / \partial y = \partial Y_F / \partial y = 0 \text{ at } y = \infty \quad (5.2.c)$$

Equations (5.1) and (5.2) can be written more compactly in non-dimensional form. We rescale the independent variables with $l/2$ to obtain $\xi = x/(l/2)$, $\eta = y/(l/2)$ so that $\xi = \pm 1$ in the two corners of figure 5.1. The species mass fractions are normalized as $y_F = Y_F/Y_{FF}$, $y_O = Y_O/Y_{OO}$. Hence, both y_F and y_O are bounded by zero and unity. Similarly, the non-dimensional temperature is $\tau = (T - T_o)/(T_f - T_o)$, whereby $\tau = 0$ on all boundaries and $\tau \rightarrow 1$ at the flame sheet. Finally, the non-dimensional mass flux past the divider is $Pe = \rho v c_p L / \lambda$. Additional physical quantities, which are important to our subsequent analysis, are the global stoichiometric index

$$\phi = \frac{v Y_{FF}}{Y_{OO}} \quad (5.3)$$

where v is the ratio of mass of oxidizer to mass of fuel in the one-step reaction; the Zel'dovich number β , which is a measure of the temperature sensitivity of the reaction

$$\beta = \alpha \frac{E}{RT}, \quad \alpha = 1 - \frac{T_o}{T_f}; \quad (5.4)$$

the Damkohler number, Da , as a ratio of the diffusion time to the reaction time

$$Da = \frac{L^2 / (\lambda / \rho c_p)}{[A Y_{OO} \exp(-E/RT_f)]^{-1}} \quad (5.5)$$

With the adiabatic flame temperature T_f defined as $T_f = T_o + Q Y_{FF} / c_p (1 + \phi)$, the non-dimensional reaction term becomes

$$w = y_O y_F \exp \left[\frac{-\beta(1-\tau)}{1-\alpha(1-\tau)} \right] \quad (5.6)$$

The non-dimensional conservation equations (5.1) can now be written as

$$\text{Pe} \frac{\partial y_O}{\partial \eta} = \nabla^2 y_O - \phi \text{Daw} \quad (5.7.a)$$

$$\text{Pe} \frac{\partial y_F}{\partial \eta} = \nabla^2 y_F - \text{Daw} \quad (5.7.b)$$

$$\text{Pe} \frac{\partial \tau}{\partial \eta} = \nabla^2 \tau + (1 + \phi) \text{Daw} \quad (5.7.c)$$

with $\nabla^2 = \partial^2 / \partial \xi^2 + \partial^2 / \partial \eta^2$. The dimensionless equations (5.2) become

$$\tau=0, y_O=0, y_F=1 \text{ at } (\xi=-1, \eta \geq 0), (-1 < \xi < 0, \eta=0) \quad (5.8.a)$$

$$\tau=0, y_O=1, y_F=0 \text{ at } (\xi=1, \eta \geq 0), (0 < \xi < 1, \eta=0) \quad (5.8.b)$$

$$\partial \tau / \partial \eta = \partial y_O / \partial \eta = \partial y_F / \partial \eta = 0 \text{ as } \eta \rightarrow \infty \quad (5.8.c)$$

Equations (5.7) and (5.8) can be formulated in terms of the excess enthalpy function $H = \tau + y_O + y_F - 1$, the mixture fraction $Z = (1 - Z_f) y_F + Z_f (1 - y_O)$, and τ . Here $Z_f = (1 + \phi)^{-1}$ is the value of Z along the stoichiometric contour. The minimum value of Z is zero at the oxidizer surface, where $y_O = 1$ and $y_F = 0$ and its maximum value is unity at the fuel surface, where $y_O = 0$, $y_F = 1$. For our problem, the maximum possible value of H is zero and the minimum possible value is -1 . Functions Z and H satisfy the homogeneous forms of equations (5.7.a) and (5.7.b), which amounts to a balance between convection and diffusion. The system of equations (5.7) become

$$\text{Pe} \frac{\partial \tau}{\partial \eta} = \nabla^2 \tau + (1 + \phi) \text{Daw} \quad (5.9.a)$$

$$\text{Pe} \frac{\partial Z}{\partial \eta} = \nabla^2 Z \quad (5.9.b)$$

Note that the solution for H is $H=0$ everywhere; the total enthalpy in the gas is constant.

The boundary conditions for equations (5.9) are

$$\tau=0, Z=1 \text{ at } (\xi=-1, \eta \geq 0), (-1 < \xi < 0, \eta=0) \quad (5.10.a)$$

$$\tau=0, Z=0 \text{ at } (\xi=1, \eta \geq 0), (0 < \xi < 1, \eta=0) \quad (5.10.b)$$

$$\partial Z / \partial \eta = \partial \tau / \partial \eta = 0 \text{ at } \eta \rightarrow \infty \quad (5.10.c)$$

The simplest case is $Pe=0$, which produces a purely diffusive problem. The equation for Z is easily solved to give $Z = \pi^{-1} \left[\pi/2 - \tan^{-1} \left\{ \tan(\pi\xi/2) / \tanh(\pi\eta/2) \right\} \right]$. The stoichiometric contour is the arc along which $Z=Z_f$, see figure 5.1. The trailing diffusion flame lies very near this arc, as shown.

These solutions for H and Z can be utilized to produce estimates for the heat flux to the bounding surfaces. This becomes especially straightforward in the case of infinite rate chemistry because the flame is attached to the divider, see figure 5.1. On the fuel side, $\nabla Z = (1 - Z_F) \nabla y_F$, whereas on the oxidizer side $\nabla Z = -Z_F \nabla y_O$. From the constancy of H we have either $\nabla y_F = -\nabla \tau$ or $\nabla y_O = -\nabla \tau$, giving

$\nabla \tau = -(1 - Z_F)^{-1} \nabla Z$ on the fuel side and $\nabla \tau = Z_F^{-1} \nabla Z$ on the oxidizer side. From the preceding solution for Z we find

$$\nabla Z = \hat{\xi} \left[\frac{-\sinh(\pi\eta/2) \cosh(\pi\eta/2)}{2(\sin^2 \pi\xi/2 + \sinh^2 \pi\eta/2)} \right] + \hat{\eta} \left[\frac{\sin \pi\xi/2 \cos \pi\xi/2}{2(\sin^2 \pi\xi/2 \sinh^2 \pi\eta/2)} \right] \quad (5.11)$$

Along the lower surface $-1 < \xi < 1, \eta=0$ we find

$$\nabla \tau = \frac{-\hat{\eta}}{2(1 - Z_F) \tan \pi\xi/2}, \quad -1 < \xi < 0 \quad (5.12.a)$$

$$\bar{\nabla} \tau = \frac{\hat{\eta}}{2Z_F \tan \pi \hat{\xi} / 2}, \quad 0 < \hat{\xi} < 1 \quad (5.12.b)$$

Along the vertical walls at $\hat{\xi} = -1$ and $\hat{\xi} = +1$, we find

$$\bar{\nabla} \tau = \frac{\hat{\xi}}{2(1 - Z_F) \tan \pi \hat{\eta} / 2}, \quad \hat{\xi} = -1 \quad (5.13.a)$$

$$\bar{\nabla} \tau = \frac{-\hat{\xi}}{2Z_F \tan \pi \hat{\eta} / 2}, \quad \hat{\xi} = +1 \quad (5.13.b)$$

From Equation (5.12.a) the heat flux to the divider is infinite because the flame is attached to the divider. However, the fluxes to the nearby surface may possibly be accurately represented by these equations. Part of our goal in this article is to ascertain the accuracy of Eqs. (5.12.a) and (5.13.a) away from the divider, and thus to determine the practical usefulness of infinite-rate Burke-Schumann heat flux calculations.

Equations (5.9) and (5.10) will serve as a benchmark for comparing the Burke-Schumann results and the heat-transfer model results of Section 5.5. These equations will be solved numerically using an Alternating Direction Implicit (ADI) method. Because the use of the mixture fraction and excess enthalpy functions de-couples the species equations from the energy equation, equation (5.9.b) is solved first. Then, using the definitions of Z and H , equation (5.9.a) is solved. The non-linear reaction term in equation (5.9.a) is handled by using the results of the previous iteration, thus linearizing the numerical system.

5.4 Simplified Heat Transfer Model “B”

In model “B” the flame arc becomes a constant temperature line, $\tau=1$, extending downstream from the point r_q , see figure 5.2. The boundary conditions on the surfaces are $\tau=0$ and at $\eta \rightarrow \infty$; we have the zero gradient condition $\partial\tau/\partial\eta=0$ as before. The governing equation is $\nabla^2\tau=0$ in the case of zero convection; $\nabla^2\tau=Pe\partial\tau/\partial\eta$ in the case with uniform and identical convection from the fuel and oxidizer reservoirs adjacent to the divider. The introduction of scaled coordinates $\Xi=\xi/r_q$ and $N=\eta/r_q$ places the flame leading edge at the intersection of the circular arc $R=\sqrt{\Xi^2 + N^2}=1$ and the line $Z=Z_f$. Here r_q is the quenching distance defined as the distance from the divider plate to the point of maximum reactivity. The flame usually quenches a very small distance upstream of the point of maximum reactivity, hence there is no inconsistency in defining quenching distance in this manner. In the general case this transformation offers no advantages for solution because the scaling merely changes the separation distance between the two vertical walls from two to $2/r_q$. When r_q becomes small, however, the vertical walls effectively disappear, and the flame sheet lies along the radially-directed arc $\theta=\pi Z_f$, $1 < R < \infty$. There are no length scales remaining in this problem, leaving a universal heat flux distribution to the lower surface given by $\partial\tau(\Xi,0)/\partial N = g(\Xi; Z_f)$. Here Z_f is the sole remaining parameter in the analysis. In terms of the original coordinates we have

$$\frac{\partial\tau(\xi,0)}{\partial\eta} = \frac{1}{r_q} g\left(\frac{\xi}{r_q}; Z_f\right) \quad (5.14)$$

The maximum flux occurs at the point where the derivative of $\partial\tau(\xi,0)/\partial\eta$ vanishes.

The above expression in equation (5.14) is universal to the extent that the flame curvature can be neglected. If r_q is not sufficiently small, the curvature of the flame towards the vertical axis (see figure 5.1) becomes important and the equation loses accuracy, producing an over-estimate for the surface heat flux. From equation (5.14) the integrated flux along the surface is a function only of Z_f , i.e.,

$$\int_{-\infty}^{\infty} (\partial\tau/\partial\eta)d\xi = \int_{-\infty}^{\infty} g(\Xi; Z_f)d\Xi \equiv Q(Z_f). \quad \text{The function } Q(Z_f) \text{ is not symmetric about}$$

$Z_f=1/2$ because the quench radius is asymmetric with respect to Z_f . It has been shown in reference 2 that Q increases as Z_f decreases, largely because of the increase in the flame temperature. This feature, we observe, is not built into this simplified model.

As shown in previous works [2,9,10] the model configuration of figure 5.1 can be mapped via conformal mapping methods into the configuration shown in figure 5.3. In this latter configuration the flame is in fact a radial arc¹. The heat flux to the surface is $\partial\tau/\partial\eta = (\partial\tau/\partial\nu)(\partial\nu/\partial\eta)$. Analogous to the previous derivation, we define the scaled coordinates $U=u/r_q$, $V=v/r_q$, where $r_q = \sqrt{u_q^2 + v_q^2}$ and $\sqrt{U^2 + V^2} = 1$ at the semicircular arc containing the flame leading edge. Then $\partial\tau/\partial\eta = (\partial\tau/\partial V)(\partial V/\partial\nu)(\partial\nu/\partial\eta)$, with $\partial\tau(U,0)/\partial V \equiv g(u/r_q; Z_f)$, $\partial V/\partial\nu = 1/r_q$ and $\partial\nu/\partial\eta = (\pi/2)\cos\pi\xi/2$ at the surface $\eta=0$. Thus

$$\frac{\partial\tau}{\partial\eta} = g\left(\frac{\sin\pi\xi/2}{r_q}; Z_f\right) \frac{\pi\cos\pi\xi/2}{2r_q} \quad (5.15.a)$$

$$r_q = \sqrt{u_q^2 + v_q^2} = \sqrt{\sin^2(\pi\xi_q/2) + \sinh^2(\pi\eta_q/2)} \quad (5.15.b)$$

For small ξ_q and η_q we find $r_q = (\pi/2)r_q$ in which case equation (5.15.a) corresponds with equation(5.14).

Numerical solutions of this heat transfer model are generated in Section 5.5 for the heat flux to the surface.

5.5 Results and Discussion

To begin the analysis, comparisons are made between the finite-rate chemistry model “A”, the Burke-Schumann, and the conduction heat transfer model “B” predictions of the heat flux distribution to the lower cold boundary. Here, it is assumed that the diffusing reactants at $\eta=0$ have the constant temperature, T_0 . In figures 5.4a-b the results from each model are presented for a vertical flame with $Z_f=1/2$ at two different quenching distances. Comparisons are also made for a fuel-lean and a fuel-rich flame in figures 5.5a and 5.5b respectively. The results presented are for the Burke-Schumann (B-S) solution for the heat flux, the heat flux obtained by solving the finite rate chemistry equations (model “A”), and the heat flux from the simplified heat transfer model “B”.

Examination of the stoichiometric flames in figures 5.4a and 5.4b reveal two important features. First, the Burke-Schumann solution given by equations (5.12.a,b) offers very different results for both large and small quench distances when compared to either the heat conduction and the finite chemistry models. Second, the simple heat conduction model captures most of the characteristics of the finite chemistry model, although the heat flux magnitude is slightly diminished. If a scaling factor is employed, better agreement is achieved. These results are for a pure diffusion flame with no convection ($Pe=0$).

¹ This is only strictly true in the zero convection case, $Pe=0$

The reaction zone characteristics for model "A" differ from those used in model "B". The conduction model is based on a flame sheet consisting of an infinitesimally thin reaction zone, which extinguishes a finite distance r_q from the divider plate. By contrast, the finite-rate chemistry case produces a more broadly spread reaction zone. Given this condition, it is expected that the heat transfer model will under-predict the heat loss for the pure diffusion case, as well as have a narrower peak. These characteristics are indeed observed in figures 5.4-5. Consistent with this, the conduction model produces better agreement with the finite rate case as the quenching distance, r_q , decreases.

For the non-symmetric case $Z_f \neq 1/2$ (see figure 5.1), the flame shape will be defined by the following relation between the flame-shape coordinates ξ and η :

$$\xi = \frac{2}{\pi} \tan^{-1} \left\{ \frac{\tanh\left(\frac{\pi\eta}{2}\right)}{\tan\left(\frac{\pi}{2} - \pi Z_f\right)} \right\} \quad (5.16)$$

Figures 5.5a and 5.5b show the results for two non-stoichiometric cases. The simplified model follows well the trends of the finite rate case. The model produces a maximum heat flux at a slightly different location along the lower surface than predicted by the finite rate chemistry case. The conduction model shifts the maximum away from the divider. This can be attributed to the wider flame tip for the finite-rate chemistry case. Even with this shift the heat transfer model is closer to the finite rate chemistry case than the Burke-Schumann solution. There also exists a strong asymmetry for the non-stoichiometric flames. Departures towards the fuel rich side produce closer quench distances, and consequently, larger heat losses to the lower boundary. The maximum heat flux location is also closer to the divider.

Some generalizations about the shape of the heat flux profile can be made. We wish to provide a better approximation for the heat loss profiles than those given by the readily available Burke-Schumann solution. We also seek to ascertain where, if at all, the Burke-Schumann solution accurately represents the heat flux to the lower boundary.

The heat flux profiles for small quenching distances ($r_q < 0.15$) obtained from model "B" were found to collapse to a single curve. This collapse of the heat flux profiles is predicted theoretically in section 5.4 by equation (5.14). The correlations were obtained for both straight flames and non-stoichiometric flames. These curve fits were obtained by using an ordinary least squares method. The correlations are non-linear so a Gauss iteration scheme was used.

For symmetric ($Z_f = 1/2$) flames, the heat flux profile can be described by the three parameter relation given below

$$q = \frac{0.572}{r_q} e^{-\left|\frac{\xi}{r_q}\right|^{\beta_1}} \left(\left|\frac{\xi}{r_q}\right| + \beta_2\right)^{\beta_3} \quad (5.17)$$

Parameters β_1 , β_2 , and β_3 are 1.07, 1.01 and 0.8 respectively. Note that this result does not include any scaling factor; it is solely the shape of the heat flux profile obtained from the conduction model. Although this result is applicable only for small quenching distances, the same shape can be applied to larger quenching distances by changing the numerical parameters β_1 , β_2 , and β_3 .

It is more challenging to model the non-symmetric flames because several quantities must be taken into account. The maximum heat loss is shifted away from the divider, and the spatial decay rates are different on each side of the maximum. The

inflection points of the heat flux profile are located at several different distances from the maximum. To account for these characteristics a five parameter correction factor, $c(\xi)$, is introduced, viz.

$$c(\xi) = \left[\beta_4 \left(\frac{\xi}{r_q} - \beta_5 \right) + \beta_6 \left(\frac{\xi}{r_q} - \beta_5 \right)^2 \right] \exp \left(-\beta_7 \left| \frac{\xi}{r_q} - \beta_5 \right|^{\beta_8} \right) \quad (5.18)$$

With this correction factor the heat flux profiles take the form

$$q = \frac{0.572}{r_q} \left(e^{-\left| \frac{\xi}{r_q} \right|^{1.07}} \left(\left| \frac{\xi}{r_q} \right| + 1.01 \right)^{0.8} - c(\xi) \right) \quad (5.19)$$

The five-parameter values are dependent on the stoichiometry parameter ϕ . Table 5.1 shows values of β_4 to β_8 for selected ϕ values.

The above results can be used in conjunction with a scaling factor (see next section) to obtain a good approximation for the heat flux profile to the lower boundary.

The case with convection is not considered in the numerical model or in the analytical model. However, as the discussion of section 5.4 makes clear; when the quenching distance is small, the heat flux profiles should closely resemble the zero-convection case. This occurs because a rescaling of the independent variables in the governing equations with r_q will eliminate the convective terms as $r_q \rightarrow 0$. Figure 5.6 shows the results when $Pe=1$. The quenching distance is computed for the finite rate chemistry case used to determine the heat flux profile from the simple conduction model.

From figure 5.6 we observe first that the model predicts well the heat flux profile. The qualitative shape of the heat flux profile is identical to the zero convection case.

Once again, it appears all that is needed for complete agreement whenever Pe is changed is the introduction of a different numerical scaling factor in equation (5.19).

5.5.1 Scaling Factor

In order to account for the difference in reaction zone thickness between the model and the finite rate chemistry case a scaling factor S was introduced. Factor S scales the maximum heat flux from the heat transfer model to the value obtained in the finite rate chemistry case. Values of S were obtained for stoichiometric flames and then tested with non-stoichiometric flames to determine whether these values were still valid. Factor S was obtained as functions of the quenching distance, not the chemical parameters such as the Zel'dovich number, for which the dependence is much weaker than quenching distance. It is noted that the quenching distance depends on the chemical parameters. Hence, the scaling factor was correlated with the quenching distance. The relatively weaker β and Damkohler number dependence manifests itself implicitly through the effects of the reaction zone thickness on the quenching distance.

It was found that for the stoichiometric flame, S had a nearly linear dependence on r_q . The relationship is shown below

$$S = 1.72r_q + 0.66 \quad (5.20)$$

Equation (20) can be used as a direct multiplication factor in equation (5.19) for small deviations from stoichiometric flames, $0.33 < \phi < 3.0$, with S values within 10 percent of the numerical results.

5.5.2 Comparison of centerline heat losses

Examination of the temperature profile along the stoichiometric contour $Z_F = 1/2$ for vertical flames is used to verify the scaling factor as well as to identify any

shortcomings of the proposed heat transfer model. The preliminary comparison was done for a moderately small quenching distance, $r_q=0.375$, and a pure diffusion flame. The quenching distance was calculated by using the finite-rate chemistry code to solve for the quenching location, as defined by the maximum reactivity, as well as the vertical temperature distribution at the centerline. The resulting quench distance was employed in the heat conduction model and the temperature profile was calculated. A graphical comparison is shown in figure 5.7.

From figure 5.7 we observe that the heat conduction model underpredicts the heat loss to the divider plate. This is expected in view of the relative magnitude of the heat loss profiles to the lower boundary. Furthermore, as expected, if a ratio of the finite rate gradient to the heat transfer model gradient is examined it will produce the scaling factor S already examined. With this information, and noting that the scaling factor had a small dependence on the Zel'dovich and Damkohler numbers which will be ignored here, the gradient ratio should behave very similarly to the scaling factor with respect to r_q . We recall that S varied nearly linearly with the quenching distance. Examination of that relationship in equation (5.20) suggests that the heat conduction model gradient will approach the finite rate model gradient as the quenching distance becomes small.

Another feature shown in figure 5.7 is the different flame temperatures of the two codes. The heat conduction model assumes a flame temperature of 1.0 for the flame and uses that elevated value as its quasi-heat source. The finite rate model temperature is calculated from the set of partial differential equations shown in section 5.3. The finite rate model produces a lower flame temperature, as expected, since $\tau_{\text{flame}} \approx 1-O(\beta^{-1})$. This contributes to the more gradual decline in temperature towards the lower wall, and

consequentially the more linear gradient. This linear gradient supports the simplified notion of assuming a linear profile from the quench location to the wall [2,10]. However, this assumption is typically based on an adiabatic flame temperature close to unity (i.e., $\beta \rightarrow \infty$ limit), and does not take into account any heat losses through the reaction zone. The heat loss from the reaction zone in the finite-rate model “A” is evident beginning near $\eta=0.5$ and continuing to the location of the heat-transfer model flame tip at $\eta=0.375$.

5.5.3 Comparison to Finite-Chemistry Model

A comparison of our heat transfer results may be made to the finite-rate chemistry model examined in [2,10]. The heat transfer cold wall beneath the flame leading edge is given by

$$q = \frac{\vartheta}{b_q^{3/2}} \sqrt{\frac{Da}{\beta^3}} \frac{4}{\pi} (1 - Z_f)^{1/2} \sin^2(\pi Z_f) \quad (5.21)$$

where

$$\vartheta = 1 + \left\{ (1 - Z_f) \left(\frac{\sin \pi(Z_f - \delta_O)}{\sin \pi Z_f} - 1 \right) + Z_f \left(\frac{\sin \pi(Z_f + \delta_F)}{\sin \pi Z_f} - 1 \right) \right\} \quad (5.22.a)$$

$$b_q = 3.752 \left\{ 1 - \exp(-7.366 Z_f^{1.71}) \right\} Z_f^{0.36} \quad (5.22.b)$$

and $\delta_O = Z_f(1 - \tau_q)$, $\delta_F = (1 - Z_f)(1 - \tau_q)$, where τ_q , the flame leading edge quenching temperature, is given by $1 - \kappa/\beta$. It is shown in section 5.5.2 of [2] that a value of κ of between 1.5 and 2 is reasonable. We use $\kappa=1.75$. For the symmetric case $Z_f=1/2$ we find $\delta_O = \delta_F = \kappa/2\beta$, whereby $\vartheta = \cos \pi \kappa/2\beta$ and $b_q = 2.62$, giving $q = 0.21 \cos(\pi \kappa/2\beta) (Da/\beta^3)^{1/2}$.

The use of $\kappa=1.75$, and $\beta=8.0$ gives the estimate $q \cong 0.198 (Da/\beta^3)^{1/2}$. In order to relate this result to the quench distance, we employ equation (8) of [2], which gives

$$r_q = \frac{2 b_q^{3/2}}{\pi 4Z_f (1-Z_f)^{3/2}} \sqrt{\frac{\beta^3}{Da}} \quad (5.23)$$

where we have used the factor $\pi/2$ to convert the r_q of equation (8) of [2] from the $u-v$ system of coordinates to the $\xi-\eta$ coordinates used here, as outlined in section 5.4, see equation (5.15.b) et equation. The preceding numbers give $r_q \cong 3.82(\beta^3/Da)^{1/2}$, whereby, $q \cong 0.76/r_q$, which compares favorably with equation (5.17), $q \cong 0.57/r_q$, especially when we consider that the latter must be multiplied by a scaling factor greater than unity given by equation (5.20). Consequently, the heat transfer model prediction is functionally consistent with the more detailed finite chemistry model. In addition, and in contrast with reference [2], the heat transfer model produces an expression for the distribution of q along the entire surface, not only its maximum value. For this reason, it is possible to replace the factor $0.572/r_q$ in equation (5.17) with equation (5.21), using equation (5.22a,b) for ϑ and b_q respectively. The pure heat transfer formula now includes the influences of finite-rate one-step chemistry. A similar replacement, of course, may be made in equation (5.19) for the asymmetric case.

5.5.4 Zel'dovich number effects

As stated previously, the temperature gradients at the lower boundary produced by the two models show better agreement as r_q decreases. That is not to say that the profiles become more similar under this criterion. The presented profiles can be divided into three general regions: the flame tip region, the wall region, and the transition region which connects the two aforementioned regions. As will become evident from figures 5.8a and 5.8b below, the transition region between the two models have distinctly different shapes. The conduction model produces a much steeper gradient immediately

after the flame tip and a much smaller gradient at the wall. Hence the transition region is much more curved than the nearly linear temperature profile produced by finite rate chemistry model. Having noted that the profiles agree well in the wall region when the flame quenches very close to the lower boundary and that the transition regions will have their own characteristics, it is of interest to find the conditions where the flame tip regions exhibit agreement.

The finite rate model produces a flame temperature that is lower than the adiabatic flame temperature. This suggests that for the flame tip regions to agree, the finite rate model should produce a flame temperature closer to the adiabatic temperature assumed for the conduction model. This can be achieved by increasing the Zel'dovich number, β , which also has the effect of increasing the quench distance. This produces a higher flame temperature and lower heat losses through the flame tip, thus improving agreement in the flame tip region of the temperature profiles. However, the gain in agreement in one region reduces it in another, as can be seen in figures 5.8a and 5.8b. Agreement may also require an unrealistically large value of β .

The Zel'dovich number also depends on the wall temperature T_o through the relation $\beta = (E/RT^2)(T_f - T_o)$. When all quantities other than T_o are fixed, it is possible to examine the influences of wall temperature on heat flux and flame quenching distance. Since $q \approx 0.57/r_q$ and $r_q \propto (T_f - T_o)^{3/2}$, we find $q \propto (T_f - T_o)^{-3/2}$, $dr_q/dT_o \propto -(T_f - T_o)^{1/2}$, and $dq/dT_o \propto (T_f - T_o)^{-5/2}$. Thus as T_o increases, r_q vanishes at a successively decreasing rate while q increases at a successively increasing rate. Under practical conditions, we expect that the near-wall flame tip can heat the wall, raising T_o and decreasing r_q , while

increasing q . It is not clear how long this incremental process can continue, for there are upper bounds on the chemical production of heat that leads to q .

5.5.5 Characteristic Flame-Tip Width

For small r_q , a practical estimate of the width of the triple-flame structure, shown as the lowermost arc of figure 5.1, is obtained by exploiting the relationship for $q(\xi)$ given by equation (5.17). We note the closeness of β_1 , β_2 , and β_3 to unity and write $q(\xi) \approx C \exp(-\xi/r_q)(1 + \xi/r_q)$, where $C = 0.572/r_q$. This function possesses an inflection point at $\xi = r_q$, which we interpret as a measure of the triple-flame tip structure half-width, l_r .

Thus, we write

$$l_r \approx 2r_q \propto \beta^{3/2} \exp(E/2RT_f) \quad (5.24)$$

This result agrees with a previously derived estimate [3]. As the flame temperature increases, all else remaining constant, both β and the exponential factor decrease. Hence, l_r decreases exponentially and algebraically as flame temperature increases. Conversely, as the non-dimensional activation energy increases, l_r increases exponentially.

5.5.6 The q - r_q Relationship

In our study, the relation (5.17) was derived for infinite-rate chemistry and the modifications of section 5.5.3 were appended under the approximation that the infinite-rate chemistry limit was a reasonably accurate approximation. In this case, the essential prediction is $qr_q \sim O(1)$ and constant. We expect this relation to apply in a broad middle range but not at the extremes $q \rightarrow \infty$ ($r_q \rightarrow 0$) and $q \rightarrow 0$ ($r_q \rightarrow \infty$). The latter limit may be interpreted as flame liftoff, whereas the former as flame extinction. Liftoff, followed eventually by blowoff, occurs when heat losses to solid boundaries cannot be sustained.

The separation distance between surface and flame increases until the flame effectively no longer interacts with the surface. At blowoff, even gas-phase flaming becomes impossible. Extinction, on the other hand, occurs when the flame loses too much heat to the surface to survive. It produces enough heat that lifting is not necessary, but the losses to the surface become excessive. Our numerical integrations have in fact produced both limiting cases, although the detailed description is beyond the scope of this article. Nevertheless, it appears that the extinction limit is attainable without radiant losses from the flame tip, without thermal expansion of the gas, or without buoyancy. All that is required for a minimalist description is chemical heat production and conductive surface losses.

5.6 Comparison with Experimental Results

The relationships derived in section 5.5.3 allow calculations to be performed when all pertinent information about the problem is known, such as the overall heat release, stoichiometry, chemical rate data for a one-step global reaction, etc... Such data readily available for many hydrocarbon fuels such as methane (CH₄) or Propane (C₃H₈), though the accuracy of one-step reaction data is suspect as will be seen below. These two fuels are used to estimate the heat flux profiles along the nearby cold boundary and the methane estimates for the maximum heat flux are compared to experimental data.

The information used in conjunction with the equations in 5.5.3 was found in reference 13, and appears in table 5.2. The constants A, m, and n correspond to the rate equation given below.

$$\frac{d[C_x H_y]}{dt} = -A \exp(-E_a/R_u T) [C_x H_y]^m [O_2]^n \quad (5.25)$$

where A is a pre-exponential factor, m and n represent independent reaction orders, and E_a is an activation energy. All units are consistent with gmol-cm-sec.

Table 5.2 Reaction information for Methane and Propane

Fuel	A	m	n	E_a/R_u ($^{\circ}$ K)	HHV(KJ/Kg)
CH ₄ ¹	8.3×10^5	-0.3	1.3	15098	55,528
CH ₄ ²	1.1×10^{18}	1	2	15100	55,528
C ₃ H ₈	8.6×10^{11}	0.1	1.65	15098	50368

These values were used to obtain estimates for the flame temperature and quenching distance for various stoichiometries. Note that there are two different global reaction schemes used for Methane/Oxygen combustion. The two are included to show the large discrepancies in these models and how they effect the final estimates. The results appear in figure 5.9 and 5.10 for Methane and figure 5.11 for Propane.

Examination of figure 5.9 shows that the heat flux distribution is fairly flat across the lower boundary for fuel lean cases ($\phi < 1$) and become more defined when the fuel rich case ($\phi > 1$) is examined. The broadness of the heat flux profile is due to a large quenching distance of the flame. As ϕ increases, the flame tends to be able to survive closer to the lower boundary and hence produces a larger heat flux. This is a characteristic that is witnessed for both fuels and is primarily caused by the increase in the adiabatic flame temperature for fuel rich mixtures. The profiles for Methane combustion using the second global reaction scheme are much more defined. This is due to the increased rate of reaction predicted by the second scheme and hence the flame can survive closer to the cold boundary.

Two experimental studies were used to serve as benchmarks for our model. The first involved a burner-attached flame burning Methane fuel [14]. In this study, the fuel

was flowing into a quiescent oxygen environment so the present model, which assumes zero convection, may not be entirely appropriate. Additionally, the second experimental study involves both flowing fuel and oxidizer, in this case air [15]. The heat flux distribution is not examined in either of the above cases but the maximum heat flux information can be obtained. With all the above differences it is expected that the comparisons will be able to yield an order of magnitude estimate, and help validate the results from our study.

For both the studies examined a stoichiometric mixture is assumed, that is ϕ is taken to be unity. From reference 14 it is found that the maximum heat flux is on the order of 1 W/cm^2 while for the co-flowing reactant case [15] finds q''_{max} to be roughly 2 W/cm^2 . Comparisons with figure 5.9 show that the maximum heat flux for $\phi=1$ is on the order of 1 W/cm^2 , while figure 5.10 shows a maximum heat flux of order 5 W/cm^2 . Both these results show the maximum heat flux to be on the same order and agree well with experimental results thus adding credibility to the proposed heat flux distribution for burner attached flames.

5.7 Conclusions

The conductive heat transfer sub-model reproduces many of the global features of the finite rate chemistry case. The profiles at the lower boundary are similar for both models with only a scaling factor needed to produce accurate agreement. However, when examining the temperature profiles along the centerline of the lifted flame the two models can produce significantly different results for the transition region and the flame tip region, especially as the quenching distance increases. This can be partially attributed to the assumption of a flame sheet in the heat transfer model, which differs from the non-

zero flame thickness produced by finite rate chemistry. The conduction heat transfer model is unable to accurately predict the heat loss from the flame tip, even for pure diffusion flames. For this reason the conduction model is not useful for describing thermal phenomena close to the flame tip, but is very useful in examining events away from this region as is generally true for other heat transfer models of detailed flame process [5]. This limitation might be overcome by introducing a volumetric heat generation term into the conduction model that has temperature dependence, but this is a subject for future study.

For modeling finite rate chemistry influences on the heat flux, we recommend a combination of equations (5.17) [or (5.19)] and (5.21), with the later being substituted for the factor $0.572/r_q$ appearing in the formula. This combined equation accurately predicts the flux beneath the flame leading edge and also its distribution along the surface.

It is also noted that the results obtained herein may be limited to configurations closely resembling the slot configuration used in this work. The heat flux profiles for other lifted flames with different physical and flow orientations may produce different correlations. It is a limitation of the work that the methods used here will need to be followed for different problems. However, the usefulness of the results is not diminished for this lack of adaptability. The general result of our research is to show that beneath the flame tip $q \sim O(1/r_q)$, where $r_q \sim O([\beta^3/Da]^{1/2})$, to within a multiplicative function of global stoichiometry. Although this result may be deduced by simple dimensional analysis and scaling arguments, we have in addition quantified the heat flux distribution beneath the flame tip.

5.8 References

1. Nietzsche, F., *Twilight of the Idols*, R.J. Hollingdale (translation), Penguin, London, (1968)
2. Wichman, I.S., Pavlova, Z., Ramadan, B. and Qin, G, *Combustion and Flame*, **118**, 651-668 (1999)
3. Wichman, I.S. and Ramadan, B., *Phys. of Fluids*, **10**, 3145-3154 (1998)
4. Williams, F.A., Combustion Theory, 2nd Ed., Benjamin-Cummings, Menlo Park, CA. (1985)
5. Wichman, I.S., and Williams, F.A., *Combustion Science and Technology*, **32**, 91-123, (1983)
6. DiBlasi, C. and Wichman, I.S., *Combustion and Flame*, **102**, 229-240 (1995)
7. Wichman, I.S., Lakkaraju, N. and Ramadan, B., *Combustion Science and Technology*, **127**, 141-165 (1997)
8. Ramadan, B., Personal Communications, (1997-1998)
9. Wichman, I.S., *Combustion Science and Technology*, **64**, 295-313 (1989)
10. Wichman, I.S., Pavlova, Z., Ramadan, B., "Attachment of Diffusion Flames Near Cold, Chemically Inert Surfaces With and Without Reactant Flow", MSU CRL 09-24-96 (1996)
11. Rightly, M. L., Williams, F. A., *Combustion and Flame*, **101**, 287-301 (1995)
12. Hsu, P., Matthews, R.D., *Combustion and Flame*, **93** n. 4, 457-466 (1993)
13. Turns, S.R., An Introduction to Combustion second edition, McGraw-Hill, (2000)
14. Robson, K. and Wilson, M., *Combustion and Flame*, **13**, 626-634 (1969)
15. Takahashi, F. et al., 1988. ,*Journal of Heat Transfer*, **110**, 182-189 (1988)

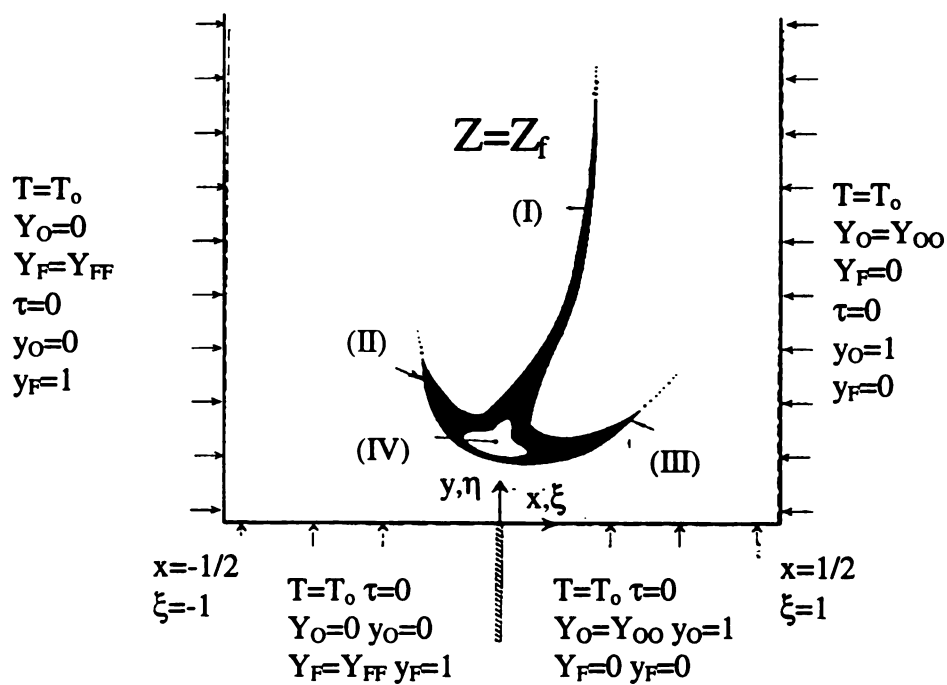


Figure 5.1 Model configuration and boundary conditions. The side and lower walls are porous to reactants. The vertical walls admit only diffusive fluxes. In the far field the diffusion flame is one-dimensional. The near field triple flame structure is shown, with (I) as the diffusion flame, (II) and (III) as rich and lean premixed flame arcs, and (IV) as the triple point or leading flame edge

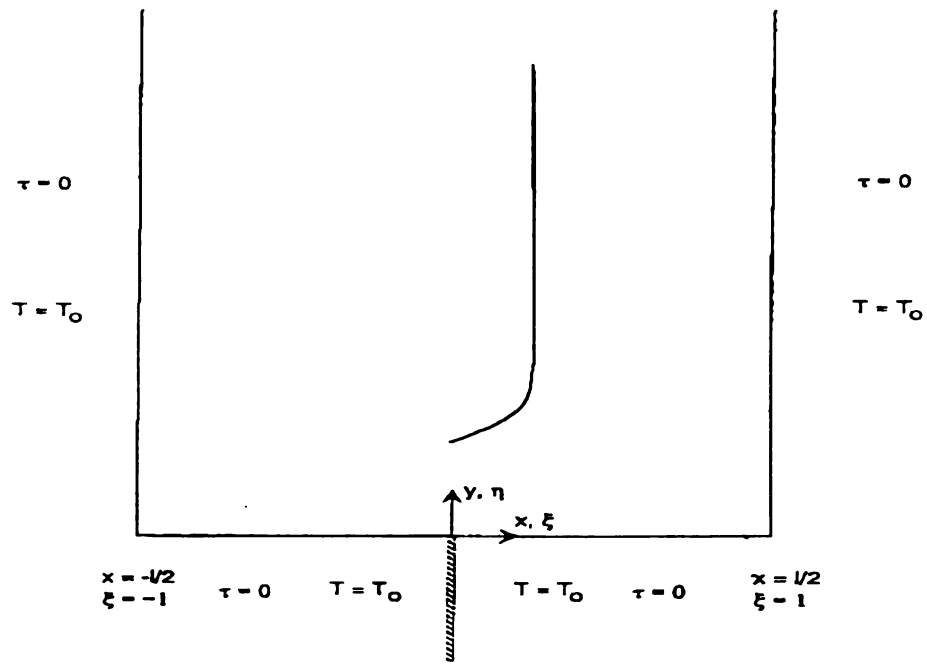


Figure 5.2 Heat transfer model for infinitesimally thin flame sheet and isothermal boundary conditions. This model is the heat transfer simplification of the flame in figure 5.1 because by far the greatest heat release is along the diffusion flame arc

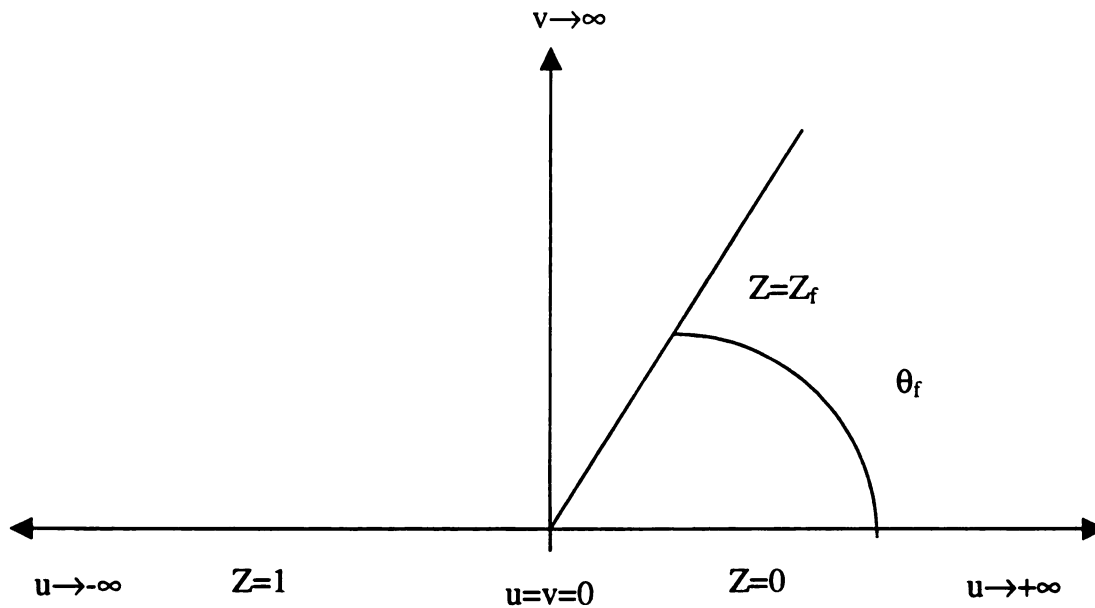


Figure 5.3 Model configuration of mixture fraction Z after conformal mapping. Note that the straight diffusion flame along $Z=Z_f$ occurs only in the case of zero convection. In addition, lines of constant Z are radially-directed arcs, $Z=\theta/\pi$

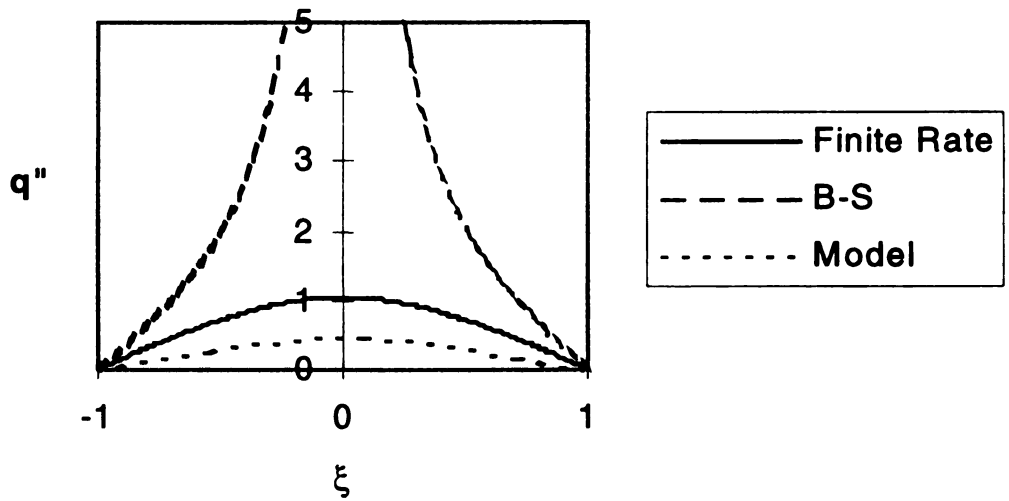
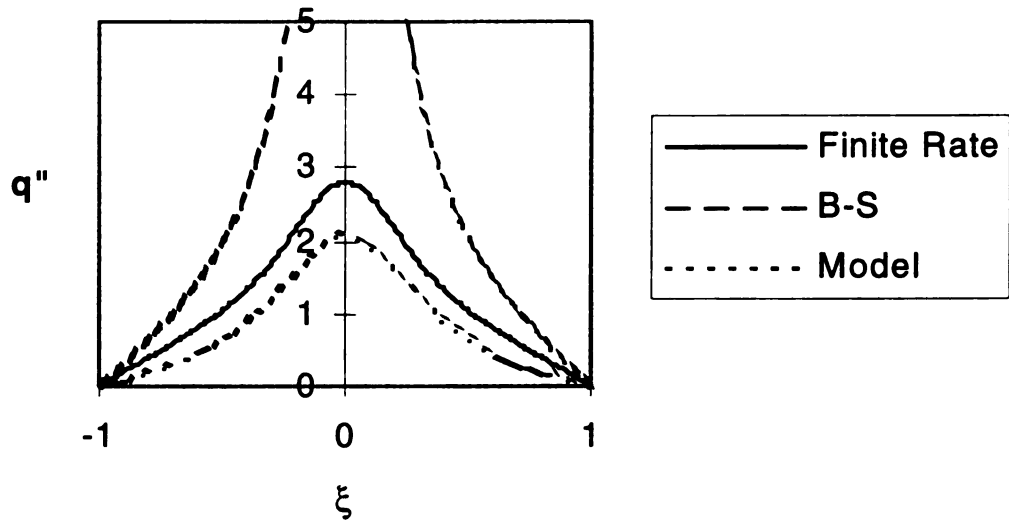


Figure 5.4 (a) Heat flux profiles comparison for straight flames $r_q=0.27$. Note the inaccuracy, generally, of the Burke-Schumann calculation of Equation(12.a,b) and the comparative similarity of the Finite-rate and Heat Transfer model results. A scaling factor renders the latter two visually indistinguishable. Heat flux comparisons for straight flame $r_q=0.9$. (b) Heat flux profiles comparisons for straight flames $r_q=0.9$. The comments to (a) apply here as well

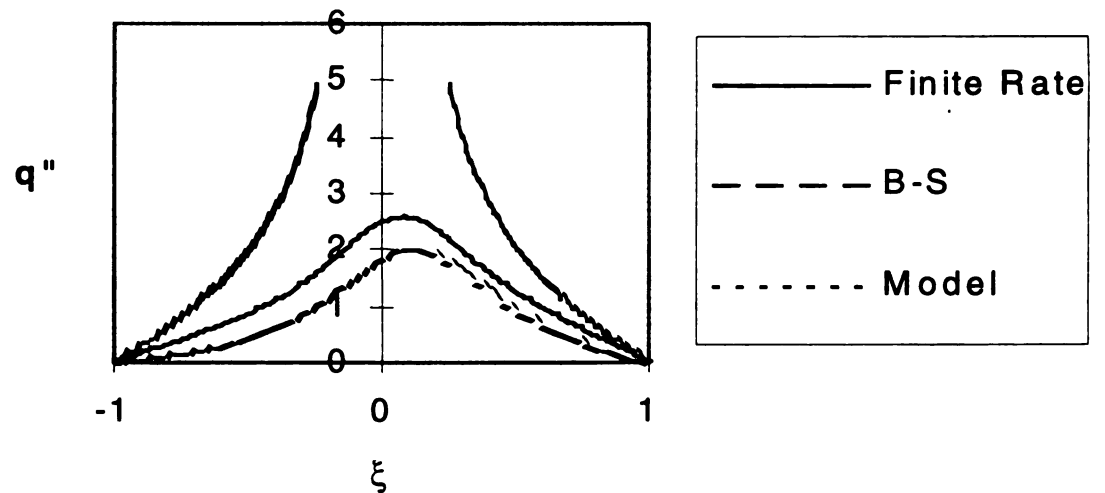
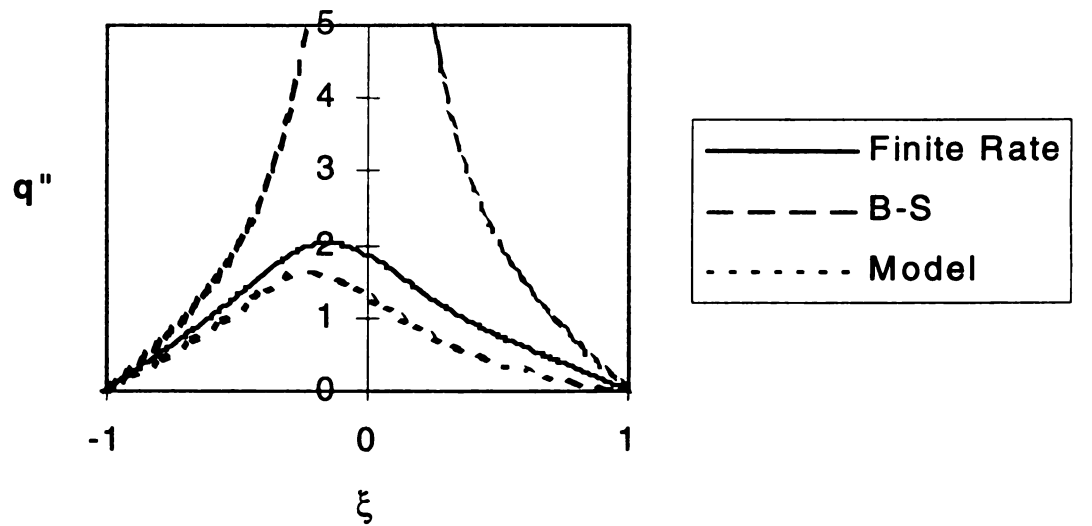
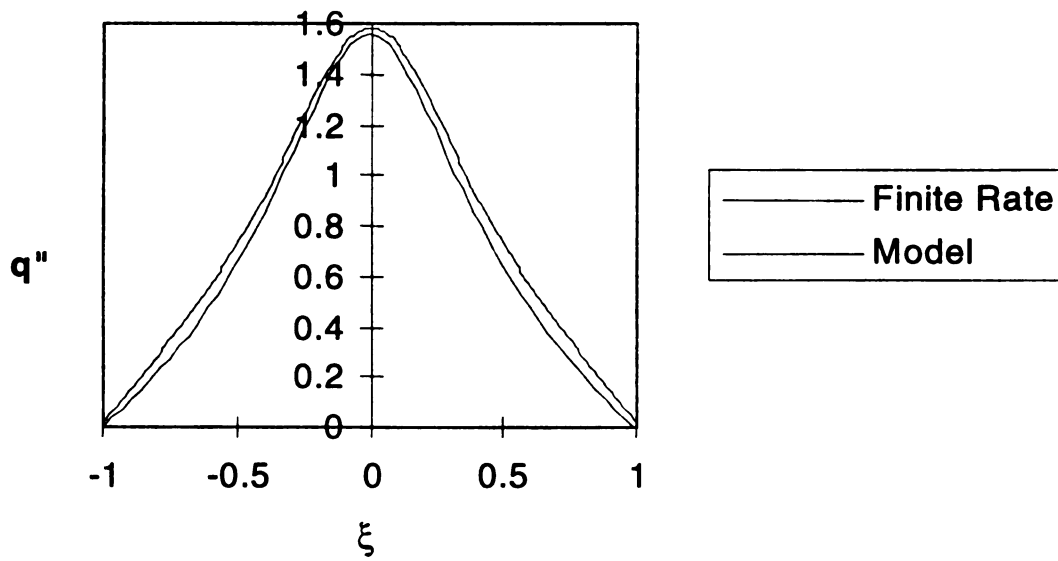


Figure 5.5 (a) Heat flux profile comparisons for fuel lean flames $\phi=0.5$, $r_q=0.38$. For this non-symmetric case the flux distribution is asymmetric. The Burke-Schumann model is once again a poor approximation to the heat flux. (b) Heat flux profile comparisons for fuel rich flames $\phi=1.5$, $r_q=0.28$. See comments in figure 5.4a

Table 5.1 Correction Factor Coefficients

ϕ	β_4	β_5	β_6	β_7	β_8
0.333	1.045	-0.179	-0.313	1.074	0.977
0.429	0.746	-0.08	-0.210	1.039	1.018
0.538	0.563	-0.096	-0.127	1.093	1.004
0.667	0.392	-0.194	-0.046	1.170	0.974
0.818	0.204	-0.084	-0.024	1.227	0.964
1.222	-0.204	0.084	-0.024	1.227	0.964
1.5	-0.392	0.194	-0.046	1.170	0.974
1.857	-0.563	0.096	-0.127	1.093	1.004
2.333	-0.746	0.08	-0.210	1.039	1.018
3.0	-1.045	0.179	-0.313	1.074	0.977



**Figure 5.6 Heat flux profile comparison for straight flame with convection
 $Pe=1, r_q=0.395$**

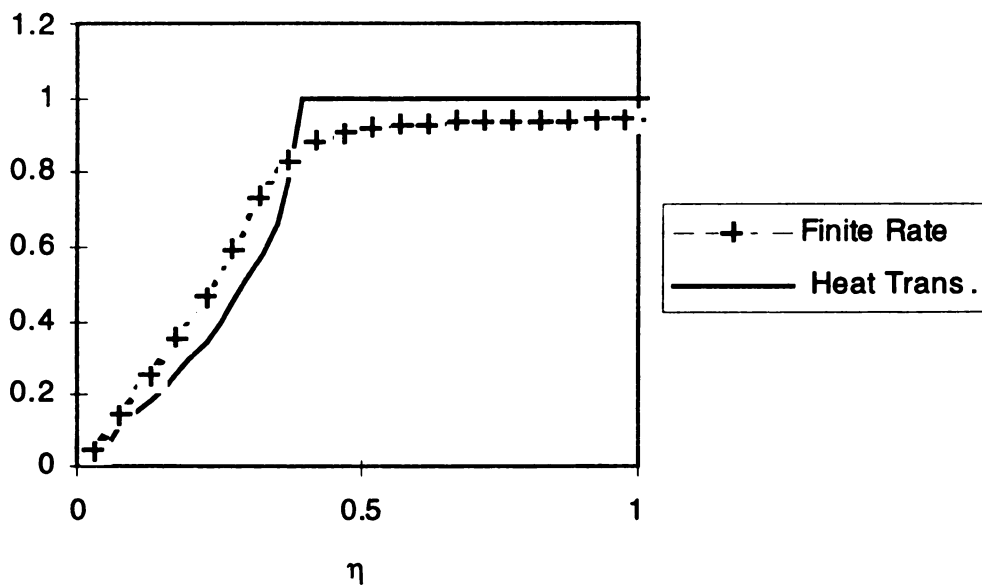


Figure 5.7 Centerline temperature distributions for a straight flame $r_q=0.375$. The broadness of the actual flame moderates the temperature variation, compared with the sharp heat transfer profile. The τ values along the diffusion flame ($\eta>0.5$) agree to within $O(\beta^{-1})$

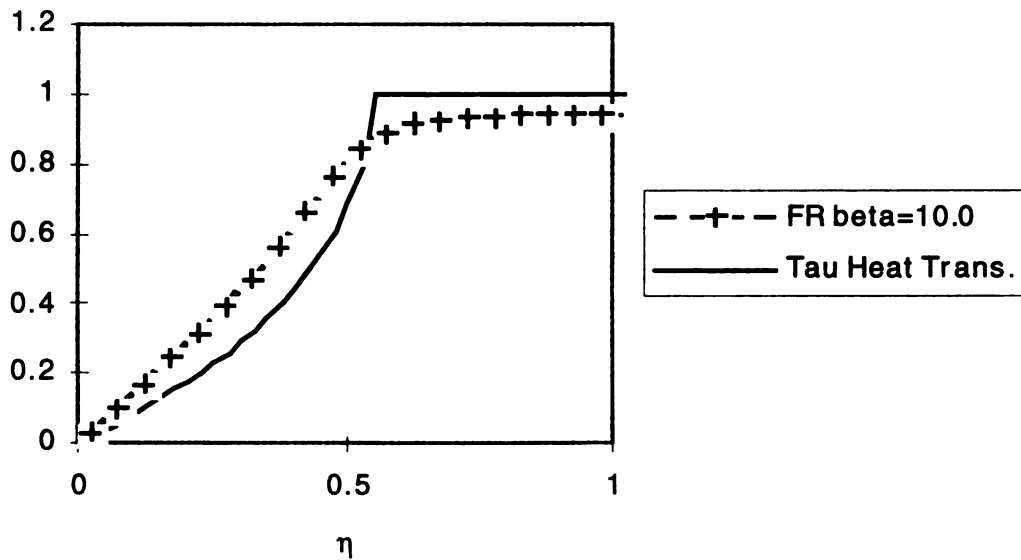
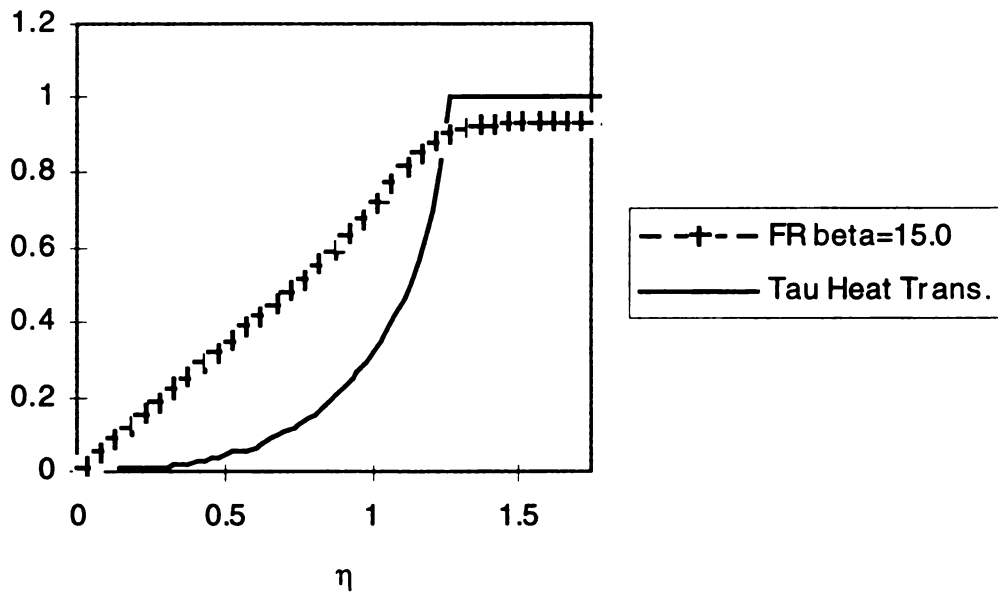


Figure 5.8 (a) Centerline temperature profile for a straight flame $r_q=0.525$. (b) Centerline temperature distribution for a straight flame $r_q=1.225$. For large quench distances the pure heat transfer temperature profile differs significantly from the finite-rate chemistry profile

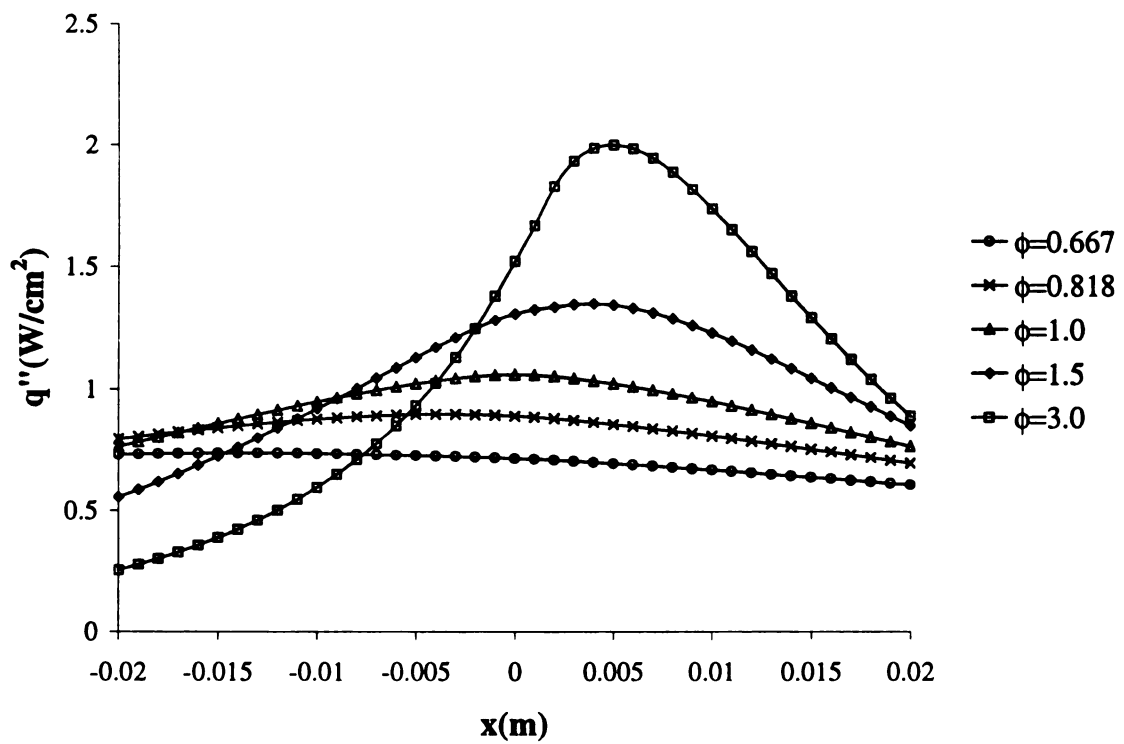


Figure 5.9 Heat flux distribution for Methane/Oxygen combustion at various stoichiometries

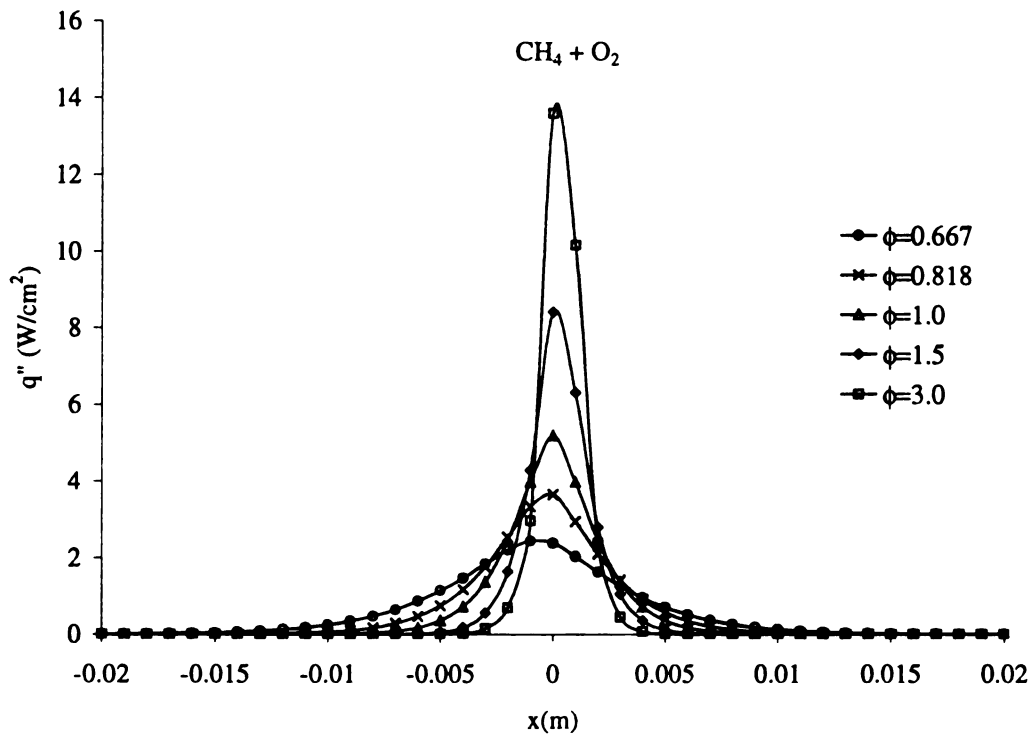


Figure 5.10 Heat flux distribution for Methane/Oxygen combustion at various stoichiometries. The second reaction mechanism given in table 5.2 is used

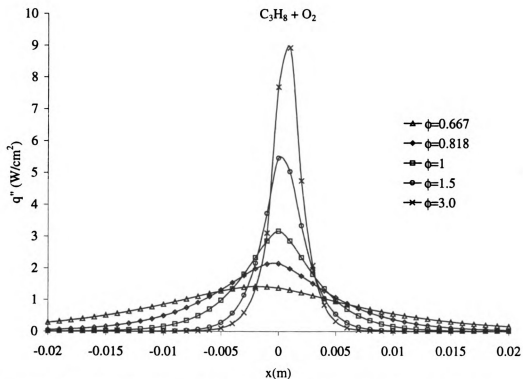


Figure 5.11 Heat flux profile for Propane/oxygen configuration. Larger heat losses than Methane are predicted

NUMERICAL TECHNIQUES

6.1 Numerical Techniques

The equations examined throughout this document represent models of more complex systems. The problems are greatly simplified by assuming the flow to be known and uniform and the fluid properties assumed constant. This eliminates the need to solve for the flow field through the Navier-Stokes equations. This model of uniform flow and constant density is a simplifying assumption to be sure; but it allows the thermo-diffusive effects, i.e. the Lewis number effects, to be examined without the complicating additions of an unknown flow field. However, even with these simplifying assumptions, the problem is still non-linear because of the chemical reaction that eliminates or creates constituents within the domain and adds thermal energy to the system to drive this transformation. Because of this non-linearity, analytical solutions become quite difficult and thrust one into the realm of asymptotic analysis. Asymptotic solutions, although insightful, are generally limited to “simpler” problems, i.e. those with only a single value for Le , simplified kinetic expressions, and one dimension. To study more complex combinations of parameters a computational solution was needed. In the text below the techniques used to solve the various systems of equations are discussed.

6.2 Transient premixed flame propagation

The governing equations for this problem have been described in chapter 4. In this section the solution techniques used and the issues that were addressed will be examined by using a generic one-dimensional equation with the same form. The following equation will be examined,

$$\frac{\partial \phi}{\partial t} = \frac{\partial^2 \phi}{\partial x^2} + f(\phi), \quad (6.1)$$

where ϕ represents a vector of dependant variables, and the function f is a non-linear function of the dependant variables.

There are several concerns that arise before numerical solutions begin. Primarily, the numerical stability of the problem as time increases. Furthermore, this stability issue is clouded with the nonlinear reaction term. It is clear that without the non-linear source term, a numerical scheme could be used that would be unconditionally stable, such as the Crank-Nicholson procedure. However, the need to linearize the equation for solution also raises stability issues. The fact that ϕ may contain more than one variable and be coupled through the reaction term is addressed by solving all the equations in the system simultaneously.

There are two ways to linearize equation (6.1): evaluate the non-linear term at the previous time step, thus producing a source term with a known value, or expand the function with a truncated Taylor series around the previous time step so that the function is represented as a linear equivalent. The discretized equations for both of these methods will be outlined below.

Along with the time lagging technique to linearize the system we apply a forward differencing for the time derivative and a central differencing for the spatial derivative. This scheme is first-order accurate in time and second in space; so in order to keep the solution reasonably accurate a small time step will be needed. An additional restriction on the size of the time step is introduced with this method. If the non-linear reaction term is going to be accurately represented by the value at the previous time step, then the time step cannot be too large. The discretized equations then become

$$\frac{\phi_i^{n+1} - \phi_i^n}{\Delta t} = \frac{\phi_{i+1}^{n+1} - 2\phi_i^{n+1} + \phi_{i-1}^{n+1}}{\Delta x^2} + f(\phi^n) \quad (6.2)$$

where the i subscript represents the node number, while the superscript n represents the time index. Furthermore, Δt and Δx are the time step and grid spacing respectively. At this point it should be pointed out that for problems where there are rapid changes in the values of the variables both temporally and spatially such as combustion wave fronts or shock waves, a non-uniform grid is usually desirable. In this way, there are more grid points in the vicinity of the sharp changes so their characteristics are captured more accurately. A non-uniform grid makes the discretization a bit more complex but does not affect the solution procedure. In the schemes used in this text a uniform grid was used, after the difference between a non-uniform and uniform mesh proved to be insignificant.

Equations (6.2) are then solved simultaneously in a block tri-diagonal format. This system will produce a banded matrix of the form $Ax=b$, where the vector x represents all the dependant variables of ϕ . Here A is a square matrix of order $C*N$, where C is the number of dependant variables and N is the number of grid points.

The lagging method of linearization produced a stable scheme only when the time step was very small. If the time step became too large, the non-linear term was unable to be accurately modeled using previous time step data. As it turned out, for the flame propagation problem, the time step using this method became so small that round off error may have become significant. This is an unacceptable situation, both from an accuracy standpoint as well as a practicality perspective. For this reason, the nonlinear term was linearized to include information from both the previous and present time indexes. This is discussed below.

The truncated Taylor series expansion of the reaction term is shown below,

$$f(\phi^{n+1}) \approx f(\phi^n) + \Delta\phi \left(\frac{\partial f}{\partial \phi} \right)^n \quad (6.3)$$

where $\Delta\phi = \phi^{n+1} - \phi^n$, and $\frac{\partial f}{\partial \phi}$ represents a n by n Jacobian matrix, with n being the number of dependant variables in ϕ . The resulting set of algebraic equations is then solved. By linearizing the system in this fashion and solving all n equations simultaneously, a stable solution can be achieved by means of a much larger time step. It is important to note that the time step must still be small to assure stability, but not as small as the lagging technique would require.

The boundary conditions of the first kind were implemented by fixing the value at the boundary node to equal that required by the boundary condition. The zero flux boundary conditions, or boundary conditions of the second kind, i.e. a fixed gradient at the boundary, were done in such a manner to ensure second order spatial accuracy. The method of image points was used so that the following discretized equation would result.

$$\phi_{i+1}^{n+1} = 2 * \Delta x * q'' + \phi_{i-1}^{n+1}. \quad (6.4)$$

In this case the i-1 node represents the image point and is found as a function of the interior node at i+1 and q'' is the heat flux at the boundary. Note that if this were to take place at the boundary where i+1 was the point outside the boundary, that would be the image point and the exterior node would be found in terms of the interior node.

6.3 Two-dimensional steady state with co-flow reactants

The governing equations for this system have the form

$$C \frac{\partial \phi}{\partial y} - D \left(\frac{\partial^2 \phi}{\partial x^2} + \frac{\partial^2 \phi}{\partial y^2} \right) = f(\phi) \quad (6.5)$$

where C and D represent constants, and f is a non-linear reaction term. The reaction term is handled identically to that of section 6.2.

Steady state schemes differ slightly from their transient counterparts in that there is no temporal evolution. In steady schemes a fixed solution is desired and there is no definite beginning and ending to the process. In this respect, the goal is to "find" the solution via iterative approaches, or in some instances a quasi-transient procedure. It should be noted that although there is no temporal evolution, the iteration itself acts as a pseudo-transient scheme so that numerical stability concerns can not totally be ignored. Furthermore, with the second dimension, the set of algebraic equations will no longer produce a block tri-diagonal form. If the set of equations is to be solved simultaneously, then a block penta-diagonal matrix will result. Since solution methods for a penta-diagonal scheme take significantly longer than those for a tri-diagonal matrix, it is desirable to utilize a tri-diagonal method in solving. This is accomplished by using an alternating direction implicit (ADI) scheme.

The ADI scheme is characterized by discretizing in one direction with an implicit manner, and the other explicitly. This set of equations is solved and the solution represents one half of a full iteration. The procedure is reversed and the formerly implicit direction is then treated as implicit and visa-versa. The solution obtained then represents one full iteration.

The discretization techniques are slightly different from those in section 6.1. The second derivatives, i.e. the diffusion term, are still modeled by second order correct central differences; but some care must be taken when examining the first derivative, i.e. the convective term. If C is large enough, the convective term become dominant and a

wave type equation exists. In this case an upwind scheme is needed to accurately model the problem. This is accomplished by using a second order accurate backward differencing shown below

$$\frac{\partial \phi}{\partial y} \approx \frac{3\phi_{i,j} - 4\phi_{i-1,j} + \phi_{i-2,j}}{2\Delta y} \quad (6.6)$$

Here, the i subscript refers to the nodes in the x -direction and the j subscripts to those in the y -direction. It is also noted that the backwards direction refers to the direction relative to the convective direction.

If C is less than some critical value, a second-order correct central differencing can be used on the convective term with no numerical instability associated with wave phenomena. This value of $C_{critical}$ can be found by examining the sign of the ϕ_{i+1} and ϕ_{i-1} terms in the discretized equation. If the condition below is satisfied, then a central differencing can be used with no loss of accuracy.

$$|C|\Delta y < 2|D| \quad (6.7)$$

Since this condition is satisfied for the co-flowing reactant problem, a central differencing was used for both the convective and diffusive terms.

The ADI method employed differed slightly from that described above. It was found that the numerical scheme was much more stable when the central differencing schemes involved evaluating the i,j term at the current iteration. This essentially resulted in the following discretized equations.

$$C \frac{\phi_{i,j+1}^k - \phi_{i,j-1}^k}{2\Delta y} - D \left(\frac{\phi_{i-1,j}^{k+1/2} - 2\phi_{i,j}^{k+1/2} + \phi_{i+1,j}^{k+1/2}}{\Delta x^2} + \frac{\phi_{i,j-1}^n - 2\phi_{i,j}^{k+1/2} + \phi_{i,j+1}^k}{\Delta y^2} \right) = f(\phi_{i,j}^k) \quad (6.8)$$

$$+ (\phi_{i,j}^{k+1/2} - \phi_{i,j}^k) \left(\frac{\partial f}{\partial \phi} \right)^k$$

Solving with the y-direction derivatives evaluated at the (k+1) iteration step completes the ADI. This scheme allows a block tri-diagonal scheme to be used for both directions, and utilizes less CPU time than solving the block penta-diagonal system.

After each iteration each point is subjected to some relaxation to improve convergence and help with numerical stability. The following equation represents how this relaxation is done:

$$\phi_{i,j}^{k+1*} = \omega\phi_{i,j}^{k+1} + (1-\omega)\phi_{i,j}^k \quad (6.9)$$

where, the k+1* superscript indicates the undated next guess in the iteration procedure. The value of ω is chosen by examination of the residuals to equation (6.5). This will be discussed in section 6.5. This iterative procedure will continue until the differences between the updated solution and the previous solution is small.

6.4 Two-dimensional Transient with Co-flow reactants

The governing equations are similar that those seen in section 6.3, with the exception that there is a $\partial\phi/\partial t$ is added to the left-hand side.

$$\frac{\partial\phi}{\partial t} + C\frac{\partial\phi}{\partial y} - D\left(\frac{\partial^2\phi}{\partial x^2} + \frac{\partial^2\phi}{\partial y^2}\right) = f(\phi) \quad (6.10)$$

Furthermore, as previously stated, a block tri-diagonal scheme is desirable due to the computational efficiency. Hence, an ADI scheme was implemented. The solution procedure follows that described by Shih [1] in which approximate factorization was used with a delta formulation of the difference equations. Equation (6.10) can be discretized into the following formulation:

$$\frac{\phi_{i,j}^{n+1} - \phi_{i,j}^n}{\Delta t} = \frac{1}{2}\left[\left(\frac{\partial\phi}{\partial t}\right)^n + \left(\frac{\partial\phi}{\partial t}\right)^{n+1}\right] + O(\Delta t^2) \quad (6.11)$$

The right-hand side of equation(6.11) is then re-written as

$$\text{RHS} = \frac{1}{2} \left[\left(-C \frac{\partial \phi}{\partial y} + D \frac{\partial^2 \phi}{\partial x^2} + D \frac{\partial^2 \phi}{\partial y^2} + f(\phi) \right)^n + \left(-C \frac{\partial \phi}{\partial y} + D \frac{\partial^2 \phi}{\partial x^2} + D \frac{\partial^2 \phi}{\partial y^2} + f(\phi) \right)^{n+1} \right] \quad (6.12)$$

The source term $f(\phi)$ is non-linear and hence cannot be handled directly at the $n+1$ time step. The linearization is handled as in section 6.2. In the delta formulation, the $\Delta\phi^n = \phi^{n+1} - \phi^n$ which appears in the linearization is kept as the dependent variable and all discretization is performed on this delta term. The variable B will represent the Jacobian matrix of $\partial f/\partial\phi$ evaluated at the n^{th} time step. Substituting equation (6.12) into equation (6.11) and introducing subscript notation to represent the derivatives yields

$$\left[I + \frac{\Delta t}{2} (C\phi_y - D\phi_{xx} - D\phi_{yy} + B) \right] \Delta\phi^n = \Delta t (-C\phi_y + D\phi_{xx} + D\phi_{yy} + f(\phi))^n \quad (6.13)$$

Here I represent the identity matrix. The approximate factorization is introduced to produce a directionally dependent representation of equation (6.13).

$$\left[N + \frac{\Delta t}{2} (C\phi_y - D\phi_{yy}) \right] N^{-1} \left[N + \frac{\Delta t}{2} (-D\phi_{xx}) \right] = \text{RHS}_2 \quad (6.14)$$

Where $N = I + B\Delta t/2$, and RHS_2 is the right-hand side of Eq(6.13). Equation (6.14) is then solved by sweeping in the y -direction and then the x -direction via the following procedure:

$$\left[N + \frac{\Delta t}{2} (C\phi_y - D\phi_{yy}) \right] \Delta\phi^* = \text{RHS}_2 \quad (6.15)$$

$$\left[N + \frac{\Delta t}{2} (-D\phi_{xx}) \right] \Delta\phi^n = N\Delta\phi^* \quad (6.16)$$

$$\phi_{i,j}^{n+1} = \phi_{i,j}^n + \Delta\phi_{i,j}^n \quad (6.17)$$

Equations (6.15,6.16) are solved via second order correct finite differencing subject to the constraints listed in section 6.3.

6.5 Error analysis

Code validation is an essential component to proper numerical analysis. This validation is commonly done by comparing experimental data to the output from the numerical method. This approach is useful when the governing equations used simulate the actual physical phenomena rather than model it. A simplified model used to predict only qualitative results will have a difficult time comparing well with experimental data. However, because of the simplicity of such models, the governing equations are generally well understood and several techniques can be used to ensure that the correct equations are being solved.

Initially, the finite difference equations (FDE) are examined for consistency. That is, a Taylor series expansion for each term is done about the i,j point. These are then substituted into the FDE and check to ensure that the original equations are obtained as the spatial or temporal terms approach zero. This will identify if the scheme is consistent or conditionally consistent. See reference 2 for more details.

Once the FDE has been solved, it is necessary to check and see if the correct equations have indeed been solved. The following describes how this was done for steady problems. The first step was to identify the optimal convergence parameter for the over-relaxation. Optimal in the sense that the residual sum of squares is minimized. Secondly, the errors are estimated by assuming the equation solved has the order of magnitude of error do the finite differencing as the original FDE.

It has long been known that when using a successive over-relaxation (SOR) procedure that the choice of the relaxation parameter ω can greatly impact the numerical schemes efficiency. However, it can also impact the accuracy of the numerical solution. This is shown by looking at the residual sum of squares. The residual is evaluated at each node and is effectively the imbalance between the right-hand side and the left-hand side of the governing finite difference equations. Each residual is then squared and summed over all interior nodes. If the numerical scheme was solving the FDE exactly, then the residual sum of squares would be zero; however, this is not the case. So, ω is varied over the range $0 < \omega < 2$ to find the value that minimizes the residuals.

Examination of the error behavior is also an important check to determine if the equations are being solved correctly. To do this it is necessary to know the accuracy of the FDE used in the model. If the problems examined are second-order accurate in both time and space, we can now assert that the true value can be given by the following equation:

$$T = R_h + Eh^2 \quad (6.18)$$

where T is the true value, R_h is the numerical result at grid spacing h such that $\Delta x = \Delta y = h$, and E is an order one constant. Taking results for three different grid sizes to be $h, h/2,$ and $h/4$ the error term can be estimated as follows.

$$E \left(\frac{h}{2} \right)^2 = \frac{R_{h/2} - R_h}{3} \quad (6.19)$$

The true value can now be estimated for the grid spacing $h/2$ and $h/4$ since the errors are known. If the errors behave in a second-order correct fashion, then the difference

between the two estimated true values should be less than the error for the $h/4$ grid spacing, and should be much less than order h^2 .

$$|T_{h/2} - T_{h/4}| < \left| \frac{R_{h/4} - R_{h/2}}{3} \right| \ll O(h^2) \quad (6.20)$$

If equation (6.20) holds true, then the numerical scheme behaves as expected and one can have reasonable confidence that the correct equations are being solved.

6.6 References

1. Shih, T. and Chyu, W. *AIAA Journal*, **29**, 1759-1760 (1991)
2. Anderson, D., Tannehill, J. and Pletcher, R. Computational Fluid Mechanics and Heat Transfer, Hemisphere Publishing (1984)

MICHIGAN STATE UNIVERSITY LIBRARIES



3 1293 02112 3728